

HAIR-CELL ADAPTATION MOTORS: A CHEMICAL-GENETIC APPROACH

By
John D. Scarborough


A dissertation submitted to The Oregon Health & Science University in conformity with the
requirements for the Degree of Doctor of Philosophy

Portland, Oregon
August 14, 2006

School of Medicine
Oregon Health & Science University

CERTIFICATE OF APPROVAL

This is to certify that the Ph.D. dissertation of
JOHN D. SCARBOROUGH
has been approved



Advisor



Member




Member



Member



Member



Member

ABSTRACT

To maintain optimal sensitivity, sensory hair cells of the inner ear rely on adaptation - the Ca^{++} -dependent closure of mechanically-activated transduction channels that follows a sustained stimulus. Manifest as a gradual decline in transduction current, adaptation occurs on fast and slow times scales by separate molecular processes. Rapid channel closure, called fast adaptation, ensues in less than a few milliseconds by an unresolved mechanism; slow adaptation occurs within tens of milliseconds when a complex of myosin-1c (Myo1c) molecules reduces tension applied to transduction channels (Holt et al., 2002).

In mouse vestibular hair cells, we found that the fast adaptation rate was modeled best as a release of a mechanical element in series with the transduction apparatus. To determine whether myosin-1c molecules of the adaptation motor accounted for this release and participated in fast adaptation, the Y61G mutation was inserted into the *Myo1c* locus by a gene-targeting strategy. Transduction and adaptation were measured in homozygous Y61G knock-in hair cells in the presence and absence of NMB-ADP, an Y61G-specific inhibitor. NMB-ADP blocked slow adaptation, as demonstrated previously in Y61G transgenic mice, but also inhibited fast adaptation, suggesting that the mechanical activity of Myo1c is required for both processes in vestibular hair cells.

To determine whether Myo1c mediates hair-cell adaptation in cochlear hair cells, mice homozygous for this sensitized (Y61G) allele were also generated to investigate Myo1c's role in the cochlea. Using these mice, we have begun preliminary experiments to test whether slow adaptation is prominent in cochlear outer hair cells and whether Myo1c activity is necessary for fast and slow adaptation in these cells.

Myosin-7a (Myo7a) has been suggested to participate in adaptation and transduction in the cochlea (Kros et al., 2002). Myo7a-deficient hair cells displayed increased slipping and reduced climbing adaptation; additionally, their bundles had to be deflected beyond their normal physiological operating range to open transduction channels. These results suggest that Myo7a plays a crucial role in hair-cell transduction, perhaps by generating force along the stereocilia length to properly align transduction elements within the plasma membrane.

To directly examine Myo7a's role in hair-cell adaptation, we extended the inhibitor-sensitization strategy to Myo7a, generating mice that expressed the analogous Y-to-G mutation in Myo7a (Y114G) under a hair-cell specific promoter (Boëda et al., 2001) with the hope that the Y114G mutation would have little effect on ATP hydrolysis and motor activity, but would sensitize Myo7a to NMB-ADP.

Y114G-Myo7a transgenics were bred with mice harboring the *Myo7a*^{sh1-8J} mutation, which we found is due to ~6.4 kb deletion. 8J homozygotes displayed the typical auditory and vestibular *shaker-1* defect, expressed trace Myo7a in cochlear hair cells, and had disorganized bundles. Thus, 8J homozygotes were an ideal background to test functional rescue by our Y114G-Myo7a transgene. We found that one or two copies of the Y114G transgene failed to rescue the 8J defect: a transgenic isoform of Myo7a was expressed, but resulted in disheveled hair bundles and profound deafness, as measured by ABR analysis. Whether the Y114G allele is functional will be assessed using a Y114G-Myo7a knock-in mouse.

Working in the Gillespie lab has been a terrific and deeply rewarding experience. Peter has been a superb scientific advisor and an outstanding mentor throughout graduate school. I am indebted to you for pushing me to the limits of my abilities, to the place where learning is greatest, for creating a fun, interactive workplace, and for your patience in respecting my role as a dad in raising a young family during graduate school. Thank you so much, Peter.

I would also like to thank Drs. John P. Adelman, Teresa Nicolson, and Richard Walker for their abiding interest in my thesis project over the years and the guidance they have given me to complete it. I also thank Dr. James Lundblad for becoming a new member of my thesis defense committee and for his helpful insight into the Myo7a project.

My thesis would not have been possible without the elegant work of Dr. Eric Stauffer and Dr. Jeffrey Holt. They have been wonderful collaborators and I feel fortunate to have been able to team up with them. To Dr. Susan K.H. Gillespie, thank you very much for your patience in teaching me molecular biology and for the very hard work you put into making the Y61G targeting vector. I also thank Emilie Miller for her contribution to Y61G project with the in vitro motility experiments, and to all the members of the Gillespie lab, past and present, for making it an extremely fun place to work and for their support and many helpful suggestions. To Beth Kempton, thank you very much for teaching me how to perform auditory brainstem analyses.

Thank you, Megan, Eve, and Ian for your unwavering love and support during these years. To my parents, thank you for your love and for planting the seed of curiosity in science and medicine.

TABLE OF CONTENTS

<i>Title</i>	<i>Page</i>
<u>ABSTRACT</u>	<u>II</u>
<u>ACKNOWLEDGEMENTS</u>	<u>IV</u>
<u>TABLE OF CONTENTS</u>	<u>V</u>
<u>LIST OF TABLES</u>	<u>XIII</u>
<u>LIST OF FIGURES</u>	<u>XIV</u>
<u>INTRODUCTION</u>	<u>1</u>
THE INNER EAR HAIR CELL	1
THE COCHLEA	1
AUDITORY TRANSDUCTION	4
THE UTRICLE AND SACCCULE	6
THE SEMICIRCULAR CANALS	7
HAIR BUNDLE STRUCTURE	7
GATING SPRING MODEL	13
ADAPTATION	14

THE MYOSIN SUPERFAMILY	22
HAIR-BUNDLE MYOSINS	22
MYOSIN-1C	24
MYOSIN-7A	25
CHEMICAL-GENETIC STRATEGY	28
<u>RESEARCH OBJECTIVES</u>	<u>30</u>
GENERATION AND CHARACTERIZATION OF Y61G-MYO1C KNOCK-IN MICE	30
CHARACTERIZATION OF THE <i>Myo7a</i>^{sh1-8J} MUTATION	30
GENERATION AND CHARACTERIZATION OF Y114G-MYO7A TRANSGENIC MICE	30
<u>MATERIALS AND METHODS</u>	<u>32</u>
CLONING OF THE Y61G-MYO1C TARGETING CONSTRUCT	32
MUTAGENESIS OF THE MYO1C SEQUENCE IN PBS-MUTØ	33
SUBCLONING OF THE LOXP-FLANKED NEOMYCIN RESISTANCE CASSETTE	34
SUBCLONING OF THE <i>DIPHTHERIA</i> TOXIN CASSETTE	35
PREPARATION OF LINEARIZED PLASMID FOR ELECTROPORATION	35
SCREENING OF RECOMBINANTS BY PCR	36
NESTED PCR (5' END PCR SCREENING STRATEGY)	37

NESTED PCR (3' END PCR SCREENING STRATEGY)	38
SOUTHERN ANALYSIS OF POTENTIAL ES CELL CLONES	40
DIGESTION	40
ALKALI TRANSFER	41
PROBE PREPARATION	42
PREHYBRIDIZATION/HYBRIDIZATION	42
WASHING	43
STRIPPING AND REPROBING	43
SOUTHERN ANALYSIS OF G8 SUBCLONES AND POTENTIAL POSITIVES	43
PCR GENOTYPING OF Y61G MICE	45
TOE AND TAIL DIGESTION	45
PCR	45
PCR GENOTYPING OF CRE MICE	47
PCR GENOTYPING FOR THE NEO CASSETTE	47
SOUTHERN ANALYSIS OF Y61G MOUSE GENOTYPES	48
DIGESTION	48
GEL TREATMENT	49
TRANSFER	49
PROBE PREPARATION	50
PREHYBRIDIZATION/HYBRIDIZATION	51
WASHING	52
STRIPPING AND REPROBING	52
RT-PCR ANALYSIS	52

RNA HARVESTING	52
CDNA SYNTHESIS	53
Y61G ANTIBODY PURIFICATION	55
PROTEIN EXTRACTION	55
SDS-PAGE	57
IMMUNOBLOT ANALYSIS	58
PROTEIN MOLECULAR WEIGHT MARKERS	59
AUDITORY-EVOKED BRAINSTEM RESPONSES OF Y61G MICE	59
CONSTRUCTION OF BACULOVIRUSES FOR MOUSE MYO1C EXPRESSION	60
SF9 EXPRESSION OF MOUSE MYO1C AND Y61G-MYO1C	62
ACTIN PREPARATION	63
PURIFICATION OF MYO1C BY Ni²⁺-NTA CHROMATOGRAPHY	64
ATPASE ANALYSIS OF MOUSE MYO1C (WILD-TYPE AND Y61G)	66
<u>MATERIALS AND METHODS II</u>	<u>69</u>
SUBCLONING MOUSE <i>MYO7A</i> EXONS INTO PCR2.1-TOPO VECTOR AND SEQUENCING	69
RT-PCR ANALYSIS OF 8J MICE	70
RNA HARVESTING	70
CDNA SYNTHESIS	70
SOUTHERN ANALYSIS OF 8J GENOTYPES	71
IMMUNOBLOT ANALYSIS OF 8J AND Y114G TRANSGENIC MICE	72
IMMUNOCYTOCHEMISTRY OF COCHLEAR HAIR CELLS	72

AUDITORY-EVOKED BRAINSTEM RESPONSES OF 8J MICE	73
<u>MATERIALS AND METHODS III</u>	75
CLONING OF THE Y114G-MYO7A TRANSGENIC CONSTRUCT	75
INSERTING THE MOUSE MYO7A PROMOTER	75
MUTAGENESIS OF 6150 SITE OF MOUSE MYO7A CDNA	76
ADDING FLANKING INSULATORS	77
SWAPPING IN THE Y114G MUTATION	78
CLONING OF THE FLASH-TAGGED MYO7A TRANSGENIC CONSTRUCT	79
SWAPPING IN THE FLASH-TAGGED MUTATION	79
PCR GENOTYPING OF Y114G TRANSGENIC MICE	79
PCR	80
PCR GENOTYPING OF FLASH-TAGGED TRANSGENIC MICE	80
RT-PCR ANALYSIS OF Y114G TRANSGENIC MICE	81
RNA HARVESTING	81
CDNA SYNTHESIS	81
RT-PCR/SOUTHERN ANALYSIS OF FLASH TRANSGENIC MICE	82
RT-PCR/<i>EcoR</i> V DIGESTION ANALYSIS OF FLASH TRANSGENIC LINES	84
IMMUNOBLOT ANALYSIS OF Y114G TRANSGENIC MICE	84
FLASH LABELING	85
RT-PCR ANALYSIS OF WILD-TYPE COCHLEA TO TEST FOR THE PRESENCE OF 38 AMINO ACIDS IN THE CODING REGION OF <i>MYO7A</i> IN EXONS 32 AND 33	86

RNA HARVESTING	86
CDNA SYNTHESIS	86
CLONING OF THE Y114G-MYO7A KNOCK-IN CONSTRUCT	88
CONSTRUCTION OF BACULOVIRUES FOR MYO7A EXPRESSION	91
SF9 EXPRESSION OF MOUSE MYO7A (WILD-TYPE AND Y114G)	91
ATTEMPTS TO PURIFY SOLUBLE MYO7A	92
RESULTS	95
<hr/>	
GENERATION AND CHARACTERIZATION OF Y61G-MYO1C KNOCK-IN	
MICE	95
SCREENING ES CLONES BY NESTED PCR AND SOUTHERN ANALYSIS	95
GENERATING Y61G MICE	102
SOUTHERN ANALYSIS OF Y61G MICE	102
RT-PCR ANALYSIS	105
IMMUNOBLOT ANALYSIS OF TISSUES FOR Y61G EXPRESSION	110
ABR ANALYSIS	110
Y61G BIOCHEMISTRY	115
EXPRESSION AND PURIFICATION OF MOUSE MYO1C	
(WILD-TYPE AND Y61G)	115
NMB-ADP INHIBITED Y61G-MYO1C	116
ELECTROPHYSIOLOGY	130
ADAPTATION IN Y61G UTRICULAR HAIR CELLS	130
NMB-ADP INHIBITS FAST AND SLOW POSITIVE ADAPTATION RATES IN	
UTRICULAR Y61G HAIR CELLS	130

NMB-ADP SLOWS NEGATIVE ADAPTATION IN UTRICULAR Y61G HAIR CELLS	133
<u>DISCUSSION</u>	136
<u>FUTURE DIRECTIONS</u>	141
<u>RESULTS II</u>	144
CHARACTERIZATION OF THE <i>Myo7a^{sh1-8J}</i> MUTATION	144
RATIONALE FOR USING 8J MICE AND CHARACTERIZING THE <i>Myo7a^{sh1-8J}</i> MUTATION	144
<i>Myo7a^{sh1-8J}</i> EXON SEQUENCING	149
SOUTHERN ANALYSIS OF WILD-TYPE AND <i>Myo7a^{sh1-8J}</i> HOMOZYGOUS MICE	161
RT-PCR ANALYSIS USING PRIMERS SPECIFIC FOR EXON 37 AND THE 3'UTR	161
IMMUNOCYTOCHEMISTRY	164
IMMUNOBLOT ANALYSIS OF TISSUES FOR MYO7A EXPRESSION	173
ABR ANALYSIS OF <i>Myo7a^{sh1-8J}</i> MICE	173
<u>DISCUSSION II</u>	180
<u>RESULTS III</u>	183

GENERATION AND CHARACTERIZATION OF Y114G-MYO7A TRANSGENIC

MICE	183
MUTANT-INHIBITOR STRATEGY	183
FLASH-FALI STRATEGY	183
GENERATING Y114G-AND FLASH-TAGGED MYO7A TRANSGENIC MICE	184
RT-PCR/SOUTHERN ANALYSIS OF FLASH TRANSGENIC LINES	187
FLASH LABELING OF INNER EAR TISSUES FROM LINES 23 AND 25	188
RT-PCR ANALYSIS OF Y114G-MYO7A TRANSGENIC MICE	195
IMMUNOBLOT ANALYSIS OF Y114G TISSUES	195
IMMUNOCYTOCHEMISTRY OF Y114G COCHLEAS	198
PHENOTPYE ANALYSIS	204
<u>DISCUSSION III</u>	<u>206</u>
<u>FUTURE DIRECTIONS III</u>	<u>213</u>
<u>SUMMARY AND CONCLUSIONS</u>	<u>219</u>
<u>REFERENCES</u>	<u>222</u>

LIST OF TABLES

<i>Number</i>		<i>Page</i>
Table 1.	Southern Probes	102
Table 2.	<i>Shaker-1</i> alleles	146
Table 3.	Primers used for <i>Myo7a</i> exon sequencing	150
Table 4.	Primers used for <i>Myo7a</i> exon (38-47) sequencing	153
Table 5.	Upstream primers for amplifying across the 8J deletion	156

LIST OF FIGURES

<i>Number</i>		<i>Page</i>
Figure 1.	Anatomy of the human ear	3
Figure 2.	Electron micrographs of hair bundles	9
Figure 3.	Electron micrographs of tip links	12
Figure 4.	Adaptation of transduction current in response to a positive stimulus	16
Figure 5.	Transduction apparatus	18
Figure 6.	Fast and slow adaptation	21
Figure 7.	Targeting strategy	97
Figure 8.	Nested PCR analysis of ES cell clones	99
Figure 9.	Southern analysis of ES cell clones	101
Figure 10.	Genotyping of Y61G mice	104
Figure 11.	Southern analysis of Y61G mice	107
Figure 12.	RT-PCR analysis of thymus from Y61G and wild-type mice	109
Figure 13.	Protein immunoblot analysis of Myo1c expression in tissues from Y61G and wild-type mice	112
Figure 14.	Auditory-evoked brainstem response analysis of Y61G mice	114
Figure 15.	Actin-activated ATPase activity of Wt-mMyo1c	119
Figure 16.	Actin-activated ATPase activity of Y61G-mMyo1c	121
Figure 17.	Inhibition of ATPase activity by NMB-ADP	123
Figure 18.	NMB-ADP inhibition of Wt-mMyo1c ATPase activity	125
Figure 19.	NMB-ADP inhibition of Y61G-mMyo1c ATPase activity	127
Figure 20.	In vitro motility of Myo1c	129

LIST OF FIGURES

<i>Number</i>		<i>Page</i>
Figure 21.	Adaptation is slowed by NMB-ADP in Y61G but not wild-type hair cells	132
Figure 22.	Fast and slow negative adaptation are slowed by NMB-ADP in Y61G utricular hair cells	135
Figure 23.	Model for fast adaptation in response to positive and negative stimuli	139
Figure 24:	Functional domains of Myo7a with shaker-1 mutations	148
Figure 25:	PCR amplification of <i>Myo7a</i> exons 38-46 from genomic DNA	155
Figure 26:	PCR amplification across the 8J deletion	158
Figure 27:	Diagram of the 8J allele and Southern analysis of 8J mutation	160
Figure 28:	RT-PCR analysis of liver RNA <i>Myo7a</i> ^{sh1-8J} and C57BL6 mice	163
Figure 29:	Genotyping 8J mice	166
Figure 30:	Phalloidin labeling of organ of Corti from 8J mice	168
Figure 31:	Localization of Myo7a in organ of Corti from mice (aged P4) by immunofluorescence and immunocytochemistry	170
Figure 32:	Localization of Myo7a in organ of Corti from mice (aged P6) by immunofluorescence and immunocytochemistry	172
Figure 33:	Protein immunoblot analysis of Myo1c expression in tissues from Y114G and 8J mice	175
Figure 34:	Protein immunoblot analysis of Myo1c expression in kidneys from wild-type and 8J mice	177
Figure 35:	Auditory-evoked brainstem response analysis of 8J mice	179
Figure 36:	Schematic diagram of the Y114G-Myo7a and FIAsh-tagged <i>Myo7a</i> transgene	186

LIST OF FIGURES

<i>Number</i>		<i>Page</i>
Figure 37:	RT-PCR/Southern analysis of FAsH-tagged <i>Myo7a</i> transgenic lines	190
Figure 38:	RT-PCR/ <i>EcoR</i> V digestion analysis of FAsH-tagged <i>Myo7a</i> transgenic lines	192
Figure 39:	Localization of inner ear <i>Myo7a</i> in FAsH-tagged <i>Myo7a</i> transgenic lines 25 by lumio green labeling	194
Figure 40:	RT-PCR analysis of cochlea and utricle from Y114G transgenic mice	197
Figure 41:	Localization of <i>Myo7a</i> in organ of Corti from single or double Transgenic mice (aged P0) by immunofluorescence and immunocytochemistry	200
Figure 42:	Immunoblot analysis of <i>Myo7a</i> expression in kidneys from single or double transgenic mice (line 56)	203
Figure 43:	RT-PCR analysis of wild-type cochlea to test for the presence of a 38 amino acid coding region of <i>Myo7a</i> in exons 32 and 33	209
Figure 44:	Targeting strategy for the Y114G knock-in construct	215

INTRODUCTION

The inner ear hair cell – a highly evolved sensor:

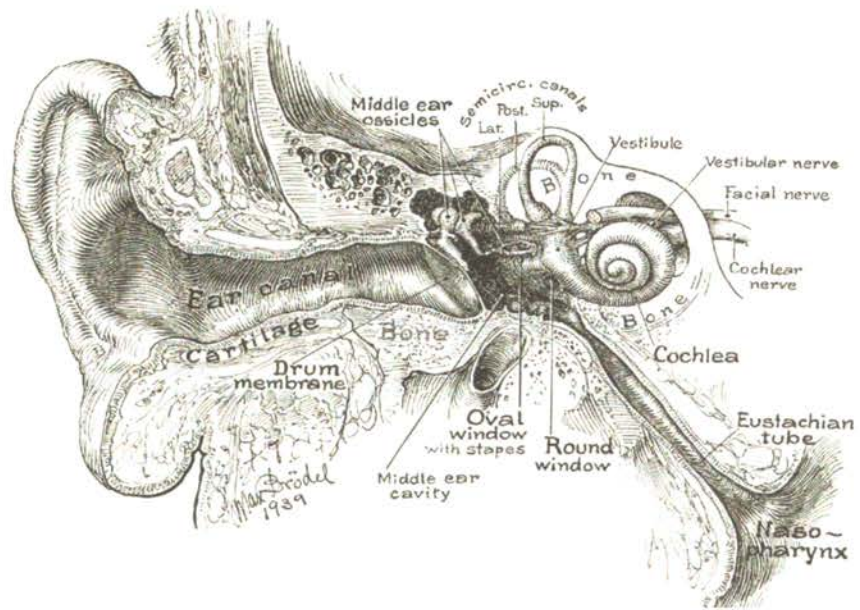
Deep within the petrous portion of the temporal bone, hair cells - the sensory receptors for sound perception and head movement - inhabit the delicate organs of the membranous labyrinth: the cochlea, utricle, saccule, and three semicircular canals. Our sense of hearing begins when fine bristles on auditory hair cells interface the aural universe by quivering in response to sound. Likewise, we navigate our gravitational world, reflexively maintaining posture and balance, when mechanoreceptive bundles on vestibular hair cells tremble in response to motions and accelerations of the head. For a sensor to accurately respond to sound and acceleration, it must perform within microseconds at atomic resolution; thus, the hair cell has evolved a *direct* transduction mechanism that functions with unparalleled speed and discrimination among the senses.

Cochlea:

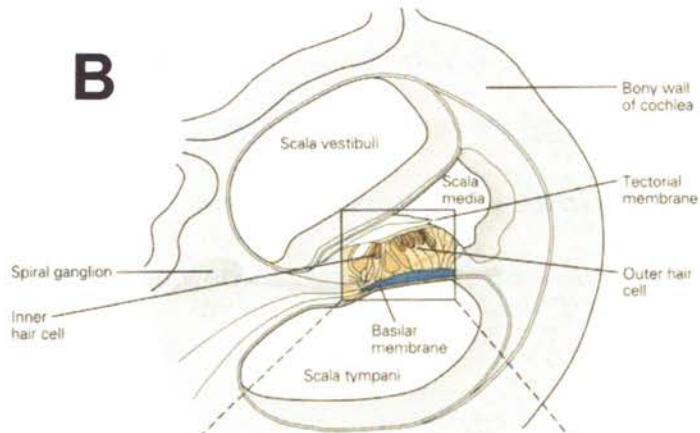
The cochlea (Fig. 1A) consists of a spiral canal making two and a half turns around a central core of bone, the modiolus. Three fluid-filled compartments - the scalae vestibuli, tympani, and media – stretch along its 33 mm length (Fig. 1B). Perilymph, a potassium-poor [4 mM], sodium-rich [142 mM] fluid ionically resembling cerebrospinal fluid, bathes the scalae tympani and vestibuli, while endolymph, a potassium-rich [157 mM] fluid produced by the stria vascularis, flows within the scala media (Wangemann and Schacht, 1996).

Figure 1. **Anatomy of the human ear.** *A*, The ear consists of the external auditory meatus, the middle ear, and the inner ear. *B*, Shown in cross section, the cochlea is a coiled tube 33 mm in length comprised of three fluid-filled compartments: the scala vestibuli, scala tympani, and scala media. *C*, A detailed view of the organ of Corti, which lies suspended in the cochlear duct. Sound ultimately produces bundle deflection of hair cells, when the elastic basilar membrane flexes in response to sound-generated fluid movements within the cochlea. The hair bundles of inner hair cells are arranged linearly, while those of outer hair cells are V-shaped. Inner hair cells transmit sensory information to the brain, since 90-95% of the afferent innervation inputs these cells. By contrast, the outer hair cells receive efferent innervation and serve to amplify faint mechanical signals. Phalangeal and pillar cells separate and support the inner and outer rows of hair cells (from Kandel et al., 2000).

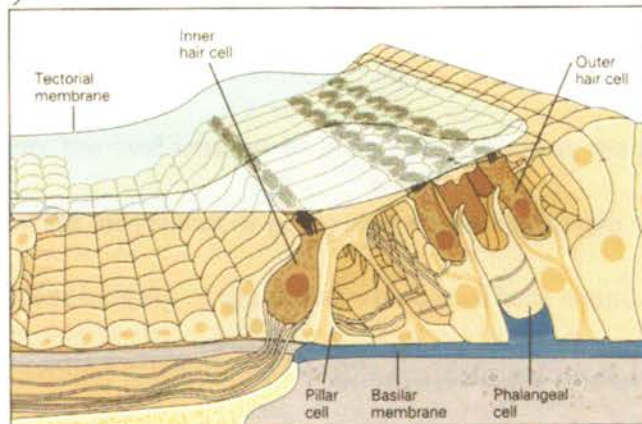
A



B



C



Separating the scalae anatomically, Reissner's membrane and a collection of flexible fibers known as the basilar membrane, or cochlear partition, lie suspended within the cochlea to form the cochlear duct (Fig. 1B). A specialized cellular structure for sound perception - the organ of Corti - rests on the cochlear partition and includes along its length an array of sound-sensing hair cells, an inner row of 3500 cells and three to four outer rows of cells that number ~12,000 (Fig. 1C). Pillar cells segregate these rows while laterally providing rigid, mechanical support. From below, Deiters' cells cup the outer hair cells for added stability and send processes obliquely toward the reticular lamina, the actual physical boundary between endolymph (scala media) and perilymph (scala vestibuli) that is formed by tight junctions at the tops of adjacent cells. From above, a stiff, gelatinous veil - the tectorial membrane - overlies all hair cell rows (Fig. 1B). Relative to the tectorial membrane, the reticular lamina descends gradually to the spiral limbus; therefore, hair bundles of the outer hair cell rows embed within the membrane's undersurface and those of the inner row attach loosely to a subreticular ridge - Henson's stripe - via wispy trabeculae (Slepecky, 1996).

Auditory Transduction:

The external ear funnels sound-pressure changes onto the tympanic membrane, putting into motion the three middle ear ossicles (malleus, incus and stapes), which focus the mechanical signal onto the oval window of the cochlea. In turn, the piston-like vibration of the stapes drives movement of perilymph within the scalae vestibuli and tympani, causing coincident bulging of the round window. These sound-generated fluid movements produce a traveling wave on the flexible cochlear partition, leading to shear

of the outer hair cell bundles against the tectorial membrane and excitation of the hair cells. Two features cause this shearing: the difference in stiffness between the tectorial and basilar membranes and their offset pivot points.

Like a prism separating light into its constituent colors, the organ of Corti deconstructs complex sounds into simpler elements based on the segment of basilar membrane being excited by a given sound frequency presented by the traveling wave. The elicited pattern of motion depends on the frequency - low frequencies cause greatest basilar membrane motion at the apex; high frequencies produce greatest movement at the base (von Békésy, 1960). Maximal motion at a given position initiates receptor potentials of the overlying hair cells, which in turn excite auditory nerve fibers innervating the region. This tonotopic arrangement results largely from the basilar membrane's mechanical properties, which vary continuously along its length - being narrow and taut at the base; wider and flaccid at the apex. Tonotopy is a common organizing strategy of the auditory system preserved at higher levels along the pathway, including auditory cortex.

Hair cells of the auditory system enrich the human experience immensely, but are not essential for survival. By contrast, hair cells of the vestibular system report crucial information about motions and positions of the head that are needed for reflexive eye movements and postural control (Goldberg et al., 2000). Though we are normally unaware of their actions in the vestibular system, damage to these hair cells is devastating.

Utricle and Sacculle:

The otolith organs, the utricle and saccule, respond to accelerations and translational movements of the head along any axis. Like hair cells of the cochlea, those of the otolith organs transduce motion into neural impulses by deflection of the hair bundle. In a person standing upright, utricles lie horizontally within the head; thus, utricular hair cells report changes in the horizontal plane. The saccule, by contrast, conveys changes in the vertical axis, because it lies vertically in the head. In lower vertebrates, the saccule also detects ground- and air-borne vibrations.

Both otolith organs enclose a continuous, oblong sensory epithelium called the macula, which is populated by nonsensory supporting cells and hair cells. Arising from the macula, hair bundles project initially into endolymph, then into a thin gelatinous layer, before piercing the undersurface of the otolithic membrane, a fibrous structure overlying the entire epithelium. Fine crystals of calcium carbonate known as otoconia decorate the top surface of the otolithic membrane, making it denser relative to the endolymph. Thus, when the head undergoes tilt or linear acceleration, force shifts the membrane relative to the sensory epithelium, and bundles are transiently displaced. Bundle deflection, in turn, produces a change in neurotransmitter release patterns, thereby affecting the firing rate of the innervating vestibular neurons. Because these neurons fire with a high rate of spontaneous activity, they encode absolute head position or linear accelerations.

Two groups of hair cells oppose each other with polarized bundle orientations along the striola, a narrow trench demarcating the otolithic membrane along its length. Hair bundles of the saccule point toward the striola; the opposite is true in the utricle.

Due to this arrangement, head tilt or linear acceleration excites some groups of hair cells while inhibiting others. Because hair cells sit in the macula with a wide range of bundle orientations, vestibular organs can respond to linear force in every direction the body moves.

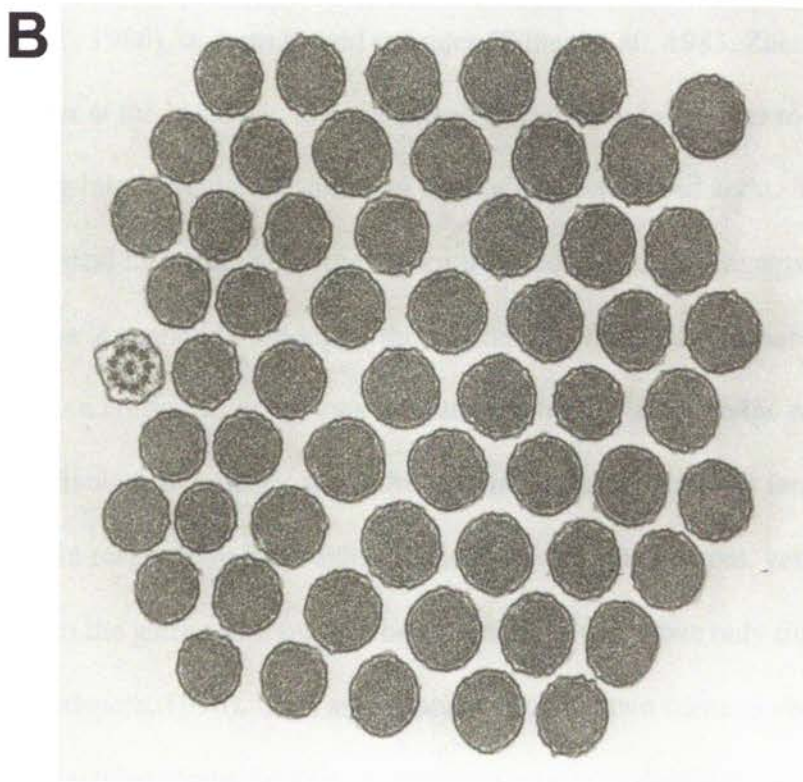
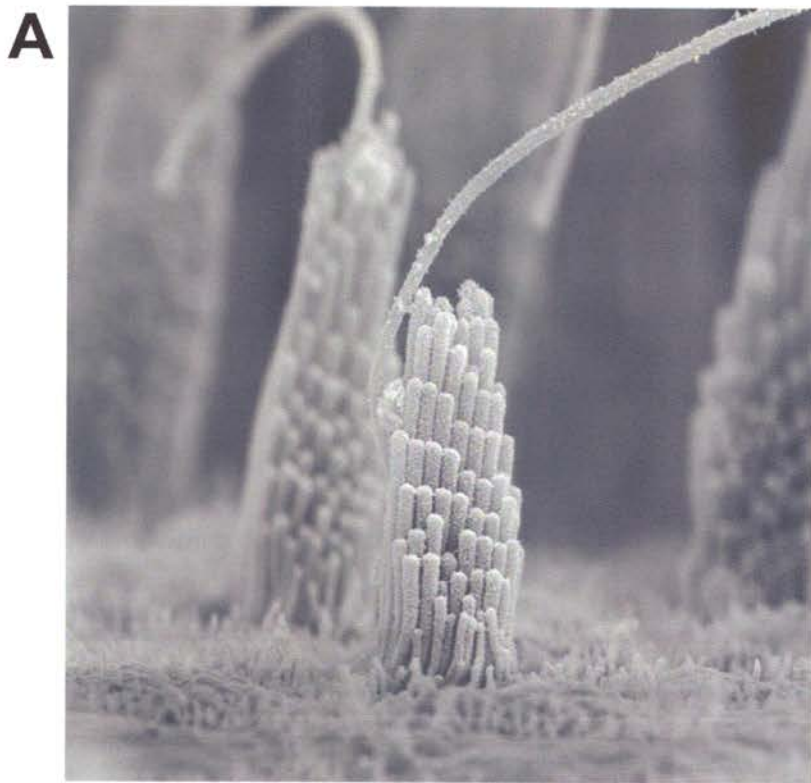
Semicircular Canals:

On either side of the head, three semicircular canals (anterior vertical, posterior vertical, and horizontal) sit at $\sim 90^\circ$ to one another, and measure changes of head position about any axis. Localized swellings at the base of each canal house the sensory epithelium - the crista ampullaris. Dwelling within each crista, hair cells (~ 7000) extend long hair bundles ($20 \mu\text{m}$) into the cupula (Lewis et al., 1985), a compliant membrane that spans across each ampulla and acts as a fluid barrier within a canal. Changes in angular acceleration cause endolymph to flow in a canal opposite the direction of head movement, deforming the cupula against the underlying hair bundles, which changes the receptor potential and transmitter release patterns in the hair cells. Because all the hair bundles within a crista are oriented in the same direction, all hair cells respond together to synchronously affect the discharge pattern of innervating nerves.

Hair bundle structure:

Hair cells transduce motion into neural signals with their apically specialized hair bundle, a stack of actin-filled stereocilia arranged in rows of increasing height (Fig. 2A). Stereocilia range in number, from 30-300, and in height; in bullfrog saccular hair cells, for example, the shortest measure $4 \mu\text{m}$, the highest $8 \mu\text{m}$. Standing beside the tallest

Figure 2. **Electron micrographs of hair bundles.** *A*, A scanning electron micrograph of a hair bundle from a mouse utricular hair cell reveals that rows of stereocilia are staggered according to height and organized in a staircase (from B. Kachar, unpublished). *B*, Transmission electron micrograph of a hair bundle in cross section. Spaced apart in a hexagonal array, each stereocilium is rigid cylinder densely packed with a core of polarized actin filaments. A single microtubule-based kinocilium sits at one end of the hair bundle (from Jacobs and Hudspeth, 1990).



row of stereocilia, the kinocilium - a vestigial, microtubular structure - degenerates shortly after birth, indicating its nonessential role in transduction (Hudspeth and Jacobs, 1979).

A diverse set of interconnecting crosslinks holds the bundle together (Goodyear et al. 2005). Near the top, *tip links* stretch along the axis of symmetry between shorter stereocilia to the side of a taller neighbor (Fig. 3A, B); *lateral links* attach stereocilia along the shafts; *ankle links*, which are prominent in amphibians, provide basal connections between stereocilia. Overall, these crosslinks result in a beveled structure, giving adjacent stereocilia a center-to center distance of 350 nm at the apex and 850 nm at the base (Denk et al., 1995).

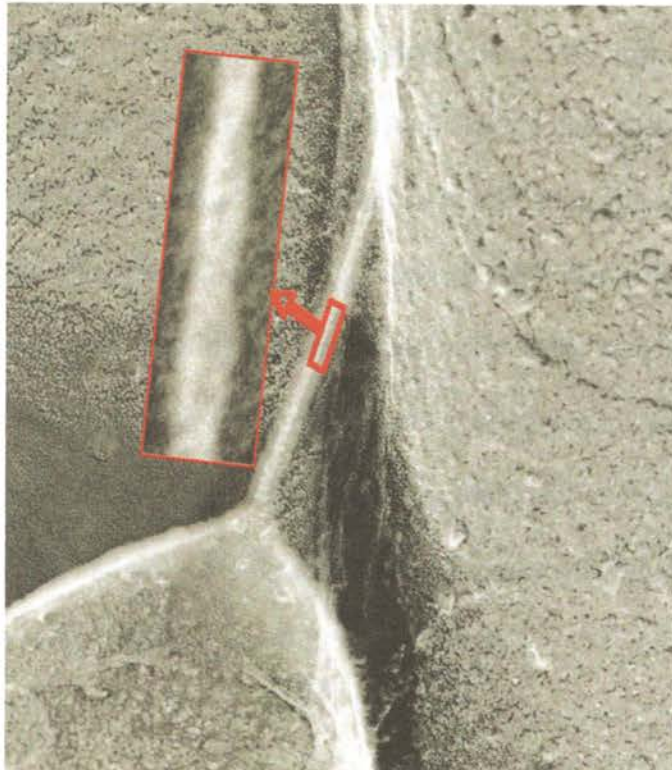
Ensheathed in plasma membrane, each stereocilium houses hundreds of polarized actin cables (Fig. 2B), cross-linked by espin and fimbrin into a paracrystalline array (DeRosier et al., 1980), to form a rigid cylinder (Tilney et al., 1983, Zheng et al., 2000). Stereocilia taper at the base, where actin filaments diminish in number to a few dozen before inserting into the cuticular plate, an anchor of crisscrossed actin. The hair bundle flexes at this apical insertion, allowing adjacent stereocilia to slide against one another when a stimulus is applied to the top of the bundle (Howard and Ashmore, 1986). This elegant design - a consequence of eons of brutal evolution - endows the hair cell with an important mechanical advantage: when the bundle traverses relatively large displacements in response to mechanical stimuli, it feels small forces, yet concentrates these forces into the gating of transduction channels, which move only tiny distances (Jacobs and Hudspeth, 1990). This arrangement explains two features about a hair cell's sensitivity: deflections along the axis of symmetry excite or diminish neurotransmitter

Figure 3. **Electron micrographs of tip links.** *A*, A transmission electron micrograph of a bullfrog saccular hair cell. Fine extracellular links (indicated with black arrows) span from the tips of stereocilia to the side of an adjacent neighbor (from Jacobs and Hudspeth, unpublished). *B*, Freeze-etch images from a bullfrog saccular hair cell reveal the double helical nature (inset) of tip-links, which are believed to attach to the gates of transduction channels (from Kachar et al., 2000).

A



B



release, while perpendicular bundle movements have no effect on a hair cell's response (Shotwell et al., 1981); miniscule displacements, on the atomic order, are felt by the bundle to open transduction channels (Hudspeth and Gillespie, 1994).

Gating Spring Model:

The prevailing view of hair-cell transduction proposes that bundle deflection towards the tallest stereocilium increases tension on elastic gating springs, which in turn transmit force directly to open channel gates (Corey and Hudspeth, 1983). Indeed, positive displacements result in an inward flow of current at the tips (Hudspeth, 1982), which increases neurotransmitter release. Conversely, when tension decreases and springs slacken, channels close. The probability of channel opening, P_{open} , therefore depends on tension applied to the gating springs; any adjustment to tension will change the transduction current.

Tip links (Fig. 3A, B) are the extracellular threads spanning adjacent stereocilia along the axis of sensitivity (Pickles et al., 1984) that were once believed to be the anatomical correlate of the gating spring. This view has fallen out of favor recently, however. Electron microscopic images of tip links (Kachar et al., 2000) suggest that they are too stiff to be the elastic gating springs, which individually measure ~ 1 mN/m (Howard and Hudspeth, 1988). These double-coiled filaments of cadherin 23 split to form two insertions into the lateral wall of a stereocilium and multiple insertions at the tip of its lower neighbor, and probably lie in series with the actual gating springs (Siemens et al., 2004, Söllner et al., 2004).

Tip links are an absolute requirement for channel gating, and form stiff connections with mechanically-gated transduction channels, which perhaps belong to the transient receptor potential (TRP) family (Corey, 2003). For example, lowering Ca^{++} concentration with the calcium chelator BAPTA breaks tip links and eliminates transduction (Assad et al., 1991). Furthermore, transduction recovers over the time-scale needed for tip-link regeneration (Zhao et al., 1996).

Adaptation:

To capture behaviorally relevant mechanical inputs above static ones, hair cells maintain sensitivity by adaptation. Following rapid bundle stimulation, the hair-cell transduction current gradually decreases toward the resting level during the course of the stimulus. This gradual decline in transduction current is underpinned by two separate, molecular phenomena termed fast and slow adaptation (Fig. 4) that both lead to channel closure (LeMasurier and Gillespie, 2005).

In an undeflected bundle, a cluster of myosins (Fig. 5) linking the transduction channel to the actin cytoskeleton actively produces modest tension (~ 10 pN) in gating springs to poise transduction channels in their most sensitive position at rest (Hudspeth, 1992). In response to negative and positive stimuli, however, the motor complex slides up and down actin filaments to continually readjust gating-spring tension and the P_{open} to the place of maximal sensitivity (Hudspeth, 1994; Gillespie, 1993), enabling hair cells to adapt to changing conditions. Thus, adaptation is a restoration of responsiveness and occurs by fast and slow Ca^{++} -dependent mechanisms that operate simultaneously in the bundle (Hudspeth and Gillespie, 1994; Wu et al., 1999; Eatock, et al., 1987).

Figure 4. **Adaptation of transduction current in response to a positive stimulus.**

The transduction current from a wild-type mouse utricular hair cell in response to a 400 ms deflection of 0.5 μm . Immediately following the positive deflection (50 μs – 1 ms), fast adaptation leads to a profound decrease of the excitatory current. Slipping adaptation ensues 10-100 ms into the stimulus, returning the current near baseline. Following the stimulus, climbing adaptation occurs when motors ascend the actin cytoskeleton to bias the resting tension in gating springs so that only ~5-15% of the channels remain open.

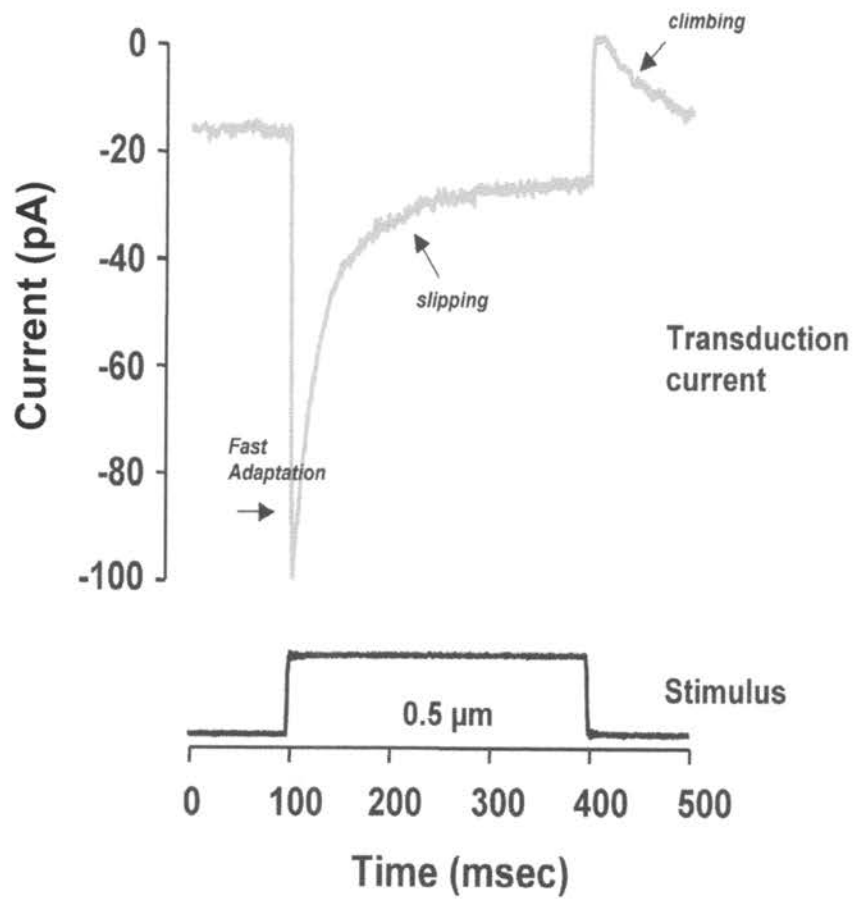
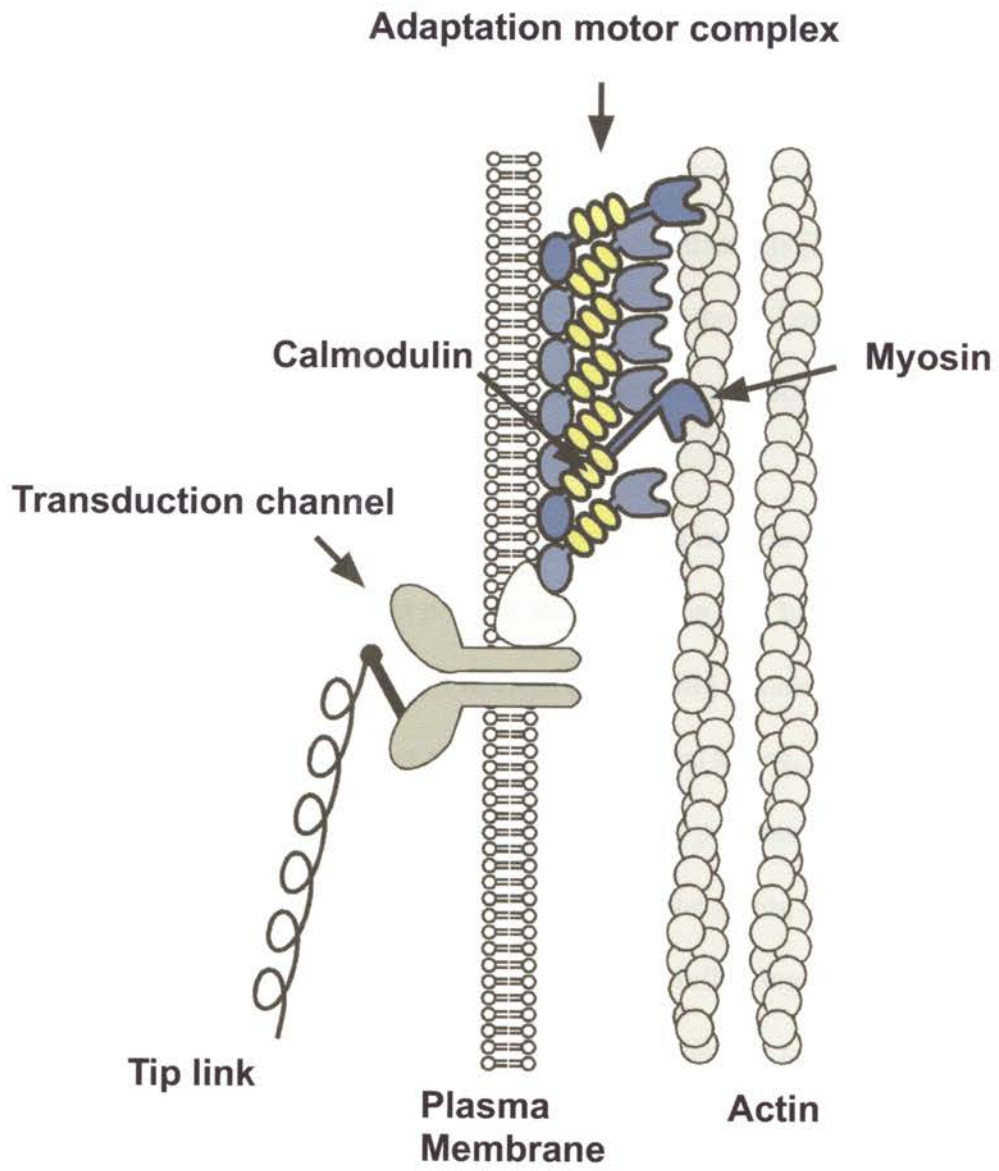


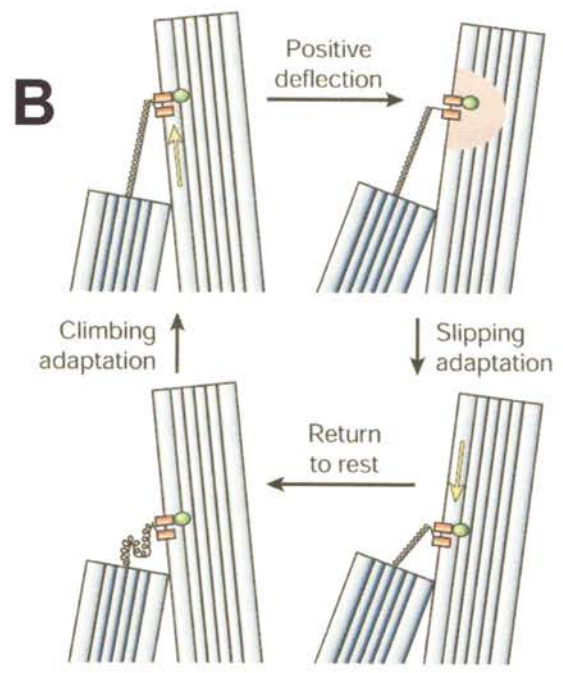
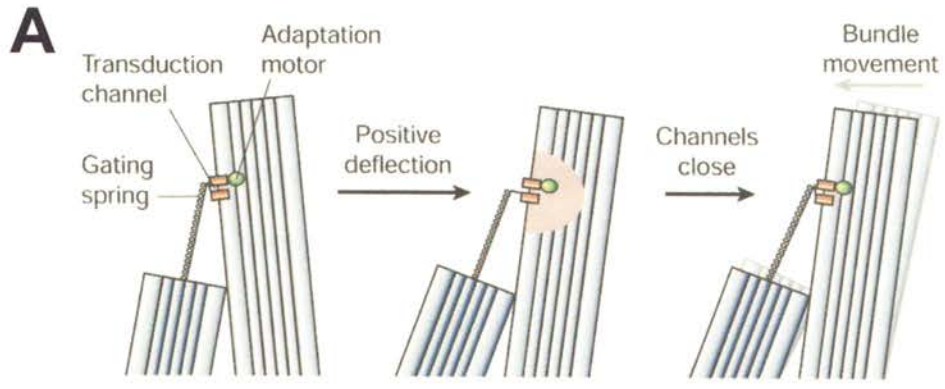
Figure 5. **Transduction apparatus.** Within the hair bundle resides an exquisitely sensitive transduction apparatus that includes a tip-link, a mechanically-gated transduction channel, and an adaptation motor complex, which is thought to be a cluster of myosins linking the channel to the actin core (P.G. Gillespie, unpublished). Tight mechanical coupling among these elements permits *direct* transduction without the need of second messengers (Corey, 1983). Indicated in blue are individual myosin molecules; in yellow are calmodulins bound to IQ domains within the myosin neck region.



At the beginning of a prolonged positive displacement, fast adaptation takes place within 0.05 - 1 milliseconds of channel opening (Corey and Hudspeth, 1979; Corey and Hudspeth, 1983), as entering Ca^{++} ions bind to a site on or near the channel to induce closure and a rapid decline in excitatory current amplitude (Fig. 4, 6A). Slow adaptation begins within 10 - 100 ms of channel opening and has two forms, slipping and climbing (Figs. 4, 6B). Slipping adaptation occurs when Ca^{++} influx binds to the adaptation motor complex, inducing rapid detachment of motors from actin filaments (Fig. 6B) and a further decrease of the current back to baseline (Fig. 4). At the end of the stimulus, Ca^{++} concentration falls and climbing adaptation ensues when motors ascend the actin cytoskeleton to reposition channels back to the resting P_{open} .

The mechanism of fast adaptation is unresolved, but may be explained by two models. The channel-reclosure model predicts that inflowing Ca^{++} binds to a site on or near the transduction channel, inducing it to close and making it more difficult to open (Howard and Hudspeth, 1988; Ricci et al., 2002; Cheung and Corey, 2005). As a result, tension is increased in the gating spring. The release model predicts that entering Ca^{++} binds to a “release” or “relaxation” element in series with the gating spring and channel (Bozovic and Hudspeth, 2003; Martin et al., 2003). When inflowing Ca^{++} binds to the release element, it causes a conformational change in the molecule such that the mechanical chain lengthens, thereby reducing tension in the gating spring and allowing the transduction channel to close. We present evidence (Stäuffer et al., 2005) for the release model in Chapter 1, pages (130-140) in experiments measuring adaptation in homozygote Y61G knock-in vestibular hair cells. Moreover, we suggest that myosin-1c (Myo1c) is the release or relaxation element.

Figure 6. **Fast and slow adaptation.** *A*, Displayed on the left is a hair bundle at rest with ~5% transduction channels open. Positive deflection fully opens all transduction channels to allow Ca^{++} entry (pink). Inflowing Ca^{++} forces channels to close and leads to a negative bundle movement opposite the direction of the stimulus. *B*, Slow adaptation mechanism. A myosin motor complex (green) continually strives to maintain gating spring tension at an optimal level by slipping or climbing the actin cytoskeleton in response to increased or decreased tension and changes in Ca^{2+} concentration. (Image from Gillespie and Walker, 2001).



Several lines of evidence suggest that myosins mediate slow adaptation. The adaptation motor actively generates force along actin filaments (Assad and Corey, 1992), and myosins are the only known actin-based motors. The motor moves with a velocity ($\sim 2 \mu\text{m s}^{-1}$) within the range measured for myosin (Assad and Corey, 1992). Bundle actin filaments are polarized with their barbed ends at the tips, permitting plus-end-directed myosins within the stereocilia to put tension on gating springs. Inhibitors of the myosin ATPase cycle, including analogs of ADP and phosphate, block adaptation (Gillespie et al., 1993; Yamoah et al., 1996).

The myosin superfamily:

The myosin superfamily encompasses eighteen different classes based on motor domain sequence similarity (Berg et al., 2001). These motor proteins generate force along actin filaments by converting the chemical energy stored in ATP into mechanical work. Three structural features are common to most myosins: a highly conserved motor head domain, each with a nucleotide binding site for ATP hydrolysis and an ATP-sensitive actin binding site; a neck domain for light chain or calmodulin binding; and a tail domain for targeted binding to various substrates.

Hair-bundle myosins:

Cells that rely on actin-based structures exploit myosins to perform essential functions. Not surprisingly, the unconventional myosins of hair cells are indispensable for proper vestibular and auditory function (Libby and Steel, 2000), since these cells include at least four actin-rich domains - the hair bundle, cuticular plate, circumferential

actin belt, and cortical actin cytoskeleton. Different myosin isoforms reside within discrete regions of the hair cell, indicating that they are tightly regulated (Hasson et al., 1997). For example, myosin-1c (Myo1c), myosin-7a (Myo7a), and myosin-15a (Myo15a) segregate to distinct compartments within the hair-bundle. In amphibians, Myo1c is localized to distal third of stereocilia whereas Myo7a is concentrated $\sim 1\mu\text{m}$ above the apical surface in association with basal crosslinks. Myo15a localizes at stereocilia tips in proportion to stereociliary length (Rzadinska et al., 2004) and might coordinate actin polymerization or assembly of the actin paracrystal. This myosin appears to play a critical role in bundle development and maintenance; shaker-2 and -2J mice, which harbor mutations in the motor domain and tail of Myo15a, respectively, develop abnormally short stereocilia (Anderson et al., 2000).

Among the myosins found exclusively in hair cells, Myo6 is vital for hair cell survival and function: loss of this protein leads to hair cell death and severe auditory and vestibular dysfunction (Avraham et al., 1995). Interestingly, this unconventional myosin moves retrogradely toward the pointed-ends of actin filaments using a unique sequence in its motor core domain (Homma et al., 2001). Since Myo6 localizes to the cuticular plate and the pericuticular necklace, a region devoid of actin but numerous in small vesicles, it might function to pull or hold down membrane at the bases of stereocilia. Indeed, hair cells deficient in Myo6 show a progressive stereocilia-fusion phenotype that begins at postnatal day 1.

Myosin-5 is absent from hair cells, but found in the auditory system. Its presence in synaptic terminals of afferent nerve fibers at the bases of inner hair cells suggests that it serves a critical role in synaptic vesicle transport (Wu et al., 2002).

Myosin-1c (Myo1c):

The unconventional myosin Myo1c is abundantly expressed in bundles (Gillespie et al., 1993) and preferentially maintained at the distal tips of stereocilia (Gillespie et al., 1993; Steyger et al., 1998; Garcia et al., 1998) where transduction takes place, strongly suggesting that it is a motor of slow adaptation. Although single molecules of Myo1c behave as a low-duty ratio motor - consistent with the idea that it transiently binds actin during its ATP cycle - several Myo1c molecules clustered together could perform as an adaptation motor (Gillespie and Cyr, 2004).

Convincing evidence that Myo1c participates in slow adaptation resulted from experiments using a mutant/inhibitor approach in transgenic mice expressing a mutant version of Myo1c (Y61G) in hair cells (Holt et al., 2002) and in Y61G knock-in hair cells (Stauffer et al., 2005), which is described in detail in Chapter 1 page (125-135). In response to application of a specific inhibitor for Y61G-Myo1c, N⁶- (2-methylbutyl) ADP (NMB-ADP), transgenic hair cells failed to adapt: transduction current remained constant during positive stimulation. By contrast, in the absence of the inhibitor, Y61G-Myo1c⁺ hair cells displayed adaptation. Moreover, introduction of NMB-ADP into wild-type hair cells had no effect on adaptation. The specificity of inhibition for Y61G revealed a critical function for Myo1c in slow adaptation of vestibular hair cells, but did not rule out the possibility of another myosin motor playing a similar role in the hair bundle.

Since the conventional transgenic mouse weakly expressed the Y61G transgene in the inner ear, it was not used to investigate Myo1c's role in the cochlea, which left unanswered the question of whether Myo1c plays a significant role in cochlear

adaptation. Currently, we are addressing this issue with preliminary experiments measuring adaptation in homozygote Y61G knock-in outer hair cells from cochlea.

Because Myo1c is a component of the adaptation motor, it seems well suited to generate the force on transduction channels required for resting tension. Myo1c localizes to the upper end of the tip link - possibly within the osmiophilic *insertional plaque* - the site proposed for active force generation and transduction. Myo1c may influence resting tension by PKA phosphorylation; activators of PKA decrease resting tension while inhibitors increase it (Ricci et al., 1997). Perhaps PKA phosphorylation of Ser 701 on Myo1c reduces the force production of the motor, leading to a lower resting P_{open} . The precise role of Myo1c in force generation is unknown; but given its prominent role in vestibular adaptation and high concentration at sites of transduction, Myo1c seems like a strong candidate to set the resting tension in all hair cells.

Myosin-7a (Myo7a):

Defects in the gene for Myo7a cause nonsyndromic deafness (Gibson et al., 1995; Liu et al., 1997) in humans and the most common deafness-blindness syndrome, Usher Ib (Weil et al., 1995; Weil et al., 1997). Similar defects in mice deficient for Myo7a highlight its importance in hair cell function (Lord and Gates, 1929; Gibson et al., 1995; Self et al., 1998). Myo7a plays a significant role in the cochlea. Kros *et al.*, examined cochlear hair cells from myosin-VIIa mutants (*shaker-1 Myo7a*^{4626SB}), and found that hair bundles had to be deflected beyond their normal physiological operating range to open transduction channels (Kros et al., 2002). This result suggests that Myo7a acts to generate force along the length of the stereocilia, perhaps by maintaining tension between

transduction components within the plasma membrane and the actin cytoskeleton. The most surprising finding of this study was that Myo7a-deficient hair cells displayed increased slipping and reduced climbing adaptation – the exact behavior predicted for a hair cell missing an adaptation motor.

A role for Myo7a in transduction and adaptation would be significant, since previous studies implicate Myo7a only in maintaining hair-bundle morphology by anchoring stereocilia crosslinks (Ernest et al., 2000; Hasson et al., 1997; Self et al., 1998). Immunolocalization in frog saccular hair cells demonstrated that Myo7a colocalized with “ankle” links in a narrow band of the hair bundle $\sim 1 \mu\text{m}$ above the basal tapers (Hasson et al., 1997). It has been proposed that Myo7a tethers these links to the actin cytoskeleton by binding vezatin (Küssel-Andermann et al., 2000), a transmembrane protein that interacts with cadherin 23, the only known constituent of the tip link (Siemens et al., 2004, Söllner et al., 2004). Furthermore, Myo7a may concentrate proteins [RI subunit of PKA, harmonin, protocadherin 15, and vezatin (Küssel-Andermann et al., 2000a; 2000b; Boëda et al., 2002)] required for proper bundle development and morphology; natural and induced mutations of Myo7a result in disorganized hair bundles and hair-cell degeneration (Gibson et al., 1995; Weil et al., 1995; Weil et al., 1997; Liu et al., 1997; Ernest et al., 2000; Self et al., 1998; Lord and Gates, 1929), producing deafness and vestibular dysfunction. Immunoelectron microscopy placed Myo7a between the plasma membrane and actin core along the length of the stereocilium in rodent hair bundles (Rzadzinska et al., 2004).

Loss of Myo7a in *shaker-1* mutants (4626SB) results in insufficient force production to tension gating springs; thus, transduction channels are closed at rest.

Unless *shaker-1* hair cells were mechanically stimulated, aminoglycoside and FM1-43 uptake failed to occur in Myo7a mutants (Richardson et al., 1997; Gale et al., 2001). These studies suggest that Myo7a, rather than Myo1c, the only known component of vestibular adaptation motor, may be the force producer setting channel resting tension (Kros et al., 2002). Biochemical analysis of rat Myo7a lends support to this idea (Inoue and Ikebe, 2003). Myo7a has a very high K_m for ATP ($> 2\text{mM}$), appropriate for a high-duty ratio motor that spends more than half of the ATPase cycle strongly bound to actin (Inoue and Ikebe, 2003). Thus, Myo7a could generate a large resting tension. Alternatively, Myo7a may confine an important regulator of *the actual* force producer (e.g., Myo1c) instead of being the force producer itself. If this scenario occurred in the hair cell, then loss of Myo7a would result in improper regulation of Myo1c, preventing it from generating the force required to keep channels open at rest.

Perhaps Myo7a is another component of the adaptation motor and cooperates with Myo1c in the same complex. This possibility seems hard to embrace for two reasons. First, given its biochemical properties (Inoue and Ikebe, 2003), it does not seem likely that Myo7a could detach and reattach actin filaments rapidly enough for slipping or climbing adaptation at ATP concentrations in hair cells. Second, immunolocalization data in rodents localized Myo7a uniformly along the length of stereocilia (Hasson et al., 1997; Rzadzinska et al., 2004) instead of near the tips, the immunolocalization site of Myo1c in frog (Steyger et al., 1998; Garcia et al., 1998). However, Myo1c also appeared uniformly along the length of stereocilia from mice (Dumont et al., 2002) and has been shown to be a motor of slow adaptation in vestibular hair cells (Holt et al., 2002; Stauffer et al., 2005). Additionally, a yeast-two hybrid screen yielded an inner ear integral

membrane protein (PHR1) that bound to the tails of both Myo1c and Myo7a (Etournay et al., 2005). Whether PHR1 links these motor proteins in a hair cell is not known.

Interestingly, no auditory or vestibular defect (Xu et al., 2004) appeared in the *PHR1* null mouse, but this mutant has not been evaluated for an adaptation phenotype.

Chemical-Genetic Strategy

Assigning precise roles to individual unconventional myosins has been unusually difficult. All bear a structurally related active site and utilize ATP for force production, complicating efforts to identify truly specific inhibitors and activators. Additionally, many cells simultaneously express several myosins that colocalize to the same subcellular region (Hasson et al., 1997; Chen et al., 2001). Gene deletions of myosins in mice have also provided little insight into their cellular roles due to lethality, developmental abnormalities, or compensatory responses (Mermall et al., 1998).

One approach to distinguishing the cellular functions of enzymes with highly similar structure and biochemical activity is the chemical-genetic strategy. First applied to the GTPase superfamily of proteins, Hwang & Miller (1987) were able to elucidate separate functions for two GTPases (EF-Tu, EF-G) intimately involved in amino-acyl tRNA loading of ribosomes. Recently, Bishop *et al.* devised a similar method of chemically decoupling any protein kinase from a signaling pathway inside the cell (Bishop et al., 2000a; Liu et al., 1998; Bishop et al., 2000b). By creating unique binding pockets not present in wild-type kinases, they sensitized protein kinases to cell-permeable molecules that do not inhibit wild-type kinases. Selective membrane-permeable inhibition extends the use of the chemical-genetic system to exploring an individual

protein's role in regulating ultrafast processes in contrast to conventional genetic methods, which are too slow at modulating the system under study.

Drawing inspiration from these previous efforts, the Gillespie lab pioneered a chemical-genetic strategy for myosin-1c (Gillespie et al., 1999) that revealed its role in slow adaptation in vestibular hair cells (Holt et al., 2002). The tyrosine residue (Y61) mutated in Myo1c to widen its nucleotide binding pocket is largely conserved across the myosin superfamily, suggesting that the same strategy could be applied to other myosin family members. Indeed, the strategy has recently been translated with success to other myosins (Myo5a) (Provance et al., 2004).

Another obvious choice is Myo7a, given its importance in hearing and vestibular function (Gibson et al., 1995; Weil et al., 1995; Liu et al., 1997; Lord and Gates, 1929), but more importantly because of its suggested but unproven roles in slow adaptation and transduction. Therefore, we extended the chemical-genetic strategy to Myo7a, described in depth in chapters 3, with the intent that it would unambiguously shed light on Myo7a's role in processes important to hair-cell function, and that it might reveal hidden capacities of this motor. In particular, we predict that Myo7a does not participate in slow adaptation, either in the cochlear or vestibular systems. Nevertheless, a surprise role for Myo7a in slow adaptation would be informative, and may indeed be the case, given the slow adaptation phenotype observed in *shaker-1* mutants (Kros et al., 2002).

RESEARCH OBJECTIVES

GENERATION AND CHARACTERIZATION OF Y61G-Myo1c KNOCK-IN MICE

A chemical-genetic strategy for Myo1c has made it feasible to examine the role of this myosin in a physiological process. Using this strategy, Holt *et al.* showed that Myo1c participates in slow adaptation of mouse utricular hair cells in Y61G expressing transgenic mice (Holt et al., 2002). To strengthen the phenotype observed and develop a more elegant system for Myo1c study, we replaced the wild-type *Myo1c* allele with the Y61G allele by a gene-targeting knock-in strategy in mice. These mice were generated to examine Myo1c's role in fast and slow adaptation in the vestibular system and to investigate its role in the cochlea.

CHARACTERIZATION OF THE Myo7a^{sh1-8J} MUTATION

We chose to characterize the *Myo7a^{sh1-8J}* mutation with the hope that this readily available mouse strain would serve as an effective *Myo7a* null mutant. To assess functional rescue of the *shaker-1* defect by either of our *Myo7a* transgenes, we bred these *Myo7a*-deficient mice with our *Myo7a* transgenic mice.

GENERATION AND CHARACTERIZATION OF Y114G- AND FLAsH-TAGGED Myo7a TRANSGENIC MICE

To directly explore the role of Myo7a in hair-cell adaptation, we extended the chemical-genetic strategy to Myo7a by engineering conventional transgenic mice that express the Y-to-G mutation in Myo7a (Y114G) under a hair-cell specific promoter. We

also pursued an alternative approach to examine the role of Myo7a in the inner ear by engineering transgenic mice with the FLAsH tag in Myo7a.

MATERIALS AND METHODS

Generation and Characterization of Y61G Knock-in Mice

Cloning of the Y61G-Myo1c targeting construct

We used the following steps in the cloning of the Y61G-Myo1c targeting construct.

1) pMG1 vector contains a *Bam*HI mouse genomic DNA clone (~13.7 kb) of *Myo1c* isolated from a BAC library by John Mercer. pMG1 is the parent vector used to construct the Y61G-Myo1c targeting vector.

2) A fragment from pMG1, *Not* I to *Age* I, was subcloned into the *Not* I, *Age* I sites of pMG-KAS, creating pMG2.

3) Another fragment from pMG1, *Age* I to *Pst* I, was subcloned into pMG2 at the *Age* I and *Nsi* I sites, respectively, thus creating pMG3. The *Pst* I and *Nsi* I fusion at the 3' end destroyed the *Nsi* I site but retained the *Pst* I site.

4) An oligo pair containing unique *Mlu* I and *Nsi* I sites was used to replace the 5' sequence of pMG3. *Aat* II and *Not* I sites flanked the oligo pair and were used to clone into the 5' multiple cloning site at *Aat* II of pMG3, thus creating pMG3.5Δ.

5) A fragment from *Sse8387I* to *Age I* from pBSmut4, containing the Y61G site (which lost a *Bgl II* site and added a *BamHI* site) and a silent mutation at serine 73 (AGT > TCC, introducing a *Sac II* site) was subcloned into *Sse8387I* and *Age I* sites of pMG3.5 Δ, thus creating pMG4.5 Δ.

6) pCR2.1-loxP *neo* plasmid was digested with *Nhe I*. The ~2.2 kb *Nhe I* piece was gel purified and cloned into a *Nhe I* site of pMG4.5 Δ located in the large intron between exons 4 and 5, thus creating pMG5.

7) An *Mlu I* flanked fragment (~1.2 kb) containing the *Diphtheria* toxin alpha cassette was then subcloned into the *Mlu I* site of pMG5, thus creating pMG 6, the finished targeting vector. The region of homology of *Myo1c* totaled ~6.5 kb - the short homology arm being ~ 0.5 kb, the long arm ~3 kb.

Mutagenesis of the *Myo1c* Sequence in pBS-mutØ to create plasmid pBS-mut4:

8) A fragment from sites *Sse8387I* to *Nhe I* in *Myo1c* of pMG1 was subcloned into the *Pst I* and *Nhe I* sites of pBK-CMV, resulting in the loss of the *Pst I* site of pBK-CMV while retaining the *Sse8387I* site. The new plasmid, pMG-mutØ, was then digested with *Hind III* and *Nsi I* and this fragment was subcloned into *Hind III* and *Pst I* sites of pBS, thus creating plasmid pBS-mutØ. This subcloning step retained the *Pst I* site but eliminated the *Nsi I* site.

9) Using mutagenic oligo PG80 (gga acg cta ccg cgg tgt ctt ctt cta tga agt acc), mutagenesis was performed to change the codon for serine 73 from AGT to TCC, introducing a *Sac* II site and creating plasmid pBS-mut1.

10) Using mutagenic oligo PG79 (cga gac cta cag att gga tcc cgg cag cat atg g), tyrosine 61 was changed to glycine 61, resulting in the loss of *Bgl* II and addition of *Bam*HI sites creating plasmid pBS-mut2.

11) Sequencing revealed two errors that were introduced by mutagenesis. To correct these errors, two separate rounds of *Pfu* mutagenesis were performed. The resulting plasmid was pBS-mut4.

12) pBS-mut4 was digested with *Sse*8387I and *Age* I and fragment subcloned into similar sites in pMG3.5 Δ , thus creating pMG4.5 Δ .

Subcloning of the loxP-flanked neomycin-resistance positive selection cassette:

Using primers (PG 77: tag cta gcc ggc tcg tat gtt gtg tgg, PG78: tag cta gcg gcg aaa ggg gga tgt gct g) to introduce flanking *Nhe* I restriction sites, we amplified the *loxP-neo* cassette from Chris Bond's plasmid and subcloned it into the pCR 2.1-TOPO vector, creating plasmid pCR2.1-neo. This plasmid was digested with *Nhe* I, and the *Nhe* I-flanked *neo* cassette fragment was gel purified using Qiagen Gel Extraction kit. pMG4.5 Δ was likewise treated with *Nhe* I, dephosphorylated with calf-intestinal phosphatase (~2 U/reaction), and gel purified with Qiagen Gel Extraction kit. Using DNA ligase, the

Nhe I-flanked neo cassette fragment was ligated with the pMG4.5 Δ fragment at an insert to vector ratio of \sim 3:1. The resulting plasmid, pMG5, contained the neomycin-resistance positive selection cassette inserted in *Nhe* I site located in the large exon between exons 4 and 5. Orientation was verified by sequencing and by diagnostic restriction enzyme digestion. The short arm of homology was thus \sim 0.5 kb and the long arm \sim 3 kb.

Subcloning of the diphtheria toxin negative selection cassette:

Using primers (PG180: ata cgc gtc tct aga act acg atc cag, PG181: ata cgc gta aag tgc cac ctg acg tc) to introduce flanking *Mlu* I restriction sites, we amplified the *Diphtheria* toxin negative selection cassette from a plasmid and subcloned into pCR 2.1-TOPO vector, creating pCR2.1-TOPO-DT. This plasmid was digested with *Mlu* I. The *Mlu* I-flanked DT cassette fragment (\sim 1.2 kb) was gel purified using Qiagen Gel Extraction kit (Qiagen, Valencia, CA). This fragment was then subcloned into pMG5 in the single *Mlu* I site in the multiple cloning site outside of the 5' *Myo1c* region of homology. Orientation was confirmed by sequencing and diagnostic restriction enzyme digestion. The resulting plasmid, pMG6, was the final targeting construct.

Preparation of linearized pMG6 for electroporation of ES Cells:

A sterile loop was used for streaking pMG6 from a glycerol stock onto an LB/ampicillin (50 μ g/ml) plate, which was incubated for 16 hours at 37°C. Two colonies were picked and used to inoculate starter cultures (3 ml) of LB/ampicillin (50 μ g/ml) for 7 hours at 37°C. Two 500 ml LB/ampicillin (50 μ g/ml) cultures were inoculated with 500 μ l of each starter culture. Genomic DNA was processed using an Endotoxin-free

MAXI kit (Qiagen Inc., Valencia, CA). The plasmid DNA yields of 338 μg and 534 μg were resuspended in either Tris (10 mM) EDTA (0.1 mM), pH 8.5, or EB Buffer (Tris 10 mM, pH 8.5), respectively. To linearize pMG6, each preparation (50 μg) was digested with *Nsi* I in a total of 350 μl for 3 hours at 37°C. Linearized pMG6 was precipitated at -20°C for 8 hours with 3 M sodium acetate pH 5.2 and ice-cold ethanol. The ethanol precipitates were kept at -20°C and then given to Jenefer Dekoning and Manfred Baetscher after they confirmed that the digests had gone to completion.

Screening of Recombinants by PCR

Jenefer DeKoning of the OHSU Transgenic Core facility electroporated ES cells (129S4 clone) on Friday 3/16/01 with a gel-purified, *Nsi* I-linearized pMG6. We received six plates of electroporated ES cells on 3/20/01, which were subsequently grown at 37°C until the ES cells were more confluent. Genomic DNA was harvested from 2 plates.

Plates were washed twice with phosphate buffered saline (PBS), 200 μl per well. An aliquot (50 μl) of lysis buffer (10 mM Tris pH 7.5, 10 mM EDTA, 10 mM NaCl, 0.5% Sarkosyl, 0.5 mg/ml Proteinase K) was added per well and then the plates were sealed with Parafilm and incubated at 55°C overnight. An aliquot (100 μl) of ice-cold ethanol/NaCl (25 ml ice-cold ethanol, 375 μl 5 M NaCl) was added to each well and incubated at room temperature for 2 hours. Plates were centrifuged at 2000 rpm for 10 minutes in a table-top centrifuge. Ethanol was dumped out onto paper towels. DNA precipitate was visible at the bottoms of all wells. An aliquot (200 μl) of ice-cold 70%

ethanol was used to wash each well three times which were let to air dry for 15 minutes. Each well was resuspended in an aliquot (150 μ l) of 10 mM Tris pH 8.0 [prefiltered through a 0.22- μ m Millipore filter (Millex GP, Millipore)]. Plates sat at room temperature for 1 hour before resuspension.

Nested PCR (5' end PCR Screening Strategy)

To identify ES clones that had recombined at the 5' end of the homology arm, polymerase chain reaction (PCR) reactions were performed on 96 samples from Plate #1 and 96 samples from Plate #2 using a nested PCR approach. If homologous recombination occurred correctly, outer primers PG91 and PG95 would serve to amplify a PCR product of 2.2 kb at the junction between the 5' homology arm of the targeting vector and the *Myo1c* gene. The amplified product would serve as a template for PCR amplification with inner primers, oligos PG92 and PG94.

Outer primers (PG91, PG95)

PG91= gcc aga ttg ggc tcc gta aag, PG95= tga ggt ggt act tca tag aag ga

Inner primers (PG92, PG94)

PG92= gcg gcc gta ttg gga cat ttc, PG94= tcc ata tgc tgc cgg gat cca

Outer PCR Reactions: 5 μ l of ES cell genomic DNA per sample was used per PCR reaction with 1.25 μ l each 10 μ M oligos PG91 and PG95, 2.5 μ l 10 \times PCR buffer, 5 μ l 5 \times Q buffer, 0.5 μ l 10 mM dNTPs, 9.25 μ l PCR water, and 0.25 μ l

Qiagen *Taq* polymerase (cat. #201223). Reactions were run in a Robocycler (Stratagene, La Jolla, CA) at 94°C 4 minutes [1 cycle], 94°C 1 minute, 55°C 2 minutes, 72°C 5 minutes [10 cycles], 94°C 1 minute, 55°C 1 minute, 72°C 4 minutes [20 cycles], 72°C 10 minutes [1 cycle].

Outer reactions were diluted 1/150 in PCR-grade water

Inner PCR Reactions: Inner PCR reactions included 1 µl of each diluted outer PCR reaction sample. 1.25 µl each 10 µM oligos PG92 and PG94, 2.5 µl 10× PCR buffer, 5 µl 5× Q buffer, 0.5 µl 10 mM dNTPs, 13.25 µl PCR water, and 0.25 µl Qiagen *Taq* polymerase (cat. #201223). Reactions were run in a Robocycler (Stratagene LaJolla, CA) at 94°C 4 minutes [1 cycle], 94°C 1 minute, 55°C 1 minute, 72°C 4 minutes [30 cycles], 72°C 10 minute [1 cycle].

DNA loading dye (2.5 µl) was added per inner PCR reaction and each sample was run on a 0.8% agarose gel (SeaKem) and separated by electrophoresis (50 volts, 3.5 hours).

Nested PCR (3' end PCR Screening Strategy)

To identify ES clones that had recombined at the 3' end of the homology arm, polymerase chain reaction (PCR) reactions were performed on all 96 samples from Plate #1 and 96 samples from Plate #2 using a nested PCR approach. The amplified product would serve as a template for PCR amplification with oligos 187 and 188. If homologous

recombination occurred correctly, outer primers 186 and 189 would serve to amplify a PCR product of 2.8 kb at the junction between the 3' homology arm of the targeting vector with the *Myo1c* gene.

Outer primers (PG186, PG189)

PG186=tat tac aat tca ctg gcc gtc gt, PG189=cat acc gcg atg ccc tca gc

Inner primers (PG187, PG188)

PG187=gtt acc caa ctt aat cgc ctt g, PG188=tat tcc tcc tgc tcc gac ttg a

Outer PCR Reactions: 5 µl of ES cell genomic DNA per sample was used per PCR reaction with 1.25 µl each 10 µM oligos PG186 and PG189, 2.5 µl 10× PCR buffer, 5 µl 5× Q buffer, 0.5 µl 10 mM dNTPs, 9.25 µl water, and 0.25 µl Qiagen *Taq* polymerase (cat. #201223). Reactions were run in a Robocycler (Stratagene, LaJolla, CA) at 94°C 4 minutes [1 cycle], 94°C 1 minute, 55°C 2 minutes, 72°C 5.5 minutes [10 cycles], 94°C 1 minute, 55°C 1 minute, 72°C 4.5 minutes [20 cycles], 72°C 10 minutes [1 cycle].

Outer reactions were diluted 1/150 in water

Inner PCR Reactions: Inner PCR reactions included 1 µl of each diluted outer PCR reaction sample, 1.25 µl each of 10 µM oligos PG187 and PG188, 2.5 µl 10× PCR buffer, 5 µl 5× Q buffer, 0.5 µl 10 mM dNTPs, 13.25 µl water, and 0.25 µl Qiagen *Taq* polymerase (cat. #201223). Reactions were run in Robocycler

(Stratagene, LaJolla, CA) at 94°C 4 minutes 1 cycle, 94°C 1 minute, 55°C 1 minute, 72°C 4 minutes for 30 cycles, 72°C 10 minutes for 1 cycle.

Southern Analysis of potential ES cell clones

The PCR screen of ES cell clones suggested several potential positives (listed below). Southern analysis was then performed to identify correct ES clones that had recombined homologously at the 5' and 3' end of targeting vector.

Potential Clones (potential positives & negatives as controls):

B2, C2, D4, D5, D9, E1, E9, E10, F3, G2, G3, G8 from plate #1

A8, A12, **B3**, B6, B10, B11, B12, C5, C9, C10, D11, E9, F4, F8, G12 from plate #2

For each potential clone, DNA samples were pooled from three sets of 96-well plates to give a volume of 360 μ l. To precipitate a pooled DNA sample, we added water (210 μ l), 3 M sodium acetate pH 5.2 (40 μ l), and ice-cold 100% ethanol (880 μ l) and kept at -20°C for 8 hours. Next, DNA samples were centrifuged at 14,000 rpm for 30 minutes at 4°C. Each sample was washed with 70% ethanol (400 μ l), and centrifuged for 5 minutes. Supernatants were removed and each DNA pellet air-dried for 5–10 minutes.

Digestion:

ES cell genomic DNA (15 μ g) was resuspended in water (99 μ l) with large-bore, “genomic DNA” tips. Next, we added 100 μ l 2 \times buffer (recipe: 600 μ l New England

BioLabs *Bam*HI buffer, 60 μ l 100 \times bovine serum albumin, 30 μ l 20 mg/ml casein, 12 μ l 50 mM spermidine, and 2.3 ml water) and pipetted gently with genomic tips. Mixtures were kept at 4°C for 3 hours, then warmed to 37°C for 1 hour. To each sample, 1.5 μ l *Bam*HI was mixed with genomic tips and digestions were incubated at 37°C. 16 hours later, an additional 0.5 μ l *Bam*HI was added and tubes were kept at 37°C for 3 more hours. To precipitate DNA, water (160 μ l), 3 M sodium acetate pH 5.2 (40 μ l), glycogen (1 μ l), and 100% ethanol (880 μ l) were mixed and then centrifuged at 14,000 rpm at 4°C for 30 minutes. Pellets were washed with 70% ice-cold ethanol, then centrifuged for 5 minutes at 14,000 rpm. Supernatants were removed and pellets air-dried for 5 minutes. Samples were resuspended in 25 μ l TE, loaded onto a 0.7% agarose (SeaKem, FMC, Rockland, MD) gel, and run for 6 hours at 40 volts. A picture of the gel was taken using an imaging system (Alpha Innotech, San Leandro, CA) to confirm a nice digestion pattern – gradual and greater abundance of high molecular weight DNA species versus lower molecular weight DNA species. *If this pattern was not noted, the gel was scrapped and new samples were processed.*

Alkali Transfer:

After taking a picture of the gel, it was soaked in 0.2 M HCl for 20 minutes, then in 0.4 N NaOH for 15 minutes. Using alkali transfer buffer (0.4 N NaOH), a downward transfer configuration was set up for >20 hours to transfer digested DNA samples onto Hybond N Plus membrane (Amersham Biosciences, San Diego, CA). Membranes were washed briefly with 2 \times SSC, then subjected to 1200 μ joules with a UV StrataLinker

(Stratagene, San Diego, CA) to crosslink DNA samples onto membranes. Membranes were stored dry between two Whatman sheets.

Probe Preparation:

We combined probe (25 ng) with water (7.5 μ l) in a 1.5 ml microfuge tube, then added 10 \times Decamer solution (2.5 μ l) (Ambion Corp., Austin, TX). This mixture was heated at 95-100 $^{\circ}$ C for 5-10 minutes, and snap-frozen in a dry ice-ethanol bath. In the following order, we added 5 \times reaction buffer (5 μ l), 32 P-dCTP (5 μ l), water (1.5 μ l), and Klenow (1 ml) and incubated the reaction at 37 $^{\circ}$ C for 8 minutes. To halt nucleotide incorporation, we added 1 μ l 0.5 M EDTA, then an aliquot (40 μ l) of water. Subsequently, the total volume was spun through a G-50 Sephadex column (prepared earlier) at 3000 rpm for 2 minutes to remove unincorporated nucleotides.

Prehybridization/Hybridization:

To prehybridize a membrane, FBI buffer (10 ml) was warmed for two hours in a roller bottle at 65 $^{\circ}$ C with 100 μ g salmon sperm DNA. At the completion of prehybridization, the probe was denatured at 95-100 $^{\circ}$ C for 10 minutes and snap-cooled on ice for 5 minutes. The denatured probe was then mixed with 2 ml of warm, prehybe solution in a 2063 tube. This solution was then added with the prehybe solution at the bottom of the roller bottle to avoid the formation of bubbles between the membrane and the bottle. Hybridization took place overnight at 65 $^{\circ}$ C with gentle tumbling.

Washing:

The membrane was given three quick washes with an aliquot (15 ml) of 2 xSSC in the bottle. The membrane was then removed and washed for 5 minutes with 300 ml 2 xSSC/0.5% SDS in a big dish on a gently moving rotator. A wash (15 minutes) with 300 ml 2 xSSC/0.1% SDS followed. To bring down the radioactivity counts down to background levels in areas without DNA, washed four times at 65°C with 0.1% SDS/0.1 xSSC 40 minutes each. Areas with expected band sizes gave Geiger counter activity, whereas areas without DNA gave minimal activity. Membranes were washed in 2 xSSC, drip-dried briefly, wrapped moist in Saran Wrap, and placed in cassettes with Kodak BioMax AR film for 18 hours at -80°C. (Fig. 9). Film was developed in the MRB 6th floor developer not ours.

Stripping & Reprobing:

To strip blots, a boiling solution of 1% SDS was poured over membrane, then cooled to room temperature. Stripped blots were then dried between two Whatman sheets. When appropriate, prehybridization and hybridization were repeated, as described above.

Southern Analysis of 1G8 Subclones and Potential Positive 2B3

Jenefer Dekoning expanded subclones (B1-B8, C1-C8) of 1G8 from plate #1. She provided us with a 96-well plate with these subclones, which were incubated at 37°C for 3 hours before harvesting genomic DNA. Plates were washed twice with phosphate

buffered saline (PBS), 200 μ l per well. 200 μ l lysis buffer (10 mM Tris pH 7.5, 10 mM EDTA, 10 mM NaCl, 0.5% Sarkosyl, 0.5 mg/ml Proteinase K) per well was added and then the plates sealed with Parafilm and incubated at 55°C overnight. Using large-bore genomic tips, we performed four phenol extractions on each sample. We then added 2 μ l of 20% SDS and 1 μ l 10 mg/ml RNase A per sample and put at 37°C for 2 hours. Subsequently, we performed two phenol/chloroform extractions followed by three chloroform extractions. The volume of each sample was brought to 400 μ l, and then supplemented with 17.2 μ l 5 M NaCl and 417 μ l isopropanol. The mixtures were spun at 14,000 rpm for 10 minutes. The supernatants were carefully removed and pellets were washed with an aliquot (500 μ l) of 70% ethanol. Supernatants were removed again and the pellets were air-dried for 5 minutes. Next, pellets were resuspended in TE pH 8.0 overnight at room temperature. DNA samples were analyzed by Southern blotting with the 5' external probe.

6-well plates with subclones 1G8-B2, 1G8-B4, 1G8-C4, 1G8-C8 were provided on 9/1/01. To confirm correct targeting in these subclones, Southern blots were performed on genomic DNA with 5' and 3' external probes. To thoroughly evaluate the possibility of random integrations of the targeting vector, Southern blots were performed with three probes: two internal probes and a vector probe.

5' external probe (*Bam*HI – *Not* I, 686 bp)

3' external probe (*Pst* I- *Pst* I, 575 bp)

5' internal probe (*Not* I – *Bgl* II, 778 bp)

3' internal probe (*Xmn* I – *Xho* I, 1022 bp)

Vector probe (*Dra* I- *Nco* I, 645 bp), specific for a region in the *Diphtheria* toxin cassette

The 5' and 3' internal probes were digested from plasmid PMG3.5Δ with appropriate enzymes, run on an agarose gel, and gel-purified with Gel extraction kit (Qiagen Inc, Valencia, CA). The vector probe was isolated from PMG6.

PCR Genotyping of Y61G Mice

Toe/tail digestion:

To prepare genomic DNA samples, toes from mice aged P2 or tails from mice aged P21 were harvested by razor blade removal and placed in a microfuge tube (0.5 ml) with 50 μl lysis solution (100 mM Tris pH 8.0, 5 mM EDTA pH 8.0, 0.2% SDS, 200 mM sodium chloride, 0.5 μg/ml Proteinase K) overnight at 55°C. The following day tubes were placed in a sandblock at 95°C for 15 minutes, then chilled on ice for 5-10 minutes. An aliquot (1.25 μl) of SDS-OUT (Pierce, Rockford, IL) was added to each tube and chilled on ice for 5 minutes. Tubes were centrifuged for 10 minutes at room temperature at 14,000 rpm to drive non-digested tissue to the bottom of each tube. An aliquot (20 μl) of each sample was then diluted in an aliquot (180 μl) of 10 mM Tris pH 8.0, pre-filtered (0.22-μm, Millex GP, Millipore).

Polymerase Chain Reaction (PCR):

These components were added in the following order to PCR tubes (0.5 ml volume DNase-free, RNase-free) on ice:

1.25 μ l of 10 μ M 5' oligo PGG 247 (gcattccagcatcctgcaacc)
1.25 μ l of 10 μ M 3' oligo PGG 248 (cagtgtcagccactgcaaacc)
2.5 μ l 10 \times PCR buffer
5 μ l 5 \times Q buffer
0.6 μ l 10 mM dNTPs
13.25 μ l PCR water [Millipore water pre-filtered with a 0.22- μ m filter (Millex GP, Millipore)]
0.25 μ l *Taq* polymerase (cat #201223 – core kit, Qiagen, Valencia, CA)
1 μ l diluted genomic DNA sample (added last and pipetted up-and-down a few times)

Total volume 25 μ l

Reaction tubes were placed in a Robocycler PCR machine (Stratagene, La Jolla, CA) and subjected to the following conditions: 95°C 5 minutes [1 cycle], 94°C 1 minute, 55°C 2 minutes, 72°C 4 minutes [5 cycles], 94°C 1 minute, 55°C 1 minute, 72°C 3 minutes [30 cycles], 72°C 10 minutes.

At the completion of PCR, reactions were digested with a cocktail including *Bam*HI restriction enzyme to reveal the genotype (wild-type, Y61G heterozygote, Y61G homozygote) of each mouse sample. Each tube received 3.3 μ l *Bam*HI buffer (New England BioLabs, Beverly, MA), 3.3 μ l 100 \times bovine serum albumin (New England BioLabs), and *Bam*HI restriction enzyme (1 μ l) before being incubated at 37°C for 2 hours. 10 \times DNA loading dye (4 μ l) was added to individual samples, which were then loaded into wells of a 1.4% agarose (SeaKem LE)/1 \times TAE gel and separated by electrophoresis (70 volts, 1 hour) in 1 \times TAE buffer.

PCR Genotyping of Cre Mice

Dr. John P. Adelman generously provided us with a Cre-deleter mouse, which expresses *Cre* recombinase ubiquitously from the two-cell stage using the human cytomegalovirus minimal promoter (Schwenk et al., 1995). Animals with the Y61G-floxed *neo* cassette were bred to the Cre-deleter mouse for two generations because the Cre transgene integrated on the X sex chromosome. The following Cre genotyping primers amplify ~490 bp band:

ctgaagatgttcgcgattatc/catcagctacaccagagacgg

PCR Genotyping for the Neo Cassette

Several primer pairs were tested for their ability to reproducibly amplify sequences of the *neo* cassette:

Neo genotyping primer pairs:

PG115**/PG114	~1000 bp
PG115**/PG78	~940 bp, worked nicely
PG113*/PG114	~620 bp
PG113*/PG78	~580 bp

	<u>Primer pair</u>	<u>Expected Sizes</u>
Wild-type	72540, PG114 PG113/PG114	40 bp nothing
Het Y61G Neo ⁺	72540, PG114 PG113/PG114	40 bp, 2300 bp 620 bp
Het Y61G Neo ⁻	72540, PG114 PG113/PG114	40 bp, 395 bp 620 bp

Southern Analysis of Y61G Mouse Genotypes

Digestion:

Freshly harvested mouse tails (~1 cm) were digested in 700 µl lysis solution [12.4 ml water, 1.5 ml Tris-Cl (pH 8.0), 0.6 ml sodium chloride (5 M), SDS (10%), 0.15 ml EDTA (0.5 M, pH 8.0), 75 µl Proteinase K (20 mg/ml)] and tumbled at 55°C in a microfuge tube (1.5 ml) overnight. The following day, samples were spun at 14,000 rpm at room temperature. Supernatants were poured into a fresh microfuge tube (1.5 ml) with an equal volume of isopropanol (700 µl). The mixture was gently tumbled by hand to precipitate a “cloud” of genomic DNA, which was then gently driven to the bottom of the tubes by short, low-speed centrifugation – 10 seconds, 2000 rpm. Supernatants were removed and DNA samples were let to sit in 150 µl Tris (10 mM) EDTA (0.1 mM) overnight at room temperature. The next morning samples were gently pipetted with genomic tips to solubilize DNA samples.

Digestions were performed as described in the ES cell Southern section, but *more often as follows*. To 40 µl genomic DNA (10-15 µg), we added 100× BSA (New

England BioLabs) (0.5 μ l), 50 mM spermidine (1.0 μ l), 10 \times enzyme buffer (5 μ l), concentrated *Bam*HI enzyme (1 μ l), and then incubated the reaction at 37°C overnight. DNA was precipitated by adding water (160 μ l), 3M sodium acetate pH 5.2 (40 μ l), glycogen (1 μ l), 100% ethanol (880 μ l), and centrifuging at 14,000 rpm at 4°C for 30 minutes. Pellets were washed with 70% ice-cold ethanol and centrifuged for 5 minutes at 14,000 rpm. Supernatants were removed and pellets air-dried for 5 minutes. Samples were resuspended in 25 μ l TE, loaded onto a 0.7% agarose (SeaKem LE, FMC, Rockland, MD) gel, and run for 16 hours at 20 volts. A picture of the gel was taken using an imaging system (Alpha Innotech, San Leandro, CA) confirm a nice digestion pattern – gradual increase and greater abundance of high molecular weight DNA species versus lower molecular weight DNA species. *If this pattern was not noted, the gel was scrapped and new mouse tails were harvested and processed.*

Gel Treatment:

After taking a picture of the gel, it was rocked gently for 45 minutes in denaturing solution (300 ml, 0.2N sodium hydroxide, 0.6 N sodium chloride), then for 15 minutes in equilibration solution (300 ml, 0.5M Tris pH 7.5, 1.5 N sodium chloride) and finally for another 30 minutes in a fresh 300 ml of equilibration solution.

Transfer:

To transfer digested DNA samples onto a membrane, we used an upward-transfer configuration. First, we soaked a sponge in 10 \times SSC [20 \times SSC is made with 175.3 grams sodium chloride, 88.2 grams sodium citrate in 800 ml water, adjusted to pH 7.0

with a few drops of hydrogen chloride (HCl, 14.0 N) then raised to a 1-liter total volume with water] within a tupperware container (18" × 11" × 3").

In a separate vessel, a gel-sized piece of GeneScreen membrane (Perkin Elmer, Wellesley, MA) was soaked at room temperature with water for 2 minutes, then in 10× SSC for 5 minutes.

We placed a sponge-sized Whatman sheet on top of the sponge and then the gel, face-up. Next, the pre-soaked membrane was placed on top of the gel while ensuring that there were no bubbles between points of contact. Two more gel-sized Whatman sheets were overlaid with no bubbles. To prevent bypassing of transfer buffer around the sides of the membrane, strips of Parafilm or Saran Wrap were laid across the container beside the four edges of the gel, and a 4-inch stack of paper towels was then placed on top. Finally, the reservoir was filled with 10× SSC halfway up the height of the sponge and a plastic cover was set on top of the paper towel stack. 18-24 hours transpired for complete transfer to occur. The membrane was rinsed briefly with 6× SSC before auto-crosslinking the DNA to the membrane with a UV StrataLinker (Stratagene, San Diego, CA).

Probe Preparation:

DNA probes were prepared as described in the ES cell Southern analysis section. We combined DNA (25 ng) with water (7.5 µl) in a microfuge tube (1.5 ml), then added 10× Decamer solution (2.5 µl) (Ambion Corp., Austin, TX). This mixture was heated at 95-100°C for 5-10 minutes, and snap-frozen in a dry ice-ethanol bath. In the following order, we added 5× reaction buffer (5 µl), ³²P-dCTP (5 µl), water (1.5 µl), and

Klenow (1 μ l), then incubated the reaction at 37°C for 8 minutes. To halt nucleotide incorporation, we added 0.5 M EDTA (1 μ l), then water (40 μ l). Subsequently, the total volume was spun through a G-50 Sephadex column (prepared earlier) at 3000 rpm for 2 minutes to remove unincorporated nucleotides.

Prehybridization/Hybridization (The Matt Thayer Method):

To prepare solution for pre-hybridization or hybridization, we added in order the following pre-warmed (50°C) components to a 2063 FALCON tube (Becton Dickinson, Franklin Lakes, NJ) sitting at 42°C in a water bath: 25% BSA (0.8 ml), 25% SDS (2.5 ml), and 2 M sodium phosphate, dibasic, anhydrous [Na_2HPO_4] pH 7.2 (2.5 ml). The last addition formed the psychologically unsettling “goop”. We added an equal volume of formamide to the “goop” and mixed gently while the tube sat at 42°C. This solution (~10 ml) was put with a GeneScreen membrane at 42°C overnight for prehybridization, either in a roller bottle or within a Seal-A-Meal bag.

This prehybe solution was replaced the following day with freshly-prepared solution, while keeping temperature at 42°C. Meanwhile, a probe was denatured at 95-100°C for 10 minutes and snap-cooled on ice for 5 minutes. The denatured probe was then mixed with fresh, pre-warmed hybe solution (2 ml) in a 2063 FALCON tube (Becton Dickinson, Franklin Lakes, NJ). This mixture was then added with the hybe solution in the bottle or Seal-A-Meal bag. Hybridization took place overnight at 42°C with gentle tumbling or rocking. The best results (highest signal-to-noise) were obtained with the Seal-A-Meal method, despite being technically tricky.

Washing:

The membrane was washed quickly three times with 2× SSC (15 ml) and then with 2× SSC/0.1% SDS (300 ml) for fifteen minutes. Thirty-minute washes (2-4) with 0.1% SDS/0.1× SSC at 65°C were required to lower the counts to background levels in areas of the membrane with no DNA. The membrane was washed briefly in 2× SSC, drip-dried, and wrapped moist in Saran Wrap. Membranes were placed in cassettes with Kodak BioMax AR film for 18 hours at -80°C. Film was developed in the developer.

Stripping & Reprobing:

To strip blots, a boiling solution of 1% SDS was poured over membrane, and cooled to room temperature. Stripped blots were then dried between two Whatman sheets. When appropriate, prehybridization and hybridization were repeated, as described above.

RT-PCR analysis

RNA Harvesting:

Brain and thymus organs were harvested from mice (aged P5-10) of one of three *Myo1c* genotypes: wild-type, Y61G heterozygote, Y61G homozygote. Tissues were snap-frozen by transferring them with fine forceps into RNase-free microfuge tubes (1.5 ml), resting in dry ice, and then stored at -80°C. Total RNA was purified from each tissue with the RNeasy kit (Qiagen, Valencia, CA).

Briefly, 30-mg pieces of tissue were homogenized with a rotor-stator in a solution containing 600 μ l buffer RLT with β -ME (1 ml RLT: 10 μ l β -ME). Lysates were then centrifuged at maximum speed for 3 minutes. The supernatant was transferred to a fresh tube and an equal volume of 70% ethanol added and mixed immediately by pipetting. This mixture was applied to an RNeasy mini column sitting in a 2 ml collection tube (2 ml). The tube was then centrifuged for 15 seconds > 10,000 rpm.

To pre-wash the column, 350 μ l RW1 buffer was added and the tube centrifuged for 15 seconds >10,000 rpm. An aliquot (10 μ l DNase I stock solution mixed with 70 μ l RDD buffer) was added directly to the silica membrane on the top and incubated at room temperature for 15 minutes. Another aliquot of buffer RW1 (350 μ l) was then added to the mini column and centrifuged for 15 seconds > 10,000 rpm. The RNeasy column was set into a new collection tube (2 ml) and 500 μ l of RPE buffer dispensed over the column before spinning for 15 seconds > 10,000 rpm. Another aliquot (500 μ l) of RPE buffer was added and then spun for 2 minutes > 10,000 rpm to dry the silica-gel membrane. The column was placed in a new tube and spun for 1 min at full speed to remove residual traces of ethanol. To elute RNA, the column was transferred to a fresh tube, 30 μ l RNase-free water was added to the membrane, and the tube was then spun for 1 minute >10,000 rpm. RNA samples were frozen at -80°C for storage.

cDNA Synthesis:

To synthesize cDNA, total RNA (~1,000 ng from a given tissue) was combined with 50 μ M Oligo (dT)₂₀ (1 μ l), 10 mM dNTP (1 μ l), and DEPC-treated water (up to 10 μ l), then incubated at 65°C for 5 minutes. The mixture was then iced for 5 minutes

before adding 10× RT buffer (2 µl), 25 mM MgCl₂ (4 µl), 0.1M DTT (2 µl), RNase OUT (1 µl), and Superscript III reverse transcriptase (1 µl). The mixture was incubated at 50°C for 50 minutes, then at 85°C for 5 minutes, and finally chilled on ice for 5 minutes. RNase H (1µl) was added per tube at 37°C for 20 minutes. PCR reactions were then performed.

Each PCR reaction included DEPC-treated water (39.1 µl), 10× PCR buffer-Mg⁺⁺ (5 µl), 50 mM MgCl₂ (1.5 µl), 10 mM dNTPs (1 µl), Primer 54 (gag agc gcc ttg act gcc cga gac) 10 µM (1 µl), Primer 238 (agc gcc ttc ctc ata acc ttc cag tc) 10 µM (1 µl), cDNA (6 µl), Platinum *Taq* polymerase (0.4 µl) (Invitrogen). Three reactions were run and then pooled. PCR products were purified with Qiagen PCR purification kit and then eluted in EB buffer (30 µl).

Samples for each genotype were digested with *Bam*H I or *Bgl* II, and then separated on 1.4% agarose gel by electrophoresis (70 volts, 1 hour). To estimate the relative fraction of wild-type versus transgenic mRNA, we treated the PCR products with the restriction enzyme *Bam*H I which only cuts Y61G RNA, or with *Bgl* II which only cuts transgenic cDNA. Ethidium bromide-stained gels were quantified using an imaging system (Alpha Innotech, San Leandro, CA). Primers (PG54/PG238) amplified a PCR product (~761 bp). Digestion of the PCR product with *Bam*H I or *Bgl* II yielded two products, 586 bp and 175 bp.

Y61G Antibody Purification

We generated an antibody selective for the Y61G mutation in Myo1c by immunizing rabbits with a peptide containing the mutation (CGGGNPYRDLQIGSRQHMERLYR, where CGGG was added for column conjugation). Antisera (#6765) were passed over a column constructed with the wild-type sequence (CGGGNPYRDLQIYSRQHMERLYR) four times; the flow-through was applied four times to a column constructed with the mutant peptide. Specific antibodies were eluted with acid and base neutralized, and concentrated. Using immunoblots with purified rat wild-type or Y61G-Myo1c, we found that >100-fold more wild-type protein was required to generate a band with equal intensity to that with Y61G-Myo1c.

Protein Extraction

Wild-type or Y61G tissues from various organs [heart, spleen, brain, thymus, adrenal, lung, cochlea, vestibular organs (utricle & saccule)] were harvested and immediately frozen in a 1.5 ml microfuge tube, resting on dry ice, and then stored at -80°C. To extract protein, 10-100 mg of frozen tissue was placed in 465 µl lysis buffer (25 mM Tris, 2.5 mM EDTA and 5× protease inhibitors –1 mg/ml phenylmethylsulfonyl fluoride [35 mg in 100% ice-cold ethanol], 1 mM leupeptin, 1 mM pepstatin on ice). A Dounce homogenizer was used to homogenize tissue.

While keeping the homogenizer on ice, tissue was homogenized until no resistance was met (between 20-40 strokes), first with the loose-fitting pestle then with

the tight-fitting one. 10 µl DNase (10 mg/ml) was added to the homogenate and kept on ice for 15 minutes. 25 µl 20% SDS was added to adjust the final concentration to 1% SDS. Samples were transferred to a 1.5 ml microfuge tube, heated to 100°C in sandblock for 5 minutes, and spun for 10 minutes at 14,000 rpm. The supernatant was transferred to a new tube, and diluted with 1% SDS/lysis buffer, if viscous. For each extract, protein concentration was measured by the BCA assay (Pierce, Rockford, IL). All sample dilutions (1/10, 1/50, 1/100) and BSA standards were made in 1% SDS/lysis buffer. BSA standards ranged either from 0, 0.01, 0.02, 0.04, 0.08, 0.12, 0.16, 0.2 or 0.1, 0.2, 0.4, 0.8, 1.2, 1.6, 2.0 µg.

25 ml of BCA Reagent A (containing sodium carbonate, sodium bicarbonate, bicinchoninic acid and sodium tartrate in 0.1 M sodium hydroxide) were combined with 0.5 ml BCA reagent B (containing 4% cupric sulfate) in a 50 ml Falcon tube at room temperature. 25 µl of a standard or sample was added per well on a 96-well non-treated polystyrene Costar plate cat# 3370 (Corning Inc., Corning, NY). 200µl of the BCA mix (A+B) was added per well and gently pipetted up-and-down three times. Each standard or sample was done in triplicate. The mix was gently rocked for 30 seconds at room temperature. The plate was covered with Parafilm, then set at 37°C for 30 minutes.

After cooling to room temperature, the plate was read at 562 nm with the ELISA plate reader and evaluated using the Softmax, Basic Endpoint Protocol program.

Standard curves were fit with a quadratic equation for best point fit with mean O.D. on the abscissa, concentration on ordinate. Protein concentration for a given sample was determined with the formula $y=A+Bx+Cx^2$.

SDS-PAGE

Proteins from each tissue extract were loaded into 15% resolving/4% stacking gels and separated by sodium dodecyl sulfate - polyacrylamide gel electrophoresis (SDS-PAGE). In the following order, components of the 15% resolving gel solution [2.2 ml MilliQ water, 3.75 ml 30% 150:1 acrylamide-to-bisacrylamide, 1.425 ml 2 M Tris pH 8.9, 37.5 μ l 200 mM EDTA, 37.5 μ l 20% sodium dodecyl sulfate, 50 μ l 15% ammonium persulfate and 6 μ l TEMED (BioRad)] were combined and briefly vortexed in a 50 ml tube before 3.2 ml was pipetted between the two glass plates of gel assembly. Immediately, 800 μ l water-saturated *n*-butanol was overlaid to give the resolving gel a clean edge. After 2 hours transpired for gel polymerization, the *n*-butanol was aspirated and the top of the gel rinsed several times with water.

Components making up a 4% stacking gel (5.79 ml water, 1.07 ml 29% acrylamide/1% bis, 1.0 ml 1 M Tris pH 6.8, 40 μ l 200 mM EDTA, 40 μ l 20% SDS, 60 μ l 15% ammonium persulfate, 8 μ l TEMED) were combined together and poured on the top. Within seconds, a fifteen-tooth comb was inserted in the top solution. 30 minutes was allowed for polymerization.

Combs were removed and wells rinsed twice with water before being submerged in running buffer (25 mM Tris, 192 mM glycine, 0.1% SDS, and 1 mM EDTA). Protein extracts were denatured in 4x sample buffer (20% glycerol, 250 mM Tris, 0.7 M β -mercaptoethanol, 0.016% bromophenol blue, 12% SDS, 20 mM EDTA), placed in a sandblock for 20 minutes at 65°C, vortexed briefly, microfuge-spun, and vortexed again before gel loading. Equal amounts of total protein from wild-type or homozygous Y61G

mice were loaded on the same gel and proteins were separated by SDS-PAGE (200 mV for 55 minutes). To enhance protein transfer onto membranes, gels were treated with 0.25 mg/ml hemoglobin (Gillespie and Gillespie, 1997) in transfer buffer [components for 2 liters included methanol (100 ml), 500 mM CAPS pH 10.5 (29.75 ml), and ice-cold deionized water (1870 ml)] for three 5 minute washes. Gels were run for 60 minutes at 100 volts in ice-cold running buffer to transfer proteins onto a PVDF (polyvinylidene fluoride) membrane (Immobilon P, Millipore) and left stirring overnight.

Immunoblot Analysis

PVDF membranes were incubated for 2 hours at room temperature in 20 ml phosphate buffered saline (PBS) containing 5% Liquid Block (Amersham Biosciences, UK). Subsequently, membranes were incubated an hour at room temperature in 10 ml of a similar solution containing either: a polyclonal antibody (R2652) specific for 15 kDa of C-terminus of mouse Myo1c at 3 µg/ml, or a polyclonal antibody (R6765) specific for Y61G-mouse Myo1c sequence, at 2.5 µg/ml. Blots were washed six times for five minutes each in 0.3% Tween-20/PBS. Blots were incubated with a horse radish peroxidase-conjugated secondary antibody (donkey anti-rabbit HRP at 1:10,000) in 5%/PBS for 1-2 hours at room temperature, and then washed six times for five minutes each in 0.3% Tween-20/PBS. Blots were placed on a sheet of Saran wrap and developed with 6 ml of an HRP substrate that produces a chemiluminescent product (SuperSignal West Pico, Pierce, Rockford, IL). For two seconds, blots were gently pressed between two Whatman sheets and Myo1c was quantified by densitometry of film (X-Omat Blue

XB-1, Kodak, Rochester, NY) images, using for calibration known amounts of purified proteins, which were included on the immunoblots.

Protein Molecular Weight Markers

Protein molecular weight markers were loaded in gels to provide a molecular weight standard. Prestained molecular weight markers (Benchmark Prestained Protein Ladder, Life Technologies) and unstained Perfect markers, 10-225 kDa range, Novagen, Madison, WI) were used. To detect unstained markers, S-protein HRP conjugate at 1:5000 dilution was included in the solution with the secondary antibody.

Auditory-evoked brainstem response analysis of Y61G mice

ABR audiometry to pure tones was used to evaluate cochlear function of wild-type (C57BL6/J) and Y61G homozygous mice, aged P23, using a protocol detailed in Mitchell et al. (1996). Auditory-evoked brainstem responses (ABRs) were elicited to tone-burst stimuli at 4, 8, 16, and 32 kHz and thresholds were obtained from left ears. Animals were anesthetized (ketamine+xylazine) and the individual ears of each mouse were stimulated with a closed tube sound delivery system sealed into the ear canal.

Briefly, mice were subcutaneously injected at the scruff of the neck with a dose of 0.1 cc ketamine and xylazine per 30 gram mouse body weight. After anaesthesia induction, mice were placed in a heated, sound-attenuating chamber and electrodes were inserted subcutaneously in the left fore limb (ground), mandible (reference), and vertex (active). Body temperature was kept at ~37°C with a Deltaphase isothermal heating pad

(Braintree Scientific, Braintree, MA). A sound tube was placed into the left ear canal of mice while keeping it as straight as possible so that the pinna and no part of the external ear obstructed the tube. Animals were tested with stimuli #414 and #269, which are low intensity stimulus trains. Absolute thresholds for each ear were calculated to determine cochlear function.

Biochemistry and Characterization of Mouse Myo1c (Wt and Y61G)

Construction of Baculovirus Expression Viruses for Mouse Myo1c and Y61G-Myo1c

Full-length mouse *Myo1c* was cloned into a p-ENTR/D-TOPO vector (Invitrogen, Carlsbad, CA); residue 61 was converted from Tyr to Gly using site-directed mutagenesis with primers (ccctaccgagacctacagatcggatcccggcagcatatggaacgc; gcgttccatatgctgccgggatccgatctgtaggtctcggtagg). We generated recombinant Wt and Y61G baculoviruses with the BaculoDirect Baculovirus Expression System (Invitrogen, Carlsbad, CA).

Briefly, an aliquot of entry vector (1-2 μ l) was combined with an aliquot of BaculoDirect Linear DNA (300 μ g in 10 μ l), 5 \times LR Clonase buffer, and TE buffer, pH 8.0 to a final volume of 16 μ l. An aliquot of LR clonase (4 μ l) was added to the mixture; reactions were incubated for an hour at room temperature before an aliquot of Proteinase K (2 μ l) was added and the mixture heated at 37°C for 10 minutes. Recombination

yielded two products: recombinant expression virus (with full-length myosin-1c sequence and C-terminal V5 and His (6×) tags), and a by-product (plasmid with the Herpes Simplex Virus *Thymidine kinase* and *lac Z* genes).

To select for high-titer recombinant expression viruses, three rounds of ganciclovir treatment were conducted. Briefly, an aliquot of the LR recombination reaction (10 µl) and Cellfectin (6 µl) was mixed in a microfuge tube (1.5 ml) for 30 minutes with Grace's Insect Medium, Unsupplemented. This mixture was added to *Sf9* cells (~1.5× 10⁶ cells in 2 ml) in a six-well plate and incubated for 5 hours at 27°C before wells were replaced with Complete Grace's Medium (CGM) and ganciclovir (100 µM). After 72 hours of ganciclovir selection, medium was collected in sterile 15 ml tubes and centrifuged at 4,000 rpm at 4°C for 5 minutes. The supernatant was transferred to a fresh sterile tube, stored at 4°C in the dark – this was considered the P1 viral stock.

Using 500 µl of the P1 stock, a second round of ganciclovir selection was conducted to generate P2 stocks. A plaque assay was then performed on the P2 stocks to produce single colonies, which were picked and grown in *Sf9* cells to generate a P2* viral stock. Briefly, 6-well plates were seeded with 2 ml, cell density ~0.75× 10⁶ *Sf9* cells/ml and left for an hour at 27°C. An aliquot (1 ml) was removed from each well and an aliquot (1 ml) of viral dilutions (ranging from 5× 10⁻⁶ - 5× 10⁻⁷) was incubated with the cells for an hour at 27 °C. The liquid (~2 ml) was removed from each well and replaced with an aliquot (2 ml) of 39°C-overlay (4% agarose, Complete Grace's Medium (CGM), and X-gal [150 µg/ml]). Plates then sat at room temperature for half an hour before being placed in a sealed container with 5 mM EDTA and incubated at 27°C for 5-6 days. Well-separated white plaques (~5-10) were picked individually with sterile Pasteur pipettes

and dispensed into a sterile aliquot (0.5 ml) of CGM in an microfuge tube (1.5 ml). An aliquot (100 μ l) was then taken from each tube and dispensed into wells containing *Sf9* cells at a cell density of 2×10^6 *Sf9* cells/ml in 2 ml. These plates were incubated at 27 °C for one week, as described above. Contents of each well were spun at 4,000 rpm. The supernatants were saved and stored in sterile tubes (15 ml) at 4°C under aluminum foil. These were considered P2* viral stocks.

An aliquot (1.5 ml) of P2* stock was added to an aliquot of *Sf9* cells (100 ml, density $\sim 1.5 \times 10^6$ cells) and shaken at 27 °C for 7 days *without ganciclovir* to generate high-titer P3 virus stocks. Estimates of P3 titers were assumed $\sim 7 \times 10^7$ - 1×10^8 plaque forming units per milliliter (pfu/ml). At each stage of viral stock development, stocks were handled sterilely, wrapped in aluminum foil, and stored at 4°C. These steps ensured the longest functional lifespan of viral stocks (according to Invitrogen recommendations).

The following P3 viral stocks were generated: Wt-mMyo1c (clones # 1, 5) and Y61G-mMyo1c (clones #2, 4). Clones #1, 5 for Wt-mMyo1c produced Ni-NTA eluates of equal purity ($\sim 100\%$ myosin) with similar lifespans of 7 days. Clones #2, 4 for Y61G-mMyo1c gave Ni-NTA eluates that were also equally pure, but with similar lifespan of only 2 days. Thus, all four clones each were used for ATPase and *in vitro* motility assays.

Sf9 Expression of Mouse Myo1c and Y61G-Myo1c

Sf9 cells were co-infected with Myo1c and calmodulin viruses at a multiplicity of infection of 4:2 (Gillespie et al., 1999). Briefly, *Sf9* cell cultures (volume: 400 ml,

density $\sim 1.2\text{-}2 \times 10^6$ cells/ml) were sterilely infected with aliquots of P3 viral stocks, (27 – 40 ml of Myo1c stocks) and (12-18 ml of *Xenopus* calmodulin virus). The cells were harvested 48 hours later and centrifuged in large bottles at 4,000 rpm at 4°C. Cell pellets were washed with ice-cold phosphate buffered saline (PBS), spun at 4,000 rpm at 4°C, supernatants decanted away, and then stored at -80°C. *The PBS wash was later determined to diminish Myo1c protein yield (PGG, unpublished results) and so should be omitted from any Myo1c purification.*

A detailed history was kept, indicating the clone of myosin used, cell density infected, moi, # hours incubated, date of pellet freeze, and date of myosin purification. Ni-NTA purifications (described in detail elsewhere) were most often performed within five days of a pellet freeze, but no longer than three weeks from a pellet freeze. No difference in recovery was noted from the time of pellet freeze to Ni-NTA purification.

Actin Preparation

Rabbit skeletal muscle acetone powder (Pel-Freez Biologicals, Rogers, AR) was used to purify F-actin. Briefly, 4 g of Pel-Freez muscle powder was mixed with an aliquot (80 ml) of buffer A (2 mM Tris pH 8.0, 0.2 mM ATP pH ~ 7 , 0.5 mM DTT, 0.1 mM CaCl₂, 0.1 mM NaN₃) and then stirred for 30 minutes in an Erlenmeyer flask sitting in an ice-water bath. This slurry was squeezed through pre-soaked (buffer A) cheesecloth, and the muscle residue re-mixed with a fresh aliquot (50 ml) of buffer A. Flow-throughs were pooled and spun at 15,000 rpm for 20 minutes at 4°C. Supernatants contained depolymerized G-actin. To polymerize the supernatants to F-actin, [KCl] was adjusted to

50 mM and [MgCl₂] to 2 mM while stirring at 4°C for 1 hour. [KCl] was then adjusted to 800 mM and stirred at 4°C for 30 minutes. Mixtures were spun for 90 minutes at 4°C at 65,000 rpm to pellet actin capable of polymerization. These pellets were rinsed with buffer A and then homogenized at 4°C with an aliquot (4-5 ml) of ice-cold buffer A. This slurry was injected into slide dialyzers (Pierce, Rockford, IL) and dialyzed for a total of 48 hours against 4 aliquots (1 liter) of buffer A at 4°C. The solution, containing G-actin capable of depolymerization, was then spun at 75,000 rpm for 30 minutes at 4°C. The G-actin solution was adjusted to final concentrations of 50 mM KCl and 1 mM MgCl₂, thereby inducing F-actin polymerization. This viscous solution was dialyzed against an aliquot (3 liters) of ATPase assay buffer (15 mM HEPES pH 7.5, 50 mM KCl, 1 mM MgCl₂, 0.1 mM EGTA, 0.005% NaN₃) overnight at 4°C, and then centrifuged at 75,000 rpm for 30 minutes. The pellet containing F-actin was resuspended in an ice-cold aliquot (1-2 ml) of ATPase assay buffer using a homogenizer sitting on ice. Final concentrations of F-actin were determined assuming 38.5 μM/A_{290 nm}. F-actin was used within 3-4 weeks and stored on ice in an ice bucket in the cold room for the duration. Fresh ice was replaced every 2 days or so to prevent the tube of actin from sitting in a pool of water.

Purification of Myosin-1c by Ni-NTA Chromatography

Frozen (-80°C) *Sf9* cell pellets of either Wt or Y61G mouse Myo1c were thawed for 5 minutes at 37°C then placed on ice. An aliquot (9 ml) of ice-cold lysis buffer (25 mM Tris pH 8.0, 0.5 mM EGTA, 0.5 mM MgCl₂, 2.4 mM β-mercaptoethanol, 0.2 mM phenylmethylsulfonyl fluoride, 1 μM leupeptin, 1 μM pepstatin) was used to resuspend

the pellets. Using a Luer-lock syringe (10 ml), the mixture was passed twice through a 22-g needle and then twice through a 25g needle into a 50 ml Falcon tube, sitting on ice. Aliquots of 5 M sodium chloride (1440 μ l) and 100 mM ATP (240 μ l) were gently mixed with the cell suspension, which was then kept on ice for 5 minutes. Lysis buffer was added to a final volume of 18 ml. Cell suspensions were centrifuged at 80,000 rpm for 30 minutes at 4°C.

Meanwhile, Ni-NTA columns were prepared. Briefly, an aliquot (1 ml) of Ni-NTA agarose resin (Qiagen, Valencia, CA) slurry (50%) was poured over a column and the resin allowed to gravity pack. Two washes were conducted: an aliquot (10 ml) of water, followed by an aliquot (20 ml) of wash buffer (300 mM sodium chloride, 25 mM Tris pH 8.0, 0.5 mM EGTA, 0.5 mM MgCl₂, 2.4 mM β -mercaptoethanol, 0.2 mM phenylmethylsulfonyl fluoride, 1 μ M leupeptin, 1 μ M pepstatin).

High-speed supernatants were pooled from the above spin and poured over the washed columns *two or three times*. Columns were then washed with an aliquot (25-50 ml) of wash buffer containing protease inhibitors. Mouse Myo1c was eluted from the column by the addition of five aliquots (300 μ l) of elution buffer (125 mM imidazole pH 8.0, 400 mM sodium chloride, 25 mM Tris pH 8.0, 2.0 mM EGTA, 2.0 mM MgCl₂, 2.4 mM β -mercaptoethanol, 0.2 mM phenylmethylsulfonyl fluoride, 1 μ M leupeptin, 1 μ M pepstatin).

The protein concentration of individual fractions was estimated by two methods: OD_{280 nm} and the Bradford test. For the Bradford test, an aliquot (10 μ l) of Ni-NTA eluate was combined with an aliquot (150 μ l) Bradford reagent in a clear glass tube, and evaluated for color change (gray-to-blue indicated a higher protein yield). At each step

of purification, small aliquots of whole lysate, high-speed supe, Ni-NTA flow-through, wash, and eluate were saved and combined with 4× sample buffer for subsequent SDS-PAGE analysis.

Ni-NTA eluates of Wt mouse Myo1c were active for 7 days after purification. Those from Y61G mouse Myo1c were active for only 2-3 days. Thus, all ATPase assays were conducted within 2 days of myosin purification.

ATPase analysis of mouse Myo1c (Wt and Y61G)

The actin-activated ATPase activities of Myo1c (mouse wild-type and Y61G) were measured using [γ - 32 P] ATP (Pollard, 1982) in 10 μ l total reaction volume. Briefly, a master mix (#1) was prepared on ice containing 10× ATP assay buffer (10 mM MgCl₂, 1 mM EGTA, 150 mM HEPES at pH 7.5, 500 mM KCl), 100 μ M ATP (containing unlabeled ATP and ~1,000,000 cpm per μ l [γ - 32 P] ATP), water or NMB-ADP. A second master mix was prepared on ice containing either water, actin, and mouse Myo1c Ni-NTA eluates or just water and actin alone. Aliquots of the master mix #1 were dispensed at the bottoms of four separate siliconized microfuge tubes (1.7 ml) sitting on ice. Aliquots of the second master mix were then dispensed onto the sides of tubes still resting on ice. Reactions were initiated by vortexing for 1-2 seconds, spinning (~ 3-5 seconds) in a microfuge, and transferring the tubes into a 37°C water bath. To minimize variability, great care was taken to perform all steps consistently, so that the same length of time transpired between each step and from sample to sample. To ensure the total [γ - 32 P] ATP hydrolysis remained under 30%, reactions were carried out between 5-30

minutes. Hydrolysis reactions were terminated by adding 67 μl stop solution (2 parts 10 N sulfuric acid, 5 parts silicotungstic acid) with a P200 pipette and vortexing ~1-2 seconds. $[\gamma\text{-}^{32}\text{P}] \text{P}_i$ was recovered by squirting in 250 μl bubble-free isobutanol:benzene (1:1), 25 μl ammonium molybdate, and then vortexing for 20-30 seconds. When all tubes had been extracted, tubes were mixed briefly, and spun together at 14,000 rpm at room temperature for 5 minutes. Using a P200 pipette, an aliquot (100 μl) of the organic phase was transferred into a scintillation vial. To aim for precision and internal consistency, the contents of each pipette tip was dabbed 6-8 times onto the side of a vial to get as much out as possible. An aliquot (2.5 ml) of scintillation cocktail (EcoLite) was added to each vial and then counts per minute were measured with a scintillation counter. Three total samples were also prepared: 1 μl $[\gamma\text{-}^{32}\text{P}] \text{ATP}$ stock, 100 μl isobutanol:benzene, and 2.5 ml scintillation cocktail (EcoLite) in a vial. To account for the intrinsic ATPase activity of actin and its inhibition by adenine nucleotides, assays were performed with control samples containing actin and appropriate nucleotides but no myosin-1c.

ATPase assays were conducted using fresh myosin Ni-NTA eluates, i.e. less than 2 days of myosin Ni-NTA purification because Ni-NTA eluates of Y61G mouse Myo1c were active for only 2-3 days and those from Wt mouse Myo1c were active for 7 days after purification.

Data were plotted as the mean \pm S.D. of four samples per concentration point of NMB-ADP. Five concentration points of NMB-ADP were always performed in a given assay. Inhibition data were fit with the equation: Velocity (% of control) = $[\text{I}]/([\text{I}] + \text{IC}_{50})$,

where $[I]$ is the concentration of the nucleotide analog and IC_{50} is the concentration yielding 50% inhibition.

MATERIALS AND METHODS II

Characterization of Myo7a^{sh1-8J} Mutation

Subcloning of *Myo7a* Exons into pCR 2.1-TOPO vector/ Sequencing

Using the Vector NTI program, flanking primer pairs (Tables 3, 4, 5) were designed to amplify individual exons of the entire mouse myosin-VIIa gene. PCR reactions were performed (as described earlier) on genomic DNA samples processed from one of three mouse strains: C57BL6/J, SJL, *Myo7a^{sh1-8J}* (stock #:003184, Jackson Laboratory, Bar Harbor, ME). Reactions were loaded onto 1.4% agarose/1× TAE gels to resolve specific PCR products from nonspecific products, if any. PCR products were purified with a gel extraction kit (Qiagen, Valencia, CA), eluted in EB buffer (30 µl), and TOPO-cloned into pCR 2.1 TOPO vector (Invitrogen, Carlsbad, CA).

Briefly, fresh gel-purified PCR product (1 µl) was combined with salt solution (1 µl), sterile water (3 µl), and TOPO vector (1 µl), and mixed gently for 5 minutes at room temperature. Reactions were placed on ice. An aliquot (2 µl) of each TOPO-cloning reaction was added to a vial (50 µl) of thawed One Shot *E.coli* cells and incubated on ice for 15 minutes. Cells were heat-shocked at 42°C for 30 seconds and combined with room-temperature SOC medium (250 µl). Tubes were shaken for 1 hour at 37°C. An aliquot (20 µl) was spread on pre-warmed LB plates containing X-gal and 50 mg ampicillin, which were then incubated at 37°C overnight.

The following day cultures (3 ml) of LB/ampicillin were inoculated with individual white colonies (5-10) and shaken at 37°C for 16 hours. Miniprep DNA was

processed from each culture (1.5 ml) using the Qiagen method (miniprep spin kit) and cloned PCR products of genomic mouse myosin-VIIa were sequenced with M13 forward or M13 reverse primers. Briefly, miniprep DNA (500-600 µg) was combined with 3.2 µl sequencing primer (1 µM) and enough sterile water to total 12 µl in volume. Sequences were analyzed by comparing raw sequences with published mouse *Myo7a* sequence using either *DNAasis v3.0* or Vector NTI.

RT-PCR Analysis of 8J Mice

RNA Harvesting

Total RNA from liver was prepared from C57BL6 or homozygous *Myo7a*^{sh1-8J} mice by methods described in Y61G knock-in characterization section.

cDNA Synthesis

We synthesized cDNA from total liver RNA using methods described previously. Primers, specific for exons 37 and 47 respectively, were used to amplify products from cDNA. Samples for each genotype were then separated on 1.4% agarose gel by electrophoresis (70 volts, 1 hour). Primers (EX 37 5'/EX 47B 3') amplified PCR products of the expected size (~1296 bp for wild-type; ~306 bp for 8J/8J homozygotes).

Southern Analysis of *Myo7a*^{sh1-8J} Genotypes

Southern analysis was performed (by the same method described earlier in the Y61G section) on genomic DNA samples processed from one of three mouse strains: C57BL6/J, SJL, homozygous *Myo7a*^{sh1-8J} (stock #: 003184, Jackson Laboratory, Bar Harbor, ME). Genomic DNA from each of these genotypes was digested with one of two restriction enzymes: *Hind* III or *Eco*R I.

To generate a DNA probe, a PCR product was amplified with primers (EX 47 5' and EX 47B 3') from C57BL6/J genomic DNA. Briefly, these components were added to PCR tubes (0.5 ml volume DNase-free, RNase-free) on ice in the following order:

2.5 µl of 10µM oligo EX 47 5' (atg gat gtg ggc ctt cag ccc at)
2.5 µl of 10µM oligo EX 47B 3' (tca gtc cag ctt ccc tgc cta)
5 µl 10× PCR buffer
10 µl 5× Q buffer
1.2 µl dNTPs (10 mM)
26.5 µl PCR-grade water [Millipore water pre-filtered with a 0.22-µm filter (Millex GP, Millipore)]
0.5 µl *Taq* polymerase (cat #201223 – core kit, Qiagen, Valencia,CA)
2 µl diluted genomic C57BL6/J DNA sample (added last and pipetted up-and-down a few times)

Total volume 50 µl

The 469 bp product was gel purified and labeled with [α ^{P32}]-dCTPs (by the same method described earlier), yielding a 3' Southern probe (see figure).

Immunoblot Analysis of 8J Mice and Y114G transgenic Mice

Tissues (kidney, retina, cochlea, utricles) from mice [8J heterozygous, 8J/8J homozygous or 8J/8J/Y114G transgenic (line 56)] were harvested and snap-frozen in an microfuge tube (1.5 ml), resting on dry ice, before storing at -80°C. Protein extraction and immunoblotting was performed as described for the Y61G-Myo1c knock-in characterization section. Equal protein amounts from tissue extracts were loaded per well into 15% resolving/4% stacking gels and separated by SDS-PAGE.

To detect mouse myosin-VIIa, membranes were incubated with 1 µg/ml of an affinity-purified rabbit anti-human polyclonal antibody (Proteus BioSciences, #25-6790, Hasson, T. et al. PNAS. 92: 9815-9819) specific for amino acids 880-1077 of the myosin-VIIa -. Blots were developed with donkey anti-rabbit HRP and an HRP substrate that produces a chemiluminescent product (SuperSignal West Pico, Pierce, Rockford, IL). Myosin-VIIa levels were quantified by densitometry of film (X-Omat Blue XB-1, Kodak, Rochester, NY) images, using for calibration known amounts of purified proteins, which were included on the immunoblots. This antibody shows cross-reactivity to human, mouse, rat, avian, amphibian myosin-VIIa (Hasson, T. Cell Motil. Cytoskel 37:127-138).

Immunocytochemistry and Phalloidin Labeling of Cochlear hair cells

Cochleas were dissected out of temporal bones from mice (aged P0–P2, P4, P6) in a dish of DMEM with HEPES (25 mM), pH 7.5. The stria vascularis and tectorial membrane were carefully removed with fine forceps before cochleas were fixed for 20

minutes in 4% paraformaldehyde. Tissues were washed twice in PBS, ten minutes each. To permeabilize, tissues were transferred to a solution containing 0.2% saponin/blocking cocktail [1 ml (100 mg/ml bovine serum albumin), 300 μ l normal donkey serum, 8.7 ml phosphate buffered saline] for 10 minutes. Subsequently, tissues were incubated overnight at 4°C with 5 μ g/ml anti-Myo7a antibody (rabbit polyclonal, Proteus) in blocking solution. Tissues were washed three times in PBS, ten minutes each. Subsequently, tissues were incubated at room temperature for 2 hours in blocking solution containing secondary antibody (donkey anti-rabbit Cy5 [Molecular Probes, Eugene, OR] diluted 1/10,000) and phalloidin-FITC (0.25 μ M). Tissues were then washed three times in PBS for ten minutes each. Tissues were mounted on glass slides in Vectashield (Vector laboratories Inc., Burlingame, CA) with glass coverslips and examined by confocal microscopy.

Auditory-evoked Brainstem Response Analysis

ABR audiometry to pure tones was used to evaluate cochlear function in mice aged P36 of the following genotypes: 8J homozygotes, 8J/+ heterozygotes, 8J homozygotes with a single copy of the Y114G-Myo7a transgene. Auditory-evoked brainstem responses (ABRs) were elicited to tone-burst stimuli at 4, 8, 16, and 32 kHz and thresholds were obtained from left ears. Animals were anesthetized (ketamine+xylazine) and the individual ears of each mouse were stimulated with a closed tube sound delivery system sealed into the ear canal. ABRs were measured by the same method as described in the Y61G characterization section with one exception: animals

were tested with stimuli #415 and #416, which are high intensity stimulus trains.
Absolute thresholds for each ear were calculated to determine cochlear function.

Genotypes Tested:

8J/8J homozygotes

8J/+ heterozygotes

8J/8J/ single copy of the Y114G transgene (line 56)

8J/8J/ two copies of the Y114G transgene (line 56) – awaiting analysis

MATERIALS AND METHODS III

Generation of Y114G-mMyo7a and FlAsH-tagged Myo7a Transgenic Mice

Cloning of the Y114G-Myo7a Transgenic Construct

We used the following steps in the cloning of the Y114G-Myo7a transgenic construct.

1) Site-directed mutagenesis was performed on a baculovirus expression construct pBB-His2a-mMyo7a to engineer *EcoR* I and *Ssp* I restriction sites on either side of the ATG start codon for *Myo7a*, changing the sequence from GTT ATC CTG to GTA ATA TTG.

The new plasmid was called pBB-7YG (*EcoR* I-*Ssp* I).

2) We digested pBB-7YG (*EcoR* I-*Ssp* I) with *EcoR* I and *Xho* I, and cloned this fragment (1086 bp) into pCR2.1-TOPO, which has no *Ssp* I sites. The new plasmid was named pCR2.1-Wt mMyo7a RI/*Xho* I.

Inserting the Mouse Myo7a Promoter

3) We PCR-amplified the minimal mouse *Myo7a* promoter (-118 to +1776, Böeda et al. 2001) with flanking *EcoR* I and *Ssp* I sites from C57BL6/J genomic DNA. The ~1.9 kb PCR product was TOPO-cloned into pCR2.1-TOPO. Sequencing revealed six single nucleotide differences (versus the C57BL6/J sequence of the *Myo7a* promoter from

Ensembl genome database). Each of these was consecutively converted to the C57BL6/J sequence by *Pfu* mutagenesis. The corrected region containing the C57BL6/J *Myo7a* promoter was then cloned into the *EcoR* I and *Ssp* I sites of pCR2.1-Wt mMyo7a *RI/Xho* I, thus creating plasmid pCR2.1-Wt mMyo7a *RI/Xho* I/7aP.

4) This plasmid (pCR2.1-Wt mMyo7a *RI/Xho* I/7aP) was digested with *EcoR* I and *Xho* I, generating a ~3.0 kb fragment containing the *Myo7a* promoter, the ATG start, and the 5' end of the *Myo7a* cDNA. This fragment was cloned into pCMV-Script, creating pCMV-Script A.

5) A plasmid (eGFP-mMyo7a-C1) from David Corey's laboratory was obtained that contained enhanced Green Fluorescent Protein (eGFP) in frame with the N-terminus of full-length mouse *Myo7a* cDNA. Sequencing of this plasmid revealed a one base-pair deletion at nucleotide 6150 (CAAAT > CAA_T) in the mouse *Myo7a* cDNA. Thus we performed *Pfu* mutagenesis to re-install the A to avoid a frameshift mutation in our transgene.

Mutagenesis of 6150 site of mMyo7a cDNA of David Corey's plasmid (eGFP-mMyo7a-C1)

6) Using *Pfu* turbo at 1 μ l per 50 μ l reaction, mutagenesis was performed with oligos (125 ng of *Myo7a* 6150 Mut A and Mut B primers) to reinstall a missing A at nucleotide site 6150 in the mouse *Myo7a* cDNA. Mutagenesis was carried out at 96°C 30" [1 cycle],

96°C 30" 55°C 1' 68°C 14', [16 cycles] on a Robocycler (Stratagene, La Jolla, CA).

Reactions were treated with *Dpn* I for 2 hours post-mutagenesis. An aliquot (10 ul) of the reaction was used to transform DH5 α cells and plated on LB/kanamycin plates (50 μ g/ml) at 37°C overnight. This plasmid containing the corrected 6150 site was digested with *Xho* I and *Kpn* I. The fragment (~5.1 kb) was subcloned into *Xho* I and *Kpn* I sites of pCMV-Script A, thus creating plasmid pCMV-Script B.

7) Using the David Corey plasmid (eGFP-mMyo7a-C1) as a DNA template, we PCR-amplified a ~0.5 kb product that spanned from the *Kpn* I site to the C-terminus of *Myo7a*. The 3' primer allowed us to install another *Kpn* I site 3' of the stop codon. This ~0.5 kb PCR product was then TOPO-cloned into pCR2.1-TOPO and verified by sequencing. Using *Kpn* I, we digested the ~0.5 kb fragment and subcloned it into the *Kpn* I site of pCMV-Script B, creating pCMV-Script C. Subclones with correct orientation were chosen.

Adding Flanking Insulators

8) To generate 5' insulators, we amplified a PCR product containing tandem ~250 bp insulators from the chicken β -*globin* locus (Chung et al., 1997) with primers that added a *Not* I site on the 5' end and an *EcoR* I on 3' end. We subcloned the *Not* I to *EcoR* I-flanked tandem insulator sequence into pCMV-Script C, positioning the insulator tandem at the start of the mouse *Myo7a* promoter and creating the plasmid pCMV-Script C/5' insulator.

9) To generate 3' insulators, we amplified a different PCR product containing tandem ~250bp insulators with primers that added *Mlu* I sites on both ends as well as an *Age* I site internal to the 3' *Mlu* I site. We cut pCMV-Script C/5' insulator with *Mlu* I and subcloned in the 3' insulator tandem *Mlu* I/*Age* I-*Mlu* I-flanked tandem insulators at the 3' end at the *Mlu* I site in pCMV-Script. Correct orientation was verified by sequencing. The resulting plasmid was called pCMV-Script Wt-*Myo7a* transgene with insulators (**Wt-*Myo7a* transgene**).

Swapping in the Y114G Mutation

9) Using site-directed mutagenesis and a plasmid called pBB Wt-*Myo7a*, we engineered the Y114G mutation into the mouse *Myo7a* sequence. The new plasmid was called (pBB Y114G-*Myo7a*). We digested this plasmid with *EcoR* V and *Cla* I, generating a ~1.386 kb DNA fragment bearing the Y114G mutation. We swapped this fragment with the similar region of **Wt-*Myo7a* transgene**, thus creating the **Y114G-*Myo7a* transgene**. We verified correct sequence of both transgenes with primers spaced apart by ~300 bp from the *Not* I site to the *Mlu* I sites. Sequencing ensured similar orientation of insulator sequences, which must be pointed in the same direction for proper function. Transgenes were linearized with *Not* I on the 5' end and *Age* I on the 3' end and sent to John Mercer and his group in at the McLaughlin Institute in Great Falls, Montana for mouse (FVB/NCr) oocyte microinjection.

Cloning of the FAsH-tagged Myo7a Transgenic Construct

Swapping in the FAsH-tagged Mutation

10) To create the FAsH-tagged *Myo7a* transgene, we used site-directed mutagenesis to insert the FAsH tag (CCPGCC motif) in frame between the second and third amino acids of genomic mouse *Myo7a*. The plasmid (pCR2.1-Wt mMyo7a *R1/Xho I/7aP*) was used as the template for mutagenesis. We swapped a fragment from this plasmid containing the FAsH-tag with the similar region of **Wt-Myo7a transgene**, thus creating the **FAsH-tagged Myo7a transgene**. The transgene was fully sequenced with primers spaced apart by ~300 bp from the *Not I* site to the *Mlu I* sites. Sequencing ensured proper orientation of insulator sequences and that no mutations were introduced. The transgene was linearized with *Not I* on the 5' end and *Age I* on the 3' end and sent to John Mercer and his group in Montana for mouse oocyte microinjection.

PCR Genotyping of Y114G Transgenic Mice

Toe/tail digestion: As described previously in the Y61G characterization section.

Polymerase Chain Reaction (PCR): The following components were added in the following order to PCR tubes (0.5 ml volume DNase-free, RNase-free) on ice.

1.25 μ l of 10 μ M 5' oligo genotyping primer A (ggg act atg tat gga tgg acc) or B (gga gtt tga tgt gcc cat cgg)
1.25 μ l of 10 μ M 3' oligo genotyping primer C (ccc aaa tgc ttc cag gat cgg) or D (ccc agt ttc ttc ttc tcc tcc)
2.5 μ l 10 \times PCR buffer
5 μ l 5 \times Q buffer
0.6 μ l 10 mM dNTPs
13.25 μ l PCR-grade water [Millipore water pre-filtered with a 0.22- μ m filter (Millex GP, Millipore)]
0.25 μ l *Taq* polymerase (cat #201223 – core kit, Qiagen, Valencia, CA)
1 μ l diluted genomic DNA sample (added last and pipetted up-and-down a few times)

total volume 25 μ l

Reaction tubes were placed in a Robocycler PCR machine (Stratagene, La Jolla, CA) and subjected to these conditions: 95°C 5 minutes [1 cycle], 94°C 1 minute, 55°C 2 minutes, 72°C 4 minutes [5 cycles], 94°C 1 minute, 55°C 1 minute, 72°C 3 minutes [30 cycles], 72°C 10 minutes.

PCR Genotyping of FAsH-tagged Transgenic Mice

The above primer pairs were also used to genotype FAsH transgenic mice. Another genotyping primer, (ggt atg ctg ccc cgg ctg ctg c), specific for genotyping FAsH lines was sometimes employed.

RT-PCR Analysis of Y114G Transgenic mice

RNA Harvesting

Using methods described earlier, three separate batches of inner ear tissue (utricle and cochlea) were harvested from ~15-20 mice (aged P5-10) and (aged P21-25) from the Y114G-*Myo7a* transgenic lines: 55, 56, 71. Total RNA was prepared, as described in Y61G knock-in characterization section.

cDNA Synthesis

To synthesize cDNA, total RNA (8 μ l) from inner ear tissues was combined with 50 ng/ μ l random hexamers (1 μ l), and 10 mM dNTP (1 μ l), then incubated at 65°C for 5 minutes. The mixture was then iced for 5 minutes before adding 10 \times RT buffer (2 μ l), 25 mM MgCl₂ (4 μ l), 0.1M DTT (2 μ l), RNase OUT 40 U/ μ l (1 μ l), and Superscript III reverse transcriptase 200 U/ μ l (1 μ l). The mixture was incubated at 25°C for 10 minutes, at 50°C for 50 minutes, at 85°C for 5 minutes, and finally chilled on ice for 5 minutes. RNase H (1 μ l) was added per tube and incubated at 37°C for 20 minutes. PCR reactions were then performed.

Each PCR reaction included DEPC-treated water (38.1 μ l), 10 \times PCR buffer-Mg⁺⁺ (5 μ l), 50 mM MgCl₂ (1.5 μ l), 10 mM dNTPs (1 μ l), genotyping primer A (ggg act atg tat gga tgg acc at 10 μ M, 1 μ l), genotyping primer C (ccc aaa tgc ttc cag gat cgg at 10 μ M, 1 μ l), cDNA (2 μ l), *Taq* polymerase (0.4 μ l) (Platinum *Taq* Invitrogen). Three reactions were run and then pooled. Samples from each Y114G-*Myo7a* transgenic line were

digested with *BamHI*, and then separated on 1.4% agarose gel by electrophoresis (70 volts, 1 hour).

Treatment of the PCR products with the restriction enzyme *BamHI*, which only cuts Y114G RNA, allowed an estimation of the relative fraction of wild-type versus transgenic mRNA. Ethidium bromide-stained gels were quantified using an imaging system (Alpha Innotech, San Leandro, CA). Primers were predicted to amplify a 573 bp PCR product for wild-type Myo7a and Y114G transgenic mRNA; however, *BamHI* digests this PCR product at Y114G, yielding two bands: 318 bp and 255 bp. PCR amplification and *BamHI* digestion was carried out the three times on separate batches of RNA to verify results.

Reaction tubes were placed in a MJ Research PCR machine and subjected to these conditions: 95°C 5 minutes [1 cycle], 95°C 45 seconds, 55°C seconds, 72°C 1:15 minutes [40 cycles], 72°C 10 minutes.

RT-PCR/Southern Analysis of FIAsh Transgenic Lines

Utricles and cochleas (10-20) were dissected from temporal bones of pups (aged P5-P10) from each of the FIAsh-tagged Myo7a transgenic lines (2, 5, 15, 23, 25) in a dish of DMEM with HEPES (25 mM). Inner ear tissues were snap-frozen by transfer with fine forceps into RNase-free microfuge tubes (1.5 ml) resting in dry ice.

Total RNA was purified (by methods described previously in the Y61G mouse characterization section) from each tissue with the RNeasy kit (Qiagen, Valencia, CA). Briefly, cDNA was synthesized using random hexamers with Superscript III (Invitrogen).

Subsequently, primers 7aprB (tgaaaatttcaggctcc) and genotyping primer C (ccc aaa tgc ttc cag gat cgg) were used to PCR amplify in a product ~710 base pairs in size. Three reactions were run and then pooled. Samples from each FLAsH-Myo7a transgenic line were then separated on 1.4% agarose gel by electrophoresis (70 volts, 1 hour).

To determine which FLAsH-transgenic line had the highest transgene copy number, an RT-PCR/Southern was performed using an oligo probe (GGT **ATG CTG CCC CGG CTG CTG C**), specific for the FLAsH-tag sequence (highlighted in bold). Briefly, equal amounts (700 ng utricle, 800 ng cochlea) of amplified (7aprB/geno C primers) products were loaded onto 1.4% agarose gels, which were run at 20 volts overnight. As described in the Y61G section, DNA was transferred onto Genescreen membrane by downward transfer, auto-crosslinked, and prehybridized using the Thayer method.

To label the 5'-OH (hydroxyl group) of the primer, an oligo stock (100 μM) was diluted to 5 μM with DNase-free water. (5 μM = 5 pmol/ μl) and subjected to [γ - 32] ATP-labeling using a *mir*Vana Probe & Marker kit (catalog #1554, Ambion, Austin, TX). Briefly, oligo DNA (5 pmol), [γ - 32] ATP 4000-7000 Ci/mmol, 10-150 mCi/ml (25 pmol), 1 μl 10 \times Kinase buffer, 1 μl T4 PNK (10 units/ μl), and nuclease-free water were combined to a total volume of 10 μl in a microfuge tube (1.5 ml), and then incubated at 37°C for one hour. The labeled oligo was passed over a column to remove unlabeled nucleotides. The membrane was hybridized with labeled probe, washed, and exposed to film according to methods described earlier.

RT-PCR/*EcoR* V Digestion Analysis of FIAsh Transgenic Lines

Cochlear total RNA from the FIAsh transgenic lines was purified and cDNA was synthesized by methods described in the previous section. The same primers 7a prB (tgaaaatttcgaggctcc) and genotyping primer C (ccc aaa tgc ttc cag gat cgg) were used to PCR amplify a product ~710 base pairs in size.

Samples from each FIAsh-Myo7a transgenic line were digested with *EcoR* V, and then separated on 1.4% agarose gel by electrophoresis (70 volts, 1 hour). Primers were predicted to amplify a 706 bp PCR product for wild-type Myo7a or a PCR product of 724 bp from FIAsh transgenic Myo7a mRNA. *EcoR* V digests these PCR products yielding two bands: 250 bp and 456 bp (for wild-type), 268 bp and 456 bp (for FIAsh). The transgenic product is slightly larger (268 bp) than the wild-type one (250 bp), thus allowing a determination of which transgenic line expresses the FIAsh transgene and an estimation of the relative fraction of wild-type versus transgenic mRNA.

Immunoblot Analysis of Y114G transgenic Mice

Tissues (kidney, retina, cochlea, utricle) from three genotypes [8J heterozygous, 8J/8J homozygous or 8J/8J/Y114G transgenic (line 56) mice] were harvested and snap-frozen in a microfuge tube (1.5 ml), resting on dry ice, before storage at -80°C. Protein extraction and immunoblotting was performed, as described for the Y61G-Myo1c knock-in characterization section. Equal amounts of protein from tissue extracts were loaded per well into 15% resolving/4% stacking gels and separated by SDS-PAGE.

Immunoblots were performed as described earlier in the 8J characterization section using the same antibody (Proteus BioSciences, #25-6790, Hasson, T. et al. PNAS. 92: 9815-9819).

FLAsH Labeling

Utricles and cochleas were dissected from temporal bones of pups (aged P3-P10) from each of the FLAsH-tagged transgenic lines (2, 5, 15, 23, 25) in a dish of DMEM with HEPES (25 mM), pH 7.5. Inner ear tissues were exposed to Lumio green (1-2.5 μ M) and 1,2-ethanedithiol (15-25 μ M) (Invitrogen, Carlsbad, CA) in DMEM with HEPES (25 mM) for 15 or 60 minutes at room temperature. To reduce non-specific background labeling, wash steps followed containing 1,2-ethanedithiol (either 300 or 750 μ M). Most experiments included four washes of 15 minutes duration.

Following Lumio green labeling and washing, tissues were briefly washed in a dish of OptiMEM (Invitrogen, Carlsbad, CA) or DMEM with HEPES (25 mM). Subsequently, tissues were fixed in a 4% solution of paraformaldehyde/phosphate buffered saline (PBS) for 25 minutes. During fixation, tissues dissections were completed (i.e., the otolithic membranes were removed from utricles, tectorial membranes were removed from cochleas) with fine forceps. Tissues were washed twice in PBS for ten minutes. To permeabilize, tissues were next transferred into a 0.2% saponin/PBS solution for 10 minutes. Washes with PBS followed (three times, ten minutes each). Subsequently, tissues were incubated for 1 hour at room temperature with Phalloidin - 633 or 660 [0.25 μ M] (Molecular Probes, Eugene, OR). Tissues were wash

three times in PBS for ten minutes. Tissues were mounted on glass slides in Vectashield (Vector Laboratories Inc., Burlingame, CA) with glass coverslips. FIAsh labeling of inner ear tissues was examined with epifluorescence and confocal microscopy.

Transferring inner ear tissue from dish to dish is tedious and often results in adherence of tissue to the sides of the transfer pipet, be it glass or plastic. To minimize this adherence, cut-off the tip of a plastic pipette used for a P200 and pipette up-and-down a few times in a solution of BSA (10-100 mg/ml) before transferring inner ear tissue. This step is crucial and prevents loss of precious tissue.

RT-PCR analysis of wild-type cochlea to test for the presence of a 38 amino acid coding region of *Myo7a* in exons 32 and 33

RNA Harvesting

Using methods described earlier, total RNA was prepared from cochlea from ~10 wild-type C57BL6 mice (aged P5-10).

cDNA Synthesis

To synthesize cDNA, total RNA (5 μ l) from cochlea was combined with 50 ng/ μ l random hexamers (1 μ l), 10 mM dNTPs (1 μ l), water (5 μ l), and then incubated at 65°C for 5 minutes. The mixture was then iced for 5 minutes before adding 10 \times RT buffer (2 μ l), 25 mM MgCl₂ (4 μ l), 0.1M DTT (2 μ l), RNase OUT 40 U/ μ l (1 μ l), and Superscript III reverse transcriptase 200 U/ μ l (1 μ l). The mixture was incubated at 25°C for 10 minutes, at 50°C for 50 minutes, at 85°C for 5 minutes, and finally chilled on ice for 5

minutes. RNase H (1 μ l) was added and incubated at 37°C for 20 minutes. PCR reactions were then performed.

The PCR reaction included DEPC-treated water (38.1 μ l), 10 \times PCR buffer-Mg⁺⁺ (5 μ l), 50 mM MgCl₂ (1.5 μ l), 10 mM dNTPs (1 μ l), 5' primer (aggtgtgagaaggaggacga) at 10 μ M (1 μ l), 3' primer (tgcagtgccaccacataactta) at 10 μ M (1 μ l), cDNA (2 μ l), Platinum *Taq* polymerase (0.4 μ l) (Invitrogen). The reaction tube was placed in a MJ Research PCR machine and subjected to these conditions: 95°C 5 minutes [1 cycle], 95°C 45 seconds, 55°C seconds, 72°C 1:15 minutes [40 cycles], 72°C 10 minutes. The PCR sample was separated on a 1.4% agarose gel by electrophoresis (70 volts, 1 hour).

Specifics of the above primers: the 5' primer spans exons 29 and 30 of *Myo7a*; the 3' primer is specific for a region close to the end exon 33. We received a plasmid from David Corey with the mouse *Myo7a* cDNA that contained an in-frame 38 amino acid region missing from exons 32 and 33. Since we used this cDNA to make our *Myo7a* transgenes, we wanted to know if wild-type cochlea encodes a *Myo7a* transcript with the 38 amino acid deletion. The predicted PCR product sizes if the 38 amino acid region were: Present – 695 bp, Absent – 581 bp.

Cloning of the Y114G-Myo7a Knock-in Construct

- 1) PCR amplify a ~6.4-kb piece from *Myo7a* genomic DNA (that spans intron 3/4 and exon 8) and TOPO-clone into pCR2.1-TOPO, creating the plasmid 6.4/7a-TOPO. There are *Hind* III sites just internal to either end of the ~6.4-kb piece.
- 2) Change Y114G in exon 4 by site-directed mutagenesis in the plasmid 6.4/7a-TOPO, creating plasmid 6.4/YG7a-TOPO.
- 3) There are *Xho* I sites flanking both *loxP* sites in the Y61G-Myo1c targeting construct. With *Xho* I, digest the Y61G-Myo1c construct (or *Nhe* I-flanked *neo* cassette in pCR2.1) and gel purify the ~2.2 kb *neomycin* cassette. Subclone the *neomycin* resistance cassette into the single *Xho* I site located near the center of the intron between exon 3 and exon 4 in plasmid 6.4/YG7a-TOPO, creating plasmid 6.4/YGneo7a-TOPO.
- 4) Digest 6.4/YGneo7a-TOPO with *Hind* III and *EcoR* I. Gel purify the ~7.7-kb fragment and subclone into DT-pCMV-Script in the *Hind* III and *EcoR* I sites, creating plasmid DT-pCMV-Script YGneo7a dIII/RI.
- 5) PCR amplify ~5.0-kb piece from mMyo7a genomic DNA (that spans a region from exons 8 through 12) and TOPO clone into pCR2.1, creating plasmid 5.0/7a-TOPO. There are *EcoR* I sites just internal to either end of the ~ 5.0-kb piece.

6) Digest plasmid 5.0/7a-TOPO with *EcoR* I, gel purify fragment, and subclone into the single *EcoR* I of plasmid DT-pCMV-Script YGneo7a dIII/RI. Check orientation. This subcloning step of the ~ 5.0-kb fragment will extend the 3' region of homology by ~4.2 kb. The final Y114G-Myo7a knock-in construct has ~ 10.5 kb of homology to genomic *Myo7a* and can be linearized with either *Not* I or *Kpn* I.

Options:

1) The intermediate plasmid DT-pCMV-Script YGneo7a dIII/RI (in step 4) could be used as a targeting vector, but the region of homology is ~6.3 kb.

2) Instead of PCR amplification, the 6.4-kb and 5.0-kb pieces described above could be digested out of BACs (that contain the right genomic region of *Myo7a*) and subcloned into the MCS of pBluescript or another plasmid. This strategy is probably safe, because the unintentional introduction of a mutation by PCR amplification would no longer be a concern. No matter how it is made, the final construct must be sequenced.

Southern Screening with *Bam*HI Digestion of Genomic DNA and Probes Outside Region of Homology:

Allele	5' Probe	3' Probe
WT	17.6 kb	17.6 kb
Targeted	9.4 kb	10.3 kb
Recombined	7.2 kb	10.3 kb

(i.e., neo gone)

Why Go With This Construct?

The region of homology is a ~10.5 kb. Putting the *neo* cassette at *Xho* I in the middle of a big intron (4.2 kb, between exons 3 and 4) is probably more safe than placing it at the *Xma* I site in the smaller intron (657 bp) between exon 4 and exon 5, because the *Xma* I site is only 120 bp downstream of exon 4 and the *neo* cassette could potentially interfere with splicing. Jim Smart, Manfred Baetscher, and Chris Bond agreed that the above construct might be the best of three different designs I showed them.

In vitro Biochemistry/Characterization of Recombination Wt and Y114G-mMyo7a

Construction of Baculovirus Expression Viruses for Mouse Myo7a and Y114G-Myo7a

Full-length mouse *Myo7a* was cloned into a p-ENTR/D-TOPO vector (Invitrogen, Carlsbad, CA). Three additional versions of mouse *Myo7a* with C-terminal truncations (after IQ1, after IQ5, after the putative coiled-coil domain) were cloned into the same entry vector (p-ENTR/D-TOPO vector); residue 114 was converted from Tyr to Gly using site-directed mutagenesis with primers (cca gct gct ctc cat cgg atc ccc aga gca cat ccg cc; ggc gga tgt gct ctg ggg atc cga tgg aga gca gct gg). Using the entry vectors with the coiled-coil truncated *Myo7a* versions, we generated recombinant Wt and Y114G baculoviruses with the BaculoDirect Baculovirus Expression System (Invitrogen, Carlsbad, CA) by methods described earlier.

Sf9 Expression of Wt Mouse Myo7a and Y114G-Myo7a

Sf9 cells were co-infected with Myo7a and calmodulin viruses at a multiplicity of infection of 4:2 (Gillespie et al., 1999). Briefly, *Sf9* cell cultures (volume: 400 ml, density $\sim 1.2\text{-}2 \times 10^6$ cells/ml) were sterilely infected with aliquots of P3 viral stocks, (27 – 40 ml of Myo7a stocks) and (12-18 ml of *Xenopus* calmodulin virus). The cells were harvested 48-72 hours later and centrifuged in large bottles at 4,000 rpm at 4°C. Cell

pellets were washed with ice-cold phosphate buffered saline (PBS), spun at 4,000 rpm at 4°C, supernatants decanted away, and then stored at -80°C.

Attempts to Purify Soluble Mouse Myo7a

Mouse Myo7a was produced using four different expression systems. All attempts to purify significant amounts of soluble protein for biochemical characterization failed.

1) A truncation of the wild-type mouse Myo7a containing the head, neck and IQ1 domains was cloned into the baculovirus vector pBB-His2a (Invitrogen, Carlsbad, CA). Residue 114 was converted from Tyr to Gly using site-directed mutagenesis with primers (cca gct gct ctc cat cgg atc ccc aga gca cat ccg cc; ggc gga tgt gct ctg ggg atc cga tgg aga gca gct gg) to yield an Y114G version of the plasmid. P3 viral stocks of Wt and Y114G were generated from these starting vectors (by methods described in Gillespie et al., 1999), which were used for expression in *Sf9* cells. The following extraction conditions were attempted with trace amounts of soluble Myo7a resulting.

- A. Standard Gillespie extraction conditions/Ni-NTA chromatography (described in the Y61G biochemistry section).
- B. Extraction conditions for rat Myo7a (described in Inoue et al., 2003)

2) The Gateway *in vitro* transcription/translation (Expressway Plus Expression System) from Invitrogen was employed to express Myo7a. Three different truncations of Myo7a (Wt or Y114G) were cloned into the pENTR/D-TOPO entry vector, then recombined with pEXP2-DEST vector for *in vitro* transcription/translation. Final pEXP2-DEST vectors included truncations of Myo7a after IQ1, IQ5, the coiled-coil domain, C-terminal tags (V5 tag, 6× His-C), and a stop codon.

3) The coiled-coil truncations of mouse *Myo7a* were cloned into a p-ENTR/D-TOPO vector (Invitrogen, Carlsbad, CA); residue 114 was converted from Tyr to Gly using site-directed mutagenesis with primers (cca gct gct ctc cat cgg atc ccc aga gca cat ccg cc; ggc gga tgt gct ctg ggg atc cga tgg aga gca gct gg). We generated recombinant Wt and Y114G baculoviruses with the BaculoDirect System (Invitrogen, Carlsbad, CA) by methods described earlier. P3 viral stocks contained the truncated *Myo7a* sequence just beyond the coiled-coil domain, C-terminal tags (V5 tag, 6× His-C) and a stop codon.

Sf9 cell cultures (volume: 400 ml, density $\sim 1.2 - 2 \times 10^6$ cells/ml) were co-infected with Myo7a and calmodulin viruses at a multiplicity of infection of 4:2 (Gillespie et al., 1999). The cells were harvested 60-72 hours later and centrifuged in large bottles at 4,000 rpm at 4°C. Pellets were separated and lysed in 5 mls of the following buffers, then spun at 100,000× g. An aliquot of the high-speed supernatant was separated by SDS-PAGE to examine which extraction conditions, if any, resulted in soluble mouse Myo7a. The extraction conditions in M*, O* resulted in trace amounts of soluble mouse Myo7a, as assayed by immunoblot for Myo7a. These results were reproduced three times.

- A. Ikebe conditions (with 320 $\mu\text{g/ml}$ calmodulin)
- B. standard lysis buffer (SLB) described earlier
- C. SLB + 10 mM ATP + 10 mM MgCl_2
- D. SLB + 1M NaCl
- E. SLB + 1M NaCl + 10 mM ATP + 10 mM MgCl_2
- F. SLB + 300 mM NaCl
- G. SLB + 300 mM NaCl + 10 mM ATP + 10 mM MgCl_2
- H. SLB + 0.25 % Tween-20
- I. SLB + 0.25 % Tween-20 + 10 mM ATP + 10 mM MgCl_2
- J. SLB + 1% Triton X-100
- K. SLB + 1% Triton X-100 + 10 mM ATP + 10 mM MgCl_2
- L. SLB + 0.5% deoxycholate
- M*. SLB + 0.5% deoxycholate + 10 mM ATP + 10 mM MgCl_2
- N. SLB + 0.1% deoxycholate
- O*. SLB + 0.1% deoxycholate + 10 mM ATP + 10 mM MgCl_2
- P. SLB + CHAPS 25 mM
- Q. SLB + CHAPS 25 mM + 10 mM ATP + 10 mM MgCl_2

4) The pENTR/D-TOPO entry vectors containing truncations (Wt or Y114G mouse Myo7a) after the coiled-coil domain were recombined with DEST-51 destination vector (Invitrogen, Carlsbad, CA), which is suitable for mammalian expression vector. These vectors were transfected into COS-7 cells with FuGene 6 (Roche, Indianapolis, IN). Transfected cells were lysed with IPER reagent (Pierce, Rockford, IL) and spun at high speed for 20 minutes at 4°C. Minimal amounts of soluble Myo7a protein were detected in the high speed supernatant by SDS-PAGE. Aliquots of the high speed supernatant were combined with actin +/- ATP in cosedimentation assays. The binding properties of mouse Myo7a with actin were complex. Mouse Myo7a could not be pelleted with actin.

RESULTS

GENERATION AND CHARACTERIZATION OF Y61G-Myo1C MICE

Screening ES Clones by Nested PCR and Southern analysis

To identify correctly targeted ES cell clones that had homologously recombined with the Y61G targeting construct, we utilized a nested PCR screening strategy and Southern analysis. The nested PCR strategy employed pairs of outer and inner PCR primers that spanned the 5' and 3' junctions of the targeting construct with the endogenous *Myo1c* locus (Fig. 7, 8).

Nested PCR analysis of the 5' end suggested several potential ES cell clones. Screening from plate #1 pointed to four clones (*1C2*, *1D5*, *1E9*, *1G8*) while plate #2 pointed to seven (*2A8*, *2B3*, *2B6*, *2B10*, *2B12*, *2C5*, *2C12*). The 3' end nested screen, however, was of limited value in suggesting targeted clones. Several outer PCR reactions (19) gave bands of the correct size, but all of the inner nested reactions failed to amplify PCR products. Therefore, results from the 5' screen guided us toward positive clones (Fig. 7, 8).

Southern analysis of potential clones (Fig. 7, 9) confirmed that two (*2B3*, *1G8*) were correctly targeted using separate external probes, 5' probe A and 3' probe B (see Table I below). Subclones (*1G8-B2*, *1G8-B4*, *1G8-C4*, *1G8-C8*) were also correctly targeted using these external probes. To test for the occurrence of multiple insertions or random integrations of the targeting vector, Southern analyses were performed on *2B3* and the *1G8* subclones with three additional probes: a 5' internal probe C, a 3' internal probe D and a vector probe E, specific for a region in the DT cassette. These Southern analyses revealed no

Figure 7. **Targeting Strategy.** Sequence coding for the Y61G mutation at amino acid residue 61 was inserted, resulting in conversion of a *Bgl* II restriction site to *Bam*HI. The loxP-flanked *neomycin*-resistance cassette was introduced into a large intron between exons 4 and 5 at a *Nhe* I restriction site.

Targeting Strategy

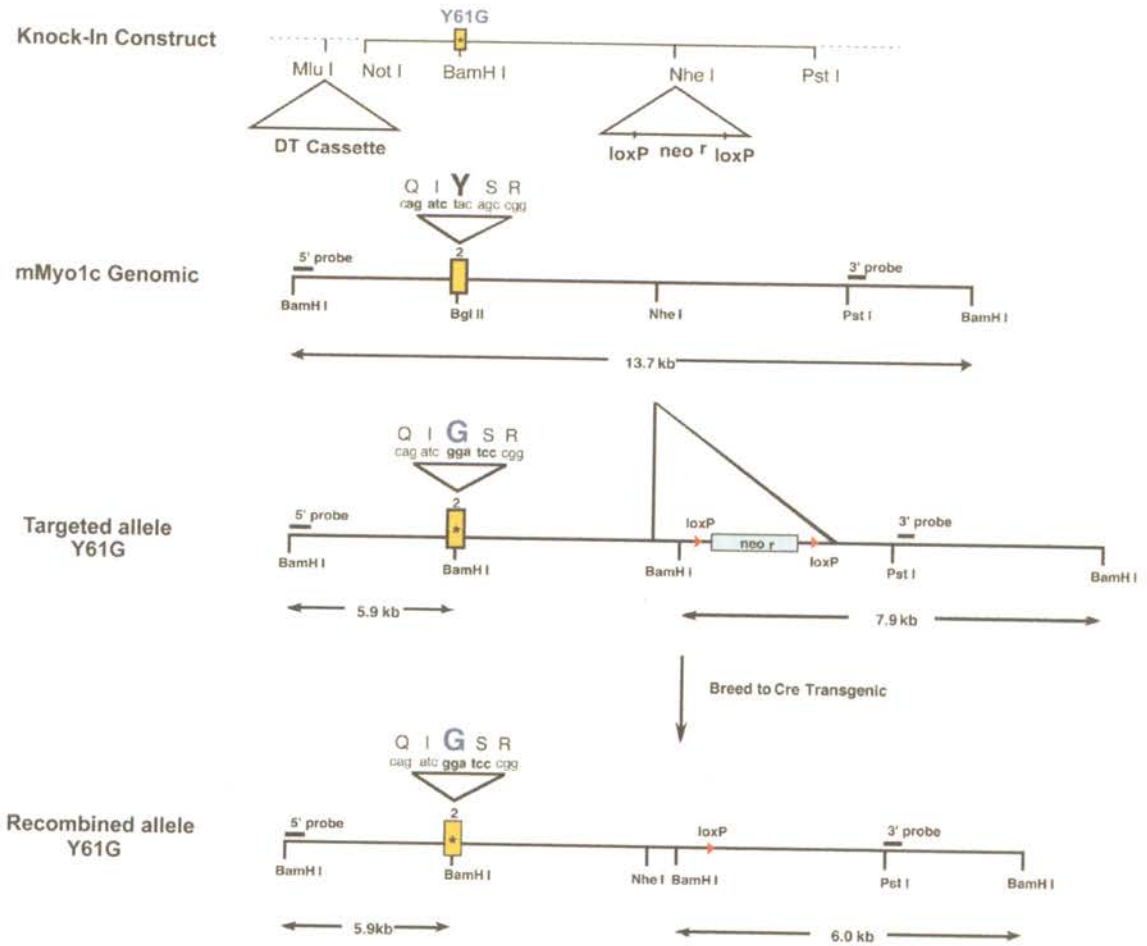
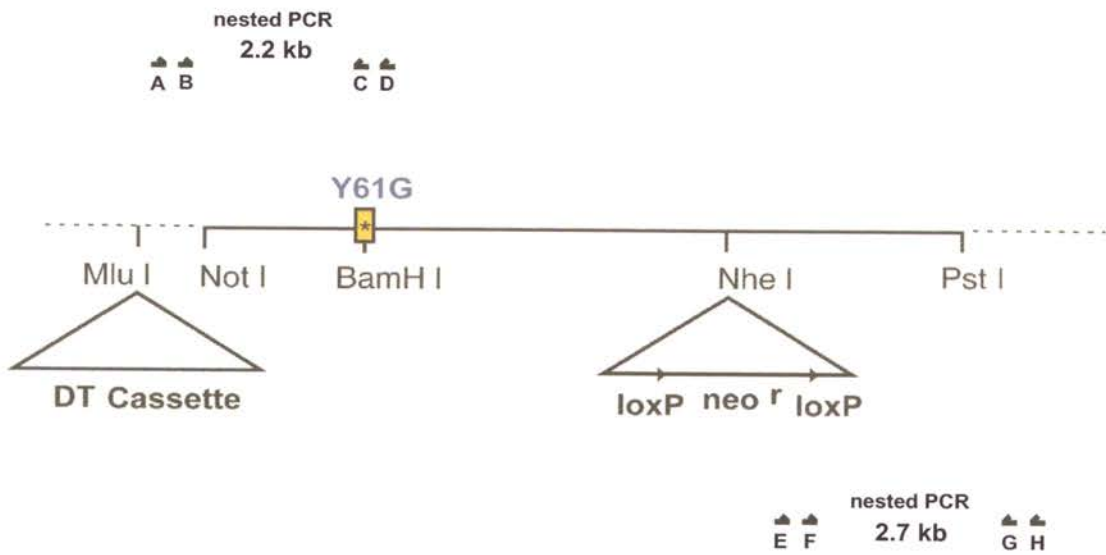


Figure 8. **Nested PCR analysis of ES cell clones.** *A*, The nested PCR screening scheme used to detect homologous recombination at the 5' and 3' junctions between the targeting construct and the endogenous *Myo1c* locus. Genomic DNA from potential ES cell clones was prepared and amplified with outer PCR primers (A/D and E/H) at each junction. Subsequently, inner primers (B/C and F/G) were used to amplify junctional PCR products. Expected sizes for the inner PCR products were 2.2 kb and 2.7 kb for the 5' and 3' junctions, respectively. *B*, An agarose (1.4%) gel showing 2.2 kb inner PCR products amplified from ES cell clones 2B3 and 1G8, indicating correct recombination at the 5' junction between the Y61G knock-in construct and the endogenous *Myo1c* locus. A 1 kb plus DNA marker ladder was loaded in far left lane.

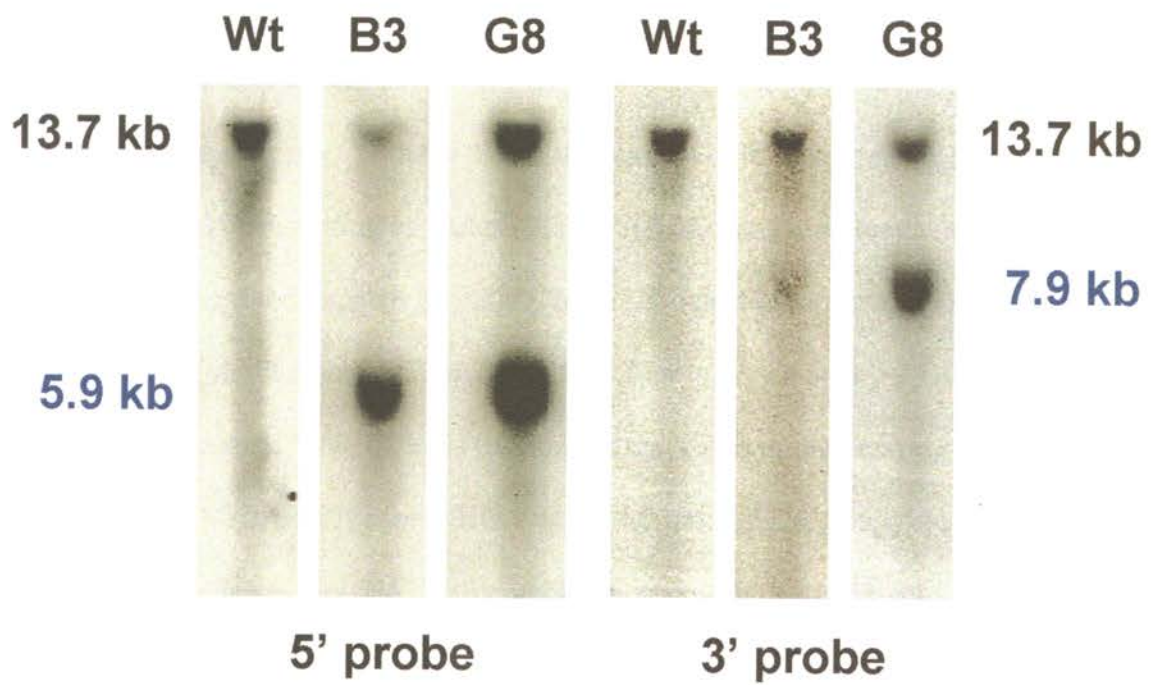
A



B



Figure 9. **Southern analysis of ES cell clones.** Detection of homologous recombination of the Y61G knock-in construct with the endogenous *Myo1c* locus in ES cell clones 2B3 and 1G8. ES cell clones were selected under G418, and 192 clones were cultured on 96-well plates. Genomic DNA from ES cells was digested with *Bam*HI, separated by agarose gel electrophoresis, and probed with 5' and 3' external probes. Expected band sizes: 5' probe – wild-type allele 13.7 kb, targeted (Y61G/Neo) allele 5.9 kb, 3' probe – wild-type allele 13.7 kb, targeted (Y61G/Neo) allele 7.9 kb.



random integrations or multiple insertions; instead, **2B3** and **IG8** subclones were indeed correctly targeted.

Table 1. Southern Probes:

- A. 5' probe [*Bam*HI – *Not* I, 686 bp]
- B. 3' probe [*Pst* I- *Pst* I, 575 bp]
- C. 5' internal probe (*Not* I – *Bgl* II, 778 bp),
- D. 3' internal probe (*Xmn* I – *Xho* I, 1022 bp)
- E. vector probe (*Dra* I- *Nco* I, 645 bp)

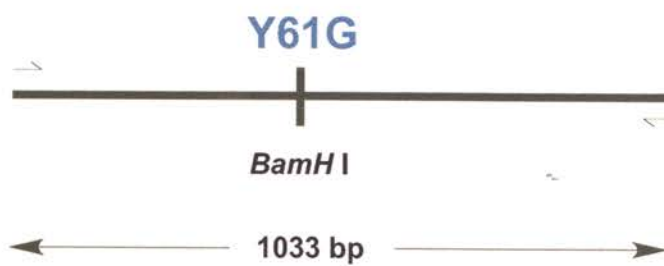
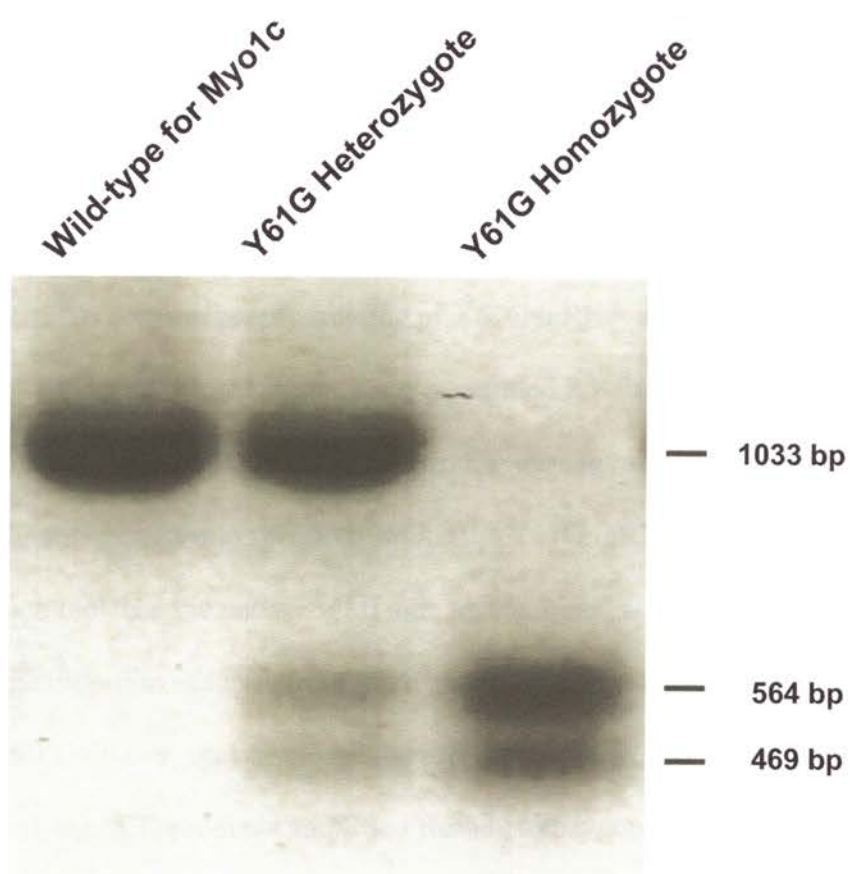
Generating Y61G mice

To generate mice with the Y61G mutation in both *Myo1c* alleles, we electroporated the targeting construct (Fig. 7, 8) into mouse embryonic stem cells (129S4) and injected targeted ES cells (**2B3**, **IG8**) into blastocysts (C57BL6/J). We generated six chimeric males from clone **IG8**, four of which were >90% agouti. One of these males (date of birth 7/23/01) transmitted the Y61G mutation to subsequent generations. Mice positive for Y61G were identified by PCR genotyping (Fig. 10) and crossed with mice expressing Cre recombinase to remove the neomycin cassette, then backcrossed to C57BL6/J mice for twelve generations.

Southern analysis of Y61G mice

We performed Southern blotting at all stages of breeding to confirm the PCR genotyping results and to track the presence and eventual removal of the neo cassette from the single Y61G line. Southern blot analysis of various mouse genotypes demonstrated successful targeting and removal of the neomycin cassette at various stages

Figure 10. **Genotyping Y61G mice.** Genomic DNA was processed from mouse tails of three different genotypes: wild-type, Y61G heterozygote, and Y61G homozygote. A 1033 bp region of *Myo1c* flanking the Y61G site by 469 and 564 bp was amplified using the following primers: gcattccagcatcctgcaacc, cagtgtcagccactgcaaacc. PCR products were subsequently digested with *BamHI*, as the Y61G mutation creates a *BamHI* restriction site, and separated by agarose (1.4%) gel electrophoresis. Predicted product sizes for each genotype were as follows: wild-type - 1033 bp; heterozygous - 1033, 564, 469 bp; homozygous - 564, 469 bp.



of breeding (Fig. 11).

RT-PCR analysis

PCR genotyping and Southern analysis of Y61G mice suggested correct targeting between the knock-in construct and the native *Myo1c* locus. These analyses also implied that neither the Y61G mutation nor the loxP-flanked neomycin cassette in the large intron between exons 4 and 5 (nor the loxP site remaining after neo excision) interfered with RNA transcription. To confirm proper splicing of Y61G mRNA and test for the presence of the Y61G site with an additional strategy, we performed RT-PCR analysis and restriction enzyme digestion on RNA harvested from mouse thymus and brain tissue.

The Y61G homozygous mice properly splice the Y61G mRNA and contain the *BamHI* site, which replaced the native *Bgl* II site. A combined analysis of RT-PCR and restriction enzyme digestion of DNA from three genotypes (wild-type, Y61G heterozygote, Y61G homozygote) disclosed the presence of the Y61G mutation (*BamHI* restriction site) in only PCR products amplified from heterozygous or homozygous samples (thymus, Fig. 12). Moreover, *Bgl* II digested RT-PCR amplified DNA products from only wild-type and heterozygous samples, indicating the absence of the tyrosine 61 (*Bgl* II site) in the homozygous samples. Digestion with *Bgl* II of wild-type sample in Fig. 12 produced two bands (761 bp and 586 bp) instead of an expected single band (586 bp), probably because the digestion did not go to completion. These results were demonstrated in brain RNA from each of the three genotypes as well.

Figure 11. **Southern analysis of Y61G mice.** *A*, Hybridizing region of the 3' external probe (*Pst* I- *Pst* I, 575 bp) and predicted sizes of *Bam*HI-digested genomic DNA fragments from alleles (Wild-type, Y61G/Neo, Y61G). *B*, Southern blot demonstrating successful targeting and Neo removal. DNA from homozygous wild-type, Y61G/Neo, or Y61G mice was digested with *Bam*HI and detected with the 3' external probe (indicated in [A]). *C*, Southern blot of five different mouse genotypes ($Myo1c^{+/+}$, $Myo1c^{+/Y61G,Neo}$, $Myo1c^{Y61G,Neo}$, $Myo1c^{+/Y61G}$, $Myo1c^{Y61G}$). Expected band sizes with the 3' external probe – wild-type allele (13.7 kb), Y61G/Neo allele (7.9 kb), and Y61G allele (6.0 kb).

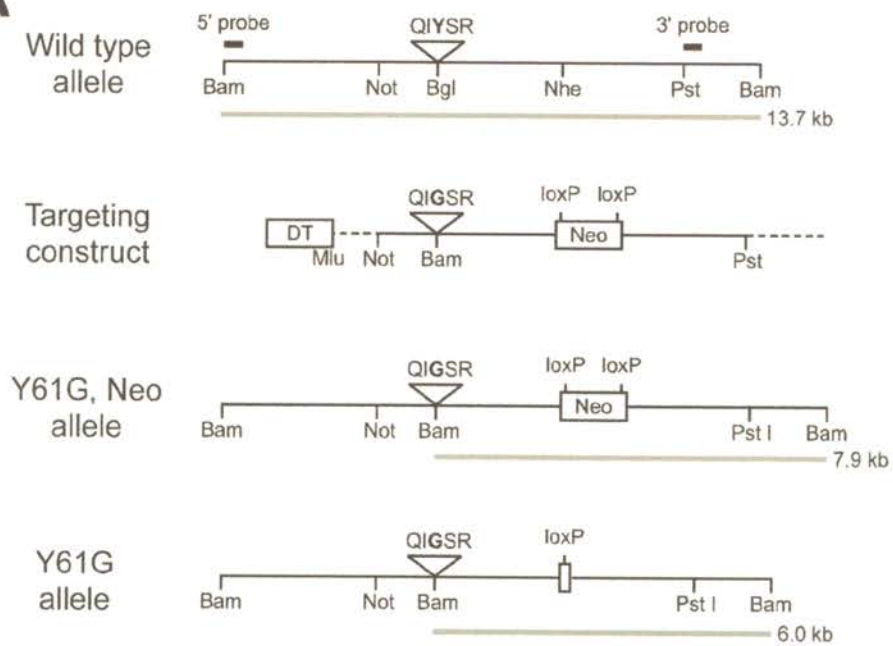
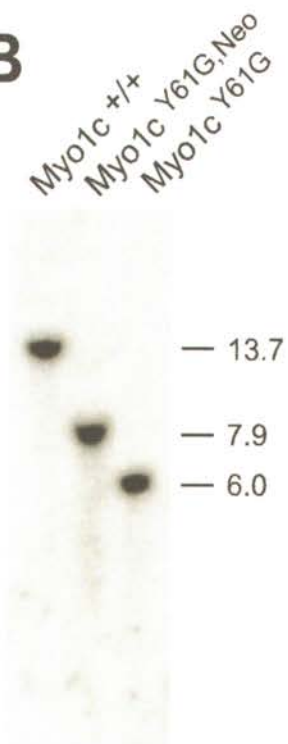
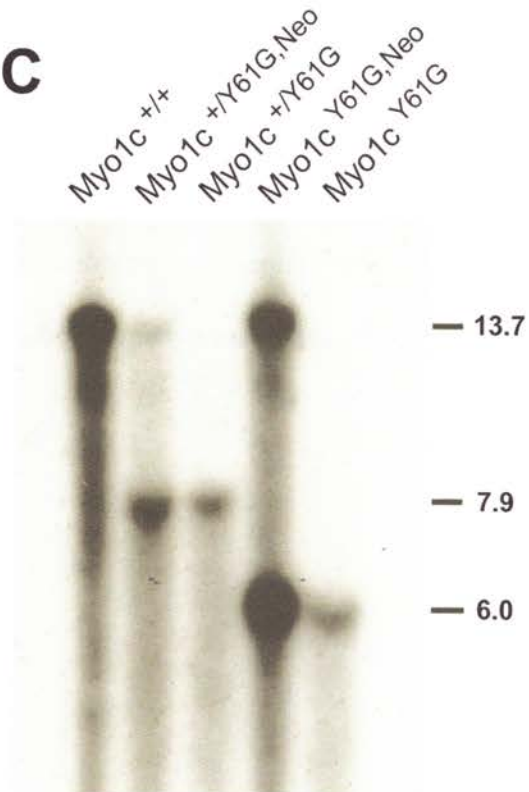
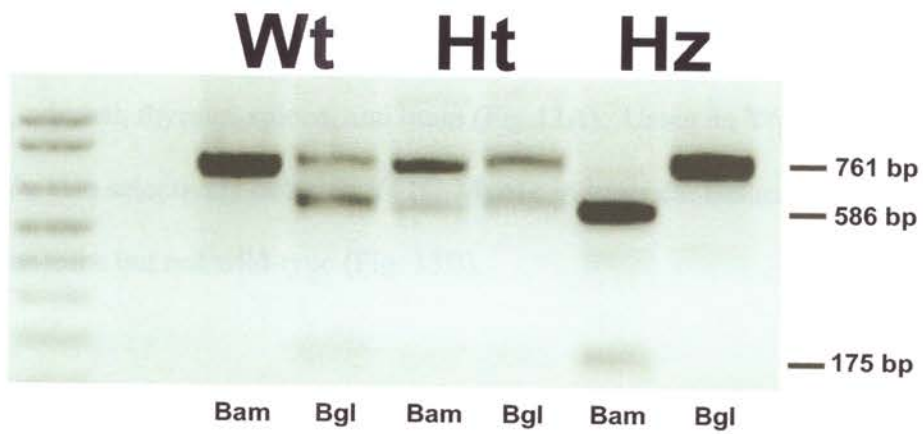
A**B****C**

Figure 12. **RT-PCR analysis of thymus from Y61G and wild-type mice.** Total RNA was processed from mouse thymus of three genotypes: wild-type, Y61G heterozygote, and Y61G homozygote. RNA was reverse-transcribed to cDNA. A 761 bp region of *Myo1c* flanking the Y61G site by 586 and 175 bp was amplified using the following primers: gag agc gcc ttg act gcc cga gac, agc gcc ttc ctc ata acc ttc cag tc. PCR products were subsequently digested with a restriction enzyme (either *Bam*HI or *Bgl* II), as the Y61G mutation creates a *Bam*HI restriction site while the wild-type sequence retains a *Bgl* II site. Digestion of PCR products went to completion except for the wild-type sample treated with *Bgl* II. Digested products were separated by agarose (1.4%) gel electrophoresis. Predicted product sizes for each genotype with *Bam*HI were as follows: wild-type - 761 bp; heterozygous - 761, 586, 175 bp; homozygous - 586, 175 bp.



Immunoblot analysis of tissues for Y61G expression

To inspect the Myo1c expression in Y61G homozygous mice in comparison with wild-type littermates, we used an antibody specific for Myo1c (R2652) and performed immunoblotting on whole organ extracts from multiple tissues. Equal amounts (1-5 μ g per sample) of protein extracts were loaded onto gels. Analysis demonstrated nearly equal band intensities between mutant and wild-type organ samples, indicating equivalent Myo1c expression in all tissues examined (figure 10A). Blot analysis also revealed that the Y61G-mMyo1c allele encodes a full-length \sim 120 kD protein, indicating that no stop codons were unintentionally introduced in the targeting vector. In the tissues sampled, Myo1c expression level was found in the following descending order of abundance: heart, lung, adrenal, thymus, spleen, and brain (Fig.13A). Using an Y61G-specific antibody, we also selectively detected Y61G-Myo1c in inner ear tissues from homozygous mice but not wild-type (Fig. 13B).

ABR analysis

Auditory-evoked brainstem responses were performed to determine whether Y61G homozygous mice hear normally, i.e., at a comparable level with wild-type C57BL/6J controls. Indeed, comparable auditory brainstem response (ABR) thresholds were observed across all frequency and stimulus intensities tested in the Y61G homozygotes and wild-type controls (C57BL6/J) at age P23 (Fig. 14). Both Y61G and C57BL/6J control mice had normal ABRs. These results suggest that the Y61G-Myo1c allele behaves similarly to wild-type Myo1c in the auditory system. The Y61G mice were backcrossed to C57BL/6J (>12 generations). Although C57BL/6 mice suffer age-

Figure 13. **Protein immunoblot analysis of Myo1c expression in tissues from wild-type and Y61G mice.** *A*, Immunoblotting of mouse tissues with R2652, a mouse Myo1c specific antibody. Equal amounts of total protein from wild-type or homozygous Y61G mice were loaded (~5µg per lane). Myo1c position (~120 kDa) indicated. Band intensities were similar between genotypes across all tissues sampled, indicating equivalent Myo1c expression in Y61G mice compared to wild-type controls. The relative level of Myo1c expression was as follows: heart, lung, adrenal, thymus, spleen, brain. Twenty ear equivalents (cochlea, utricle) were loaded per lane for inner tissues. *B*, Immunoblot analysis with R6765, an antibody selective for the mutant (mouse Y61G) sequence. Equal amounts of total protein from wild-type or homozygous Y61G mice were loaded on the same gel. Cochlea lanes were exposed to film for 20 s and vestibule lanes for 120 s.

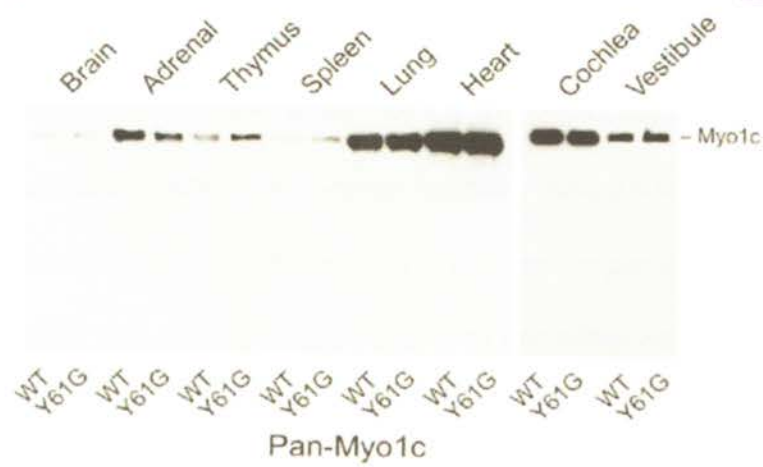
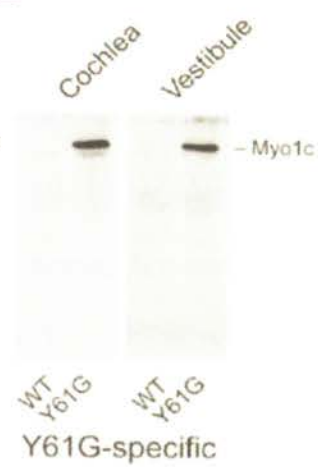
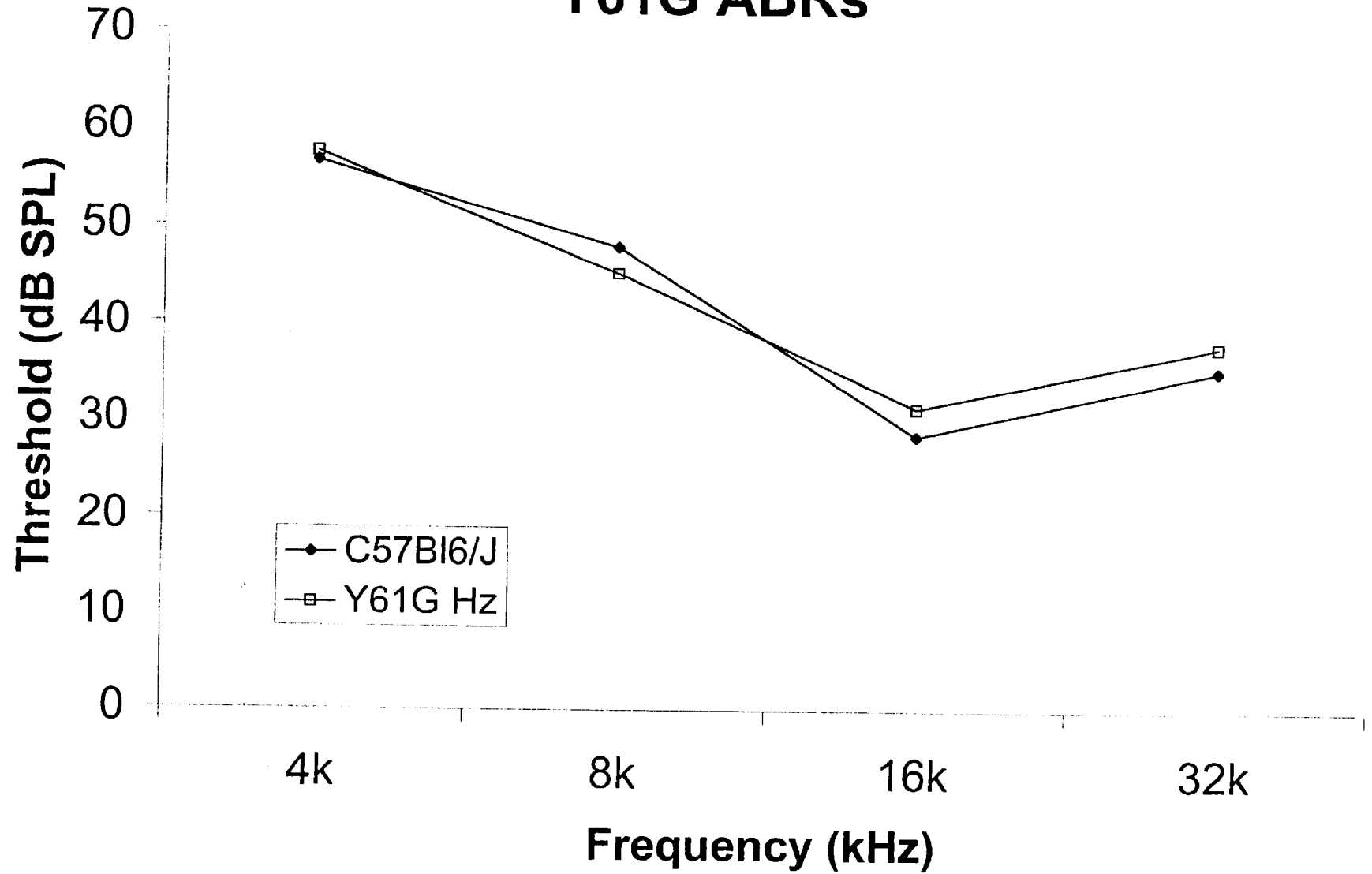
A**B**

Figure 14. **Auditory-evoked brainstem response analysis of Y61G mice.** ABR audiometry to pure tones was used to evaluate cochlear function of wild-type (C57BL6/J) and Y61G homozygous mice aged P23. Auditory-evoked brainstem responses (ABRs) were elicited to tone-burst stimuli at 4, 8, 16, and 32 kHz and thresholds were obtained from left ears to determine cochlear function. Animals were tested with low intensity stimulus trains. Comparable auditory brainstem response (ABR) thresholds were observed across all frequency and stimulus intensities tested in the Y61G homozygotes and wild-type controls (C57BL6/J). Both Y61G and control mice had normal ABRs.

Y61G ABRs



related hearing loss due to the *ah11* mutation of cadherin 23, the electrophysiology experiments (described later in this chapter) used early postnatal mouse pups with no hearing loss (Keithley et al., 2004). Perhaps measuring distortion products of otoacoustic emission (DPOAEs) would reveal a difference between Y61G mice and controls.

Y61G Biochemistry

Expression and purification of mouse Myo1c (wild-type and Y61G)

Rat Myo1c was used previously to characterize the Y61G mutation (Gillespie et al., 1999). Mouse Myo1c differs from rat Myo1c at several residues, including residue 62 (Thr in rat, Ser in mouse); therefore, the inhibition of Myo1c activity by NMB-ADP was re-investigated. Full-length wild-type and Y61G-mouse Myo1c were expressed in *Sf9* cells using baculoviruses and purified by Ni²⁺-NTA chromatography.

As detailed in the Materials and Methods, the BaculoDirect system (Invitrogen, Carlsbad, CA.) proved to be a rapid, convenient method for generating mouse Myo1c baculoviruses, taking about five weeks to manufacture 200 mls of high-titer P3 viral stocks from starting plasmids. Two different high-titer P3 viral stocks were generated for each myosin – wild-type Myo1c (clones # 1, 5); Y61G-mouse Myo1c (clones #2, 4). Because the purity, recovery, and activity (~7 days) of Myo1c were the same between clones, all four P3 viral stocks were used to produce Myo1c pellets for the ATPase and *in vitro* motility experiments described below.

To produce Myo1c, *Sf9* cells were co-infected with Myo1c and calmodulin viruses at a multiplicity of infection of 4:2 (Gillespie et al., 1999), then harvested 48

hours later because longer incubations reduced overall yield (as was determined empirically). Cell pellets were processed immediately by Ni²⁺-NTA chromatography or were frozen at -80°C. When frozen pellets were used, they were processed within two weeks of freezing because storage more than five weeks resulted in lower yields of functional Myo1c.

A typical Ni²⁺-NTA purification took four to five hours, mostly due to the time spent waiting for the high-speed supernatant and flow-through to pass through a Ni²⁺-NTA column. Preparations of 400-ml cultures (~6.4 × 10⁸ cells) yielded ~200 ug of protein, >90% of which was Myo1c. A Bradford test was done on individual Ni²⁺-NTA eluates (#1-5) to quickly estimate best protein yield. In each case, recovery was greatest in eluates #2 and #3 with a characteristic purity of Myo1c >90%, as assessed by Coomassie Blue-stained, SDS-PAGE.

NMB-ADP inhibited Y61G-Myo1c

Mouse Myo1c proteins were evaluated for their actin-activated ATPase activity (Pollard, 1982). Because the purity of Myo1c in the Ni²⁺-NTA eluates was >90%, it was assumed that most or all of the actin-activated ATPase activity in a Ni²⁺-NTA eluate came exclusively from Myo1c. Therefore, Ni²⁺-NTA eluates were used as the source of Myo1c in ATPase assays. To account for the intrinsic ATPase activity of actin and its inhibition by adenine nucleotides, assays were performed with control samples containing actin and appropriate nucleotides but no Myo1c.

Y61G-mMyo1c hydrolyzed ATP with a slightly lower K_m (9 ± 2 μM; n=4) than did Wt-mMyo1c (17 ± 5 μM; n=4), indicating that wild-type and Y61G-mMyo1c

hydrolyzed ATP to a similar degree (Fig. 15, 16). The maximal ATP hydrolytic rate (V_{\max}) of wild-type mMyo1c and Y61G-mMyo1c stored on ice was stable for ~ 7 days, but almost all of the ATPase assays were conducted within 36 hours of purification. When Ni^{2+} -NTA eluates were used within this timeframe (1-2 days), the V_{\max} of ATP hydrolysis by Y61G-mouse Myo1c was about 1.2-fold greater than that of wild-type mouse Myo1c. These results somewhat agree with the maximum velocity of ATP hydrolysis by rat Y61G-Myo1c, which was 1.4-fold greater than the V_{\max} of rat wild-type Myo1c (Gillespie et al., 1999),

NMB-ADP selectively blocked Y61G ATPase activity (IC_{50} of 1.6 μM versus 168 μM for wild-type) [Fig. 17]. Nearly ~160-fold more NMB-ADP was required to inhibit the ATPase activity of Wt-Myo1c ($K_i = 119 \pm 10 \mu\text{M}$; $n=4$) than Y61G ($0.75 \pm 0.1 \mu\text{M}$; $n=4$) [Fig. 18, 19], indicating that NMB-ADP was a potent inhibitor of mouse Y61G-Myo1c ATPase activity. This high degree of selectivity is more than that observed previously for rat wild-type and Y61G Myo1c (~59-fold), where selectivity is defined as the ratio of wild-type to Y61G K_i values. Based on these results, the mutant-inhibitor combination was deemed appropriate for investigation of the function of mouse Myo1c. The effect of NMB-ADP on the ability of Wt-Myo1c and Y61G-Myo1c to power actin filaments was examined using an in vitro motility assay. NMB-ADP selectively blocked the in vitro motility of Y61G (E. Miller, results). Motility rates for Wt-mMyo1c or Y61G-mMyo1c were 12 $\mu\text{m/s}$ versus 25 $\mu\text{m/s}$ in 2 mM ATP; 11 $\mu\text{m/s}$ versus 2 mm/s in 2 mM ATP and 0.25 mM NMB-ADP [Fig. 20].

Figure 15. **Actin-activated ATPase activity of Wt-mMyo1c.** Wt-mMyo1c was expressed with baculoviruses in *Sf9* cells and purified on Ni²⁺-NTA agarose; ATPase assays were carried out with 10 μ M ATP. Y61G-mMyo1c hydrolyzed ATP with a K_m ($17 \pm 5 \mu$ M; n=4). Plots were fit with the equation $V = (V_{max} [ATP])/([ATP] + K_m)$. ATPase activity (nmol/min) vs. [ATP] is plotted. Shown are four experiments (A, B, C, D).

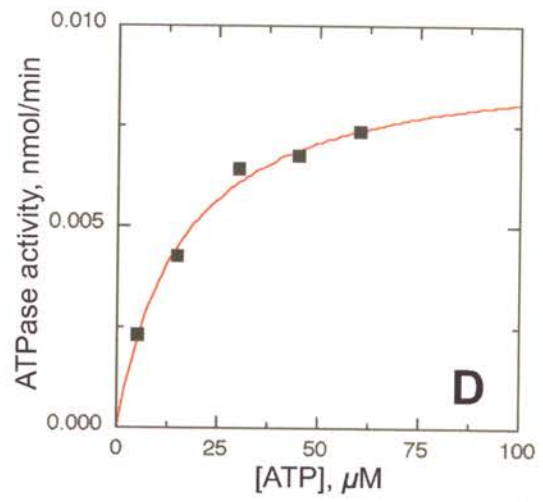
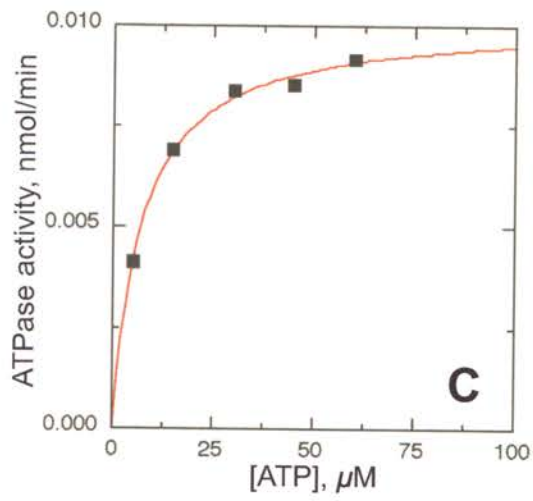
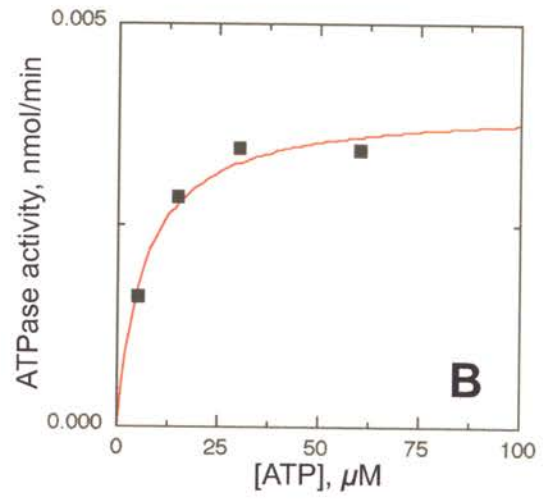
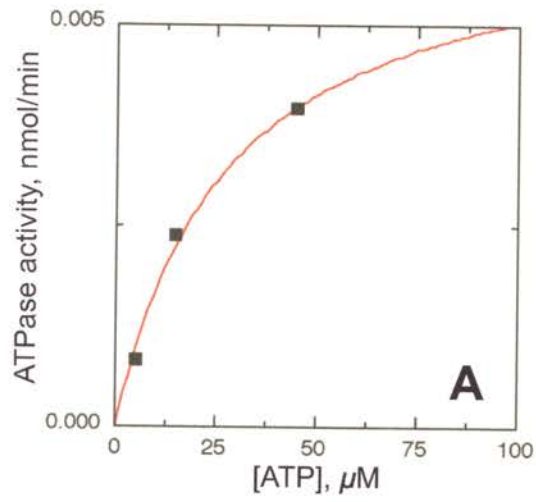


Figure 16. **Actin-activated ATPase activity of Y61G-mMyo1c.** Y61G-mMyo1c was expressed with baculoviruses in *Sf9* cells and purified on Ni²⁺-NTA agarose; ATPase assays were carried out with 10 μM ATP. Y61G-mMyo1c hydrolyzed ATP with a K_m (9 ± 2 μM; n=4). Plots were fit with the equation $V = (V_{max} [ATP])/([ATP] + K_m)$. ATPase activity (nmol/min) vs. [ATP] is plotted. Shown are four experiments (A, B, C, D).

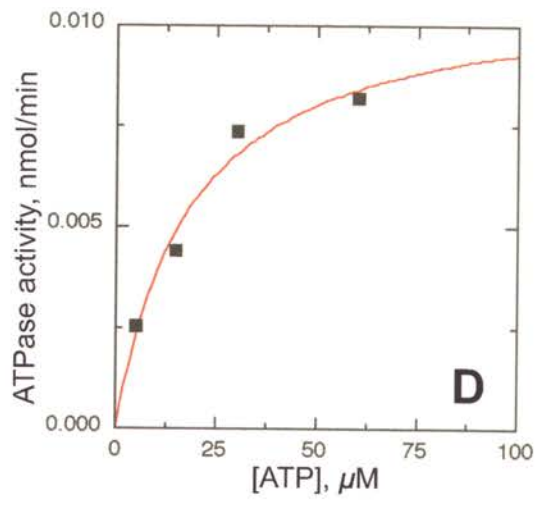
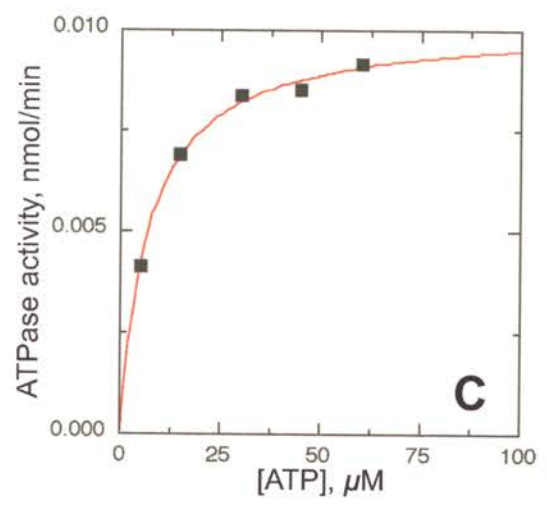
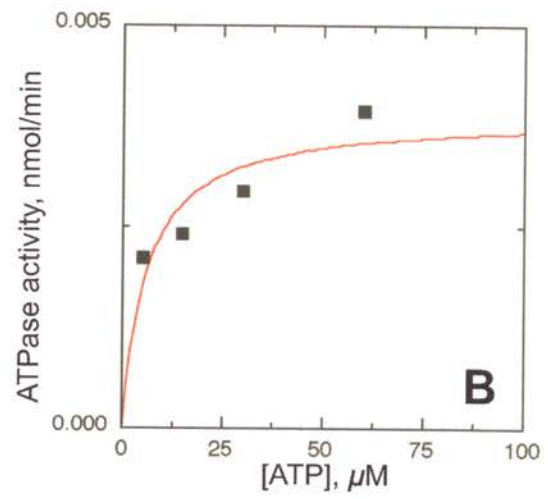
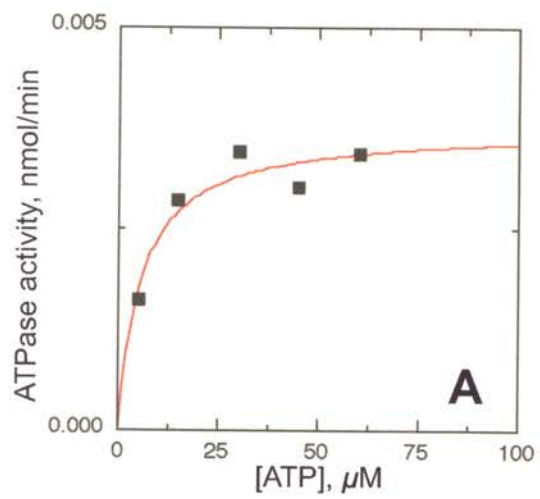


Figure 17. **Inhibition of ATPase activity by NMB-ADP.** Wild-type and Y61G-mouse Myo1c were expressed with baculoviruses in *Sf9* cells and purified on Ni²⁺-NTA agarose; ATPase assays were carried out with 10 μM ATP. Actin-activated ATPase activity of Y61G was selectively inhibited by NMB-ADP (IC_{50s} 1.6 μM vs. 168 μM for Y61G and wild-type, respectively).

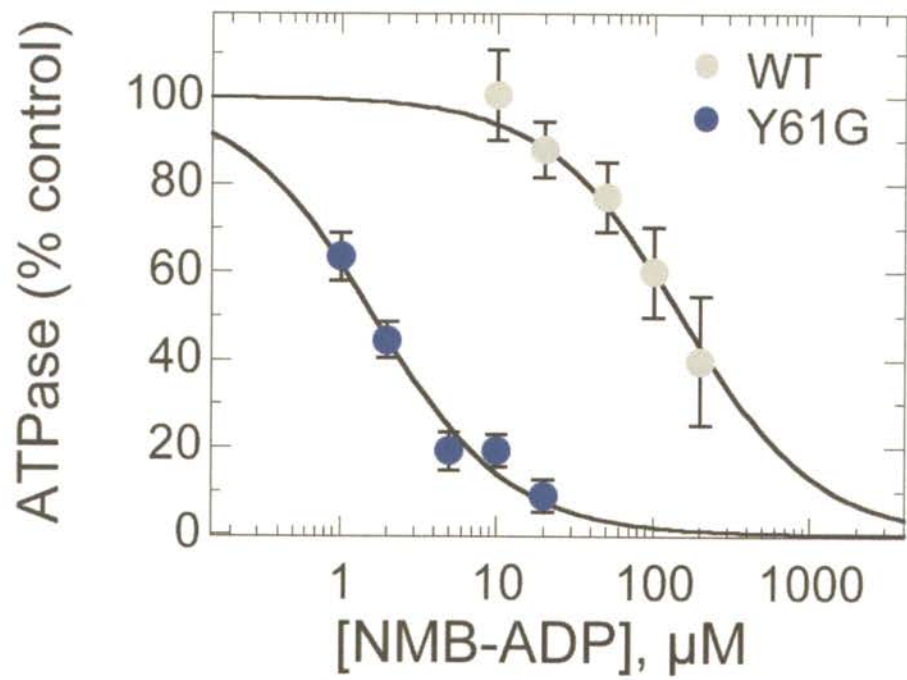


Figure 18. **NMB-ADP inhibition of Wt-mMyo1c ATPase activity.** Wild-type mMyo1c was expressed with baculoviruses in *Sf9* cells and purified on Ni²⁺-NTA agarose; ATPase assays were carried out with 10 μ M ATP. Wt-mMyo1c hydrolyzed ATP with a K_i ($119 \pm 10 \mu$ M; n=4). Myo1c% is plotted vs. [NMB-ADP], μ M. Plots were fit with the equation: velocity (% control) = $(V_{max}) * (1 - [NMB-ADP] / [NMB-ADP] + IC_{50})$. Shown are four experiments (A, B, C, D).

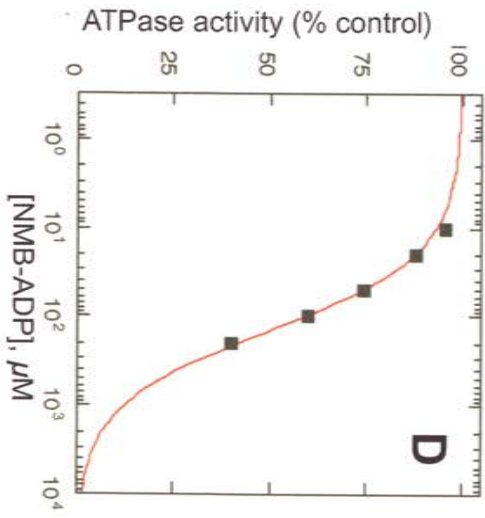
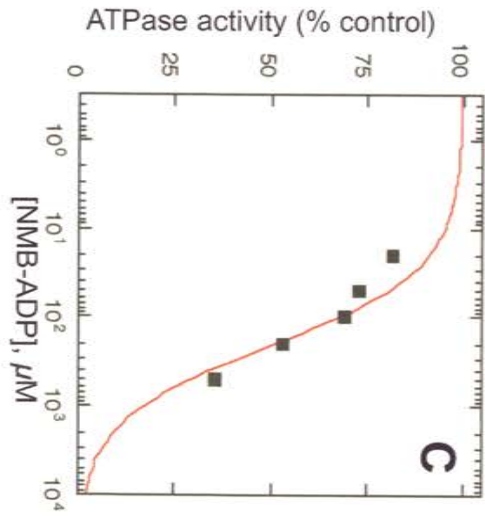
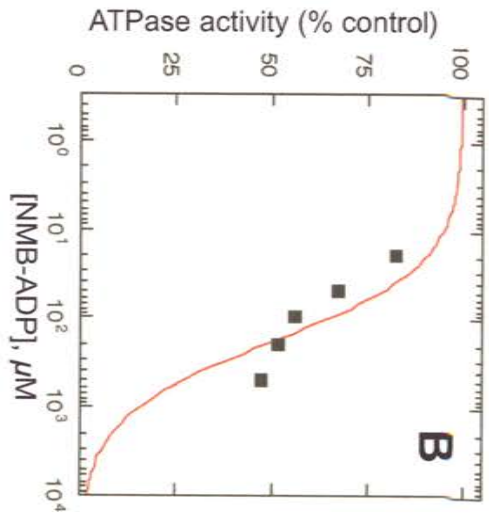
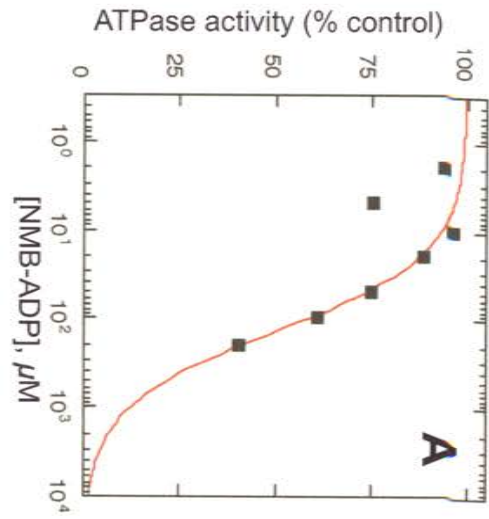


Figure 19. **NMB-ADP inhibition of Y61G-mMyo1c ATPase activity.** Y61G-mMyo1c was expressed with baculoviruses in *Sf9* cells and purified on Ni²⁺-NTA agarose; ATPase assays were carried out with 10 μM ATP. Y61G-mMyo1c hydrolyzed ATP with a K_i (0.75 ± 10 μM; n=4). Myo1c% is plotted vs. [NMB-ADP], μM. Plots were fit with the equation velocity (% control) = (V_{max})*(1-[NMB-ADP]/[NMB-ADP] + IC₅₀). Shown are four experiments (A, B, C, D).

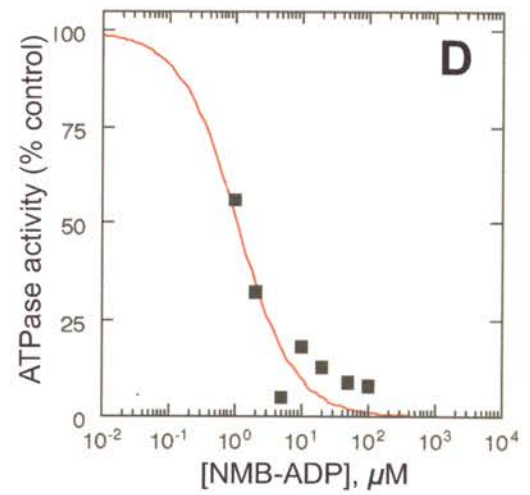
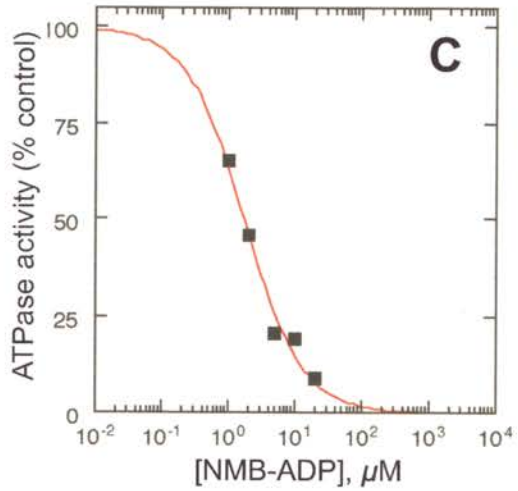
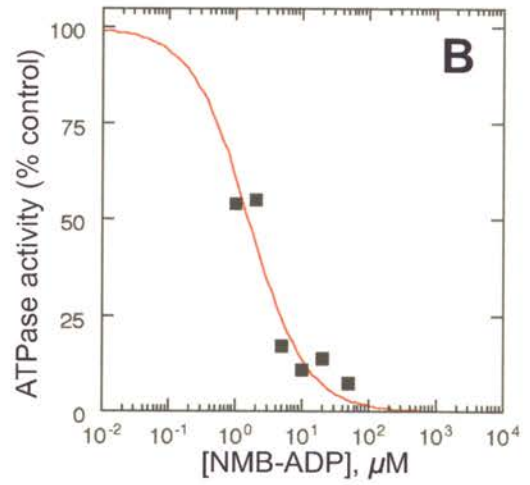
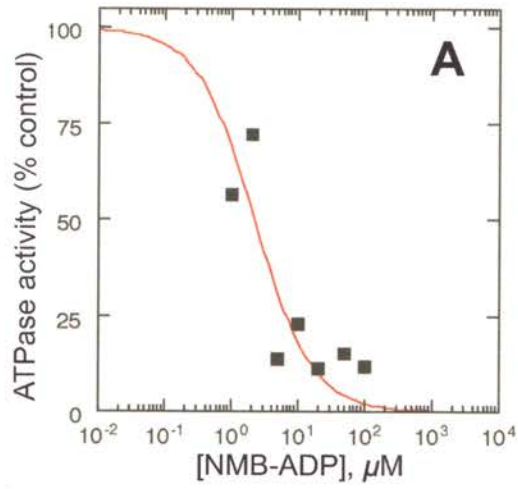
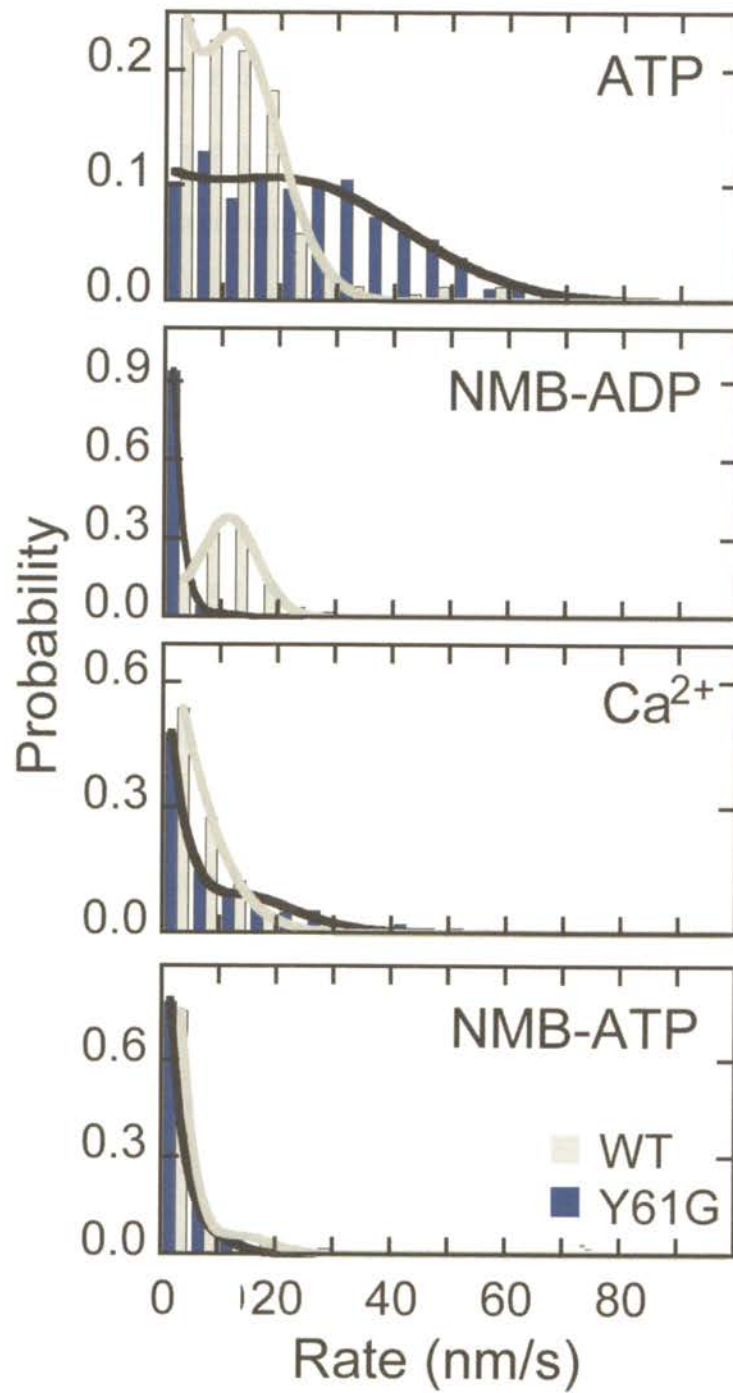


Figure 20. **In vitro motility of Myo1c.** Wild-type and Y61G-mMyo1c were expressed with baculoviruses in *Sf9* cells, then purified on Ni²⁺-NTA agarose and actin cycling. Motility assays were carried out using the following solutions: ATP, 2mM ATP, 1 mM EGTA; NMB-ADP, 2mM ATP, 250 μ M NMB-ADP, 1 mM EGTA; Ca²⁺, 2 mM ATP, 0.1 mM CaCl₂; NMB-ATP, 2mM NMB-ATP, 1 mM EGTA. Rates (nm/s) of actin filament motility were measured on coverslips coated with recombinant wild-type or Y61G-mMyo1c in the presence of ATP, NMB-ADP, calcium, or NMB-ATP. For wild-type and Y61G-mMyo1c, rates were ~12.4 nm/s vs. ~25.0 nm/s in [2 mM ATP, 1 mM EGTA] and ~11.0 nm/s vs. ~2.7 nm/s in [2 mM ATP, 0.25 mM NMB-ADP]. Motility assays were performed by Emilie Miller.



Electrophysiology

Adaptation in Y61G utricular hair cells

To determine whether Myo1c plays a role in fast adaptation, Y61G homozygous and C57BL/6 utricular hair cells were either treated with 250 μ M NMB-ADP or a control solution while recording transduction currents. Whole epithelia from utricles were isolated, and hair bundles were mechanically stimulated with stiff glass probes while adaptation was measured by whole-cell voltage-clamp recording. Under control conditions (no NMB-ADP), amplitudes of transduction currents in Y61G hair cells were similar to those measured in wild-type cells (Fig. 21 A, B).

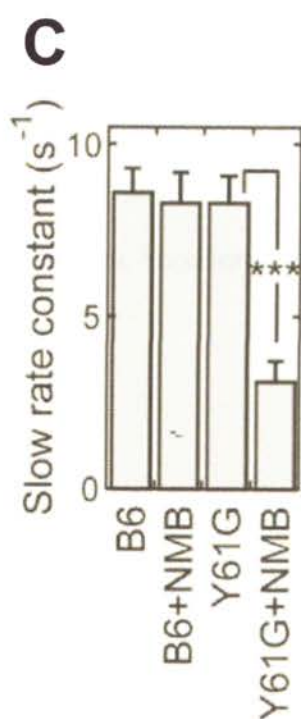
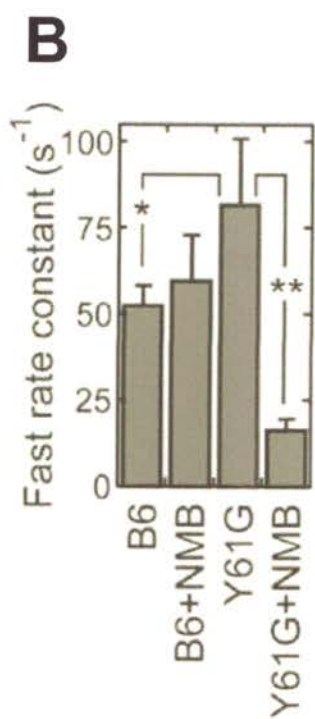
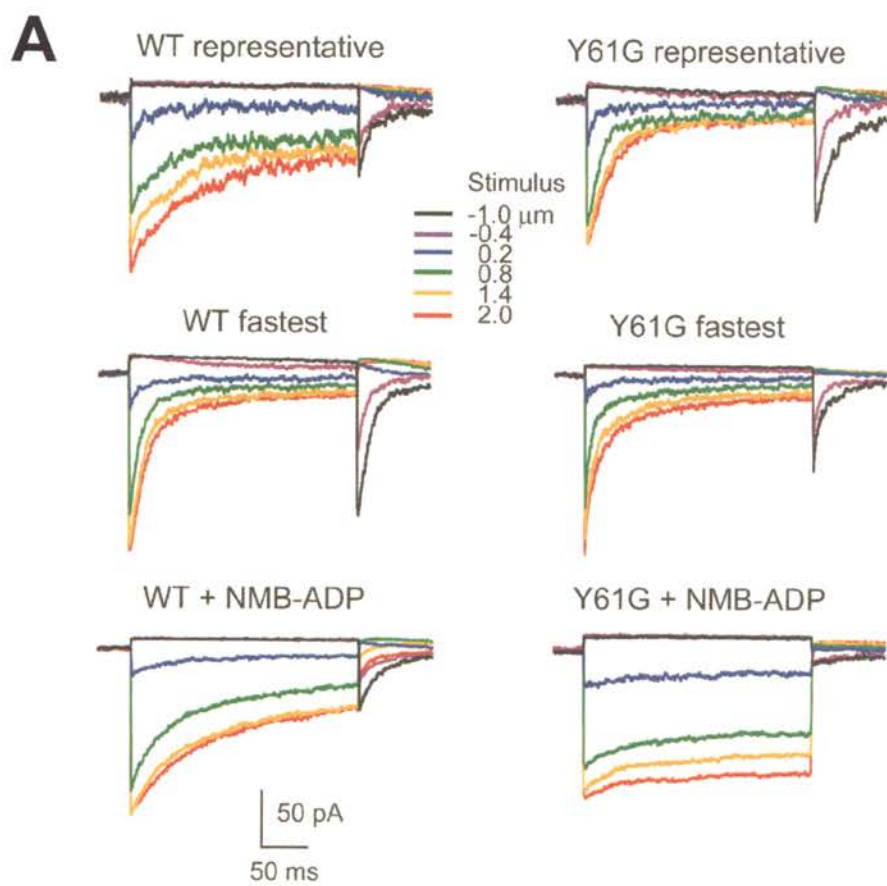
Fast adaptation, however, was significantly faster in Y61G hair cells than in wild-type hair cells (Fig. 21A). Fast positive adaptation in Y61G hair cells (16 cells; rate constant of $82 \pm 19 \text{ s}^{-1}$) was about twice that of wild-type hair cells, whether from pooled wild-type hair cells (31 cells; $46 \pm 8 \text{ s}^{-1}$) or genotyped-matched C57BL/6 ones (22 cells; $53 \pm 6 \text{ s}^{-1}$). Rate constants for slow positive adaptation in Y61G hair cells ($8.3 \pm 0.8 \text{ s}^{-1}$) were similar to those measured in wild-type cells ($9.3 \pm 1.2 \text{ s}^{-1}$) or C57BL/6 cells ($8.6 \pm 0.8 \text{ s}^{-1}$). These experiments were performed by Eric Stauffer and Jeff Holt.

NMB-ADP inhibits fast and slow positive adaptation rates in utricular Y61G hair cells

NMB-ADP had little effect on adaptation or transduction in C57BL/6 control cells (Fig. 21). By contrast, dialysis of 250 μ M NMB-ADP substantially slowed fast positive adaptation in Y61G hair cells – by roughly 80%. The rate constants for fast adaptation with and without the analog were $82 \pm 19 \text{ s}^{-1}$ vs. $16 \pm 3 \text{ s}^{-1}$. In agreement with

Figure 21. **Adaptation is slowed by NMB-ADP in Y61G but not wild-type hair cells.**

A, Examples of transduction currents in Wt and Y61G hair cells. In both cases, a representative example (top) and the fastest cell in the dataset (middle) are shown for cells filled with control dialysis solutions. In the bottom row, representative cells dialyzed with 250 μ M NMB-ADP are shown. *B*, Rate constants for fast positive adaptation using linear displacement-rate fits B6=C57BL/6. $p=0.11$; $p<0.001$. *C*, Rate constants for slow positive adaptation using linear displacement-rate fits. $p<0.0001$. Rates of fast and slow adaptation during dialysis of utricular hair cells from Y61G or control mice dialyzed with or without 250 μ M NMB-ADP. Both fast and slow adaptation are affected by NMB-ADP. Electrophysiology experiments were performed by Eric Stauffer.



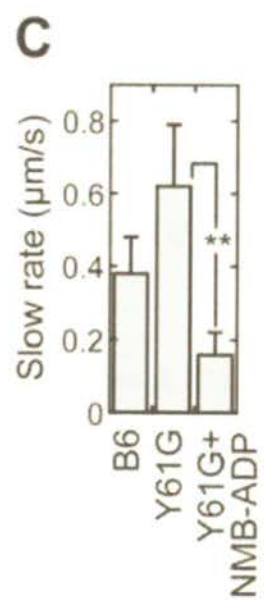
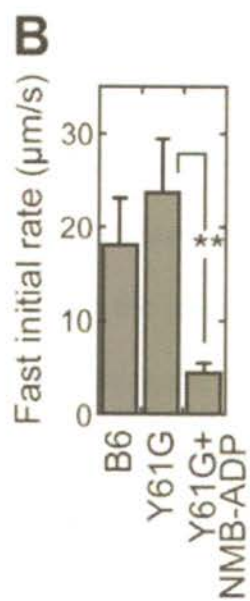
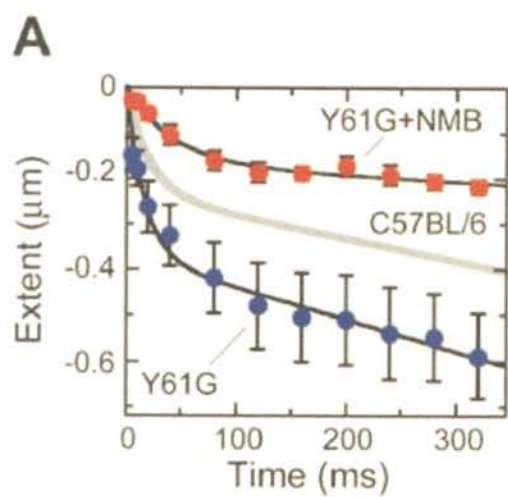
previous experiments performed in conventional Y61G transgenic hair cells (Holt et al., 2002), NMB-ADP reduced the rate constant of slow positive adaptation ($8.3 \pm 0.8 \text{ s}^{-1}$ vs. $3.1 \pm 0.5 \text{ s}^{-1}$). The robust inhibition of both slow and fast positive adaptation in Y61G homozygous cells implies that Myo1c mediates both phenomena. These experiments were performed by Eric Stauffer and Jeff Holt.

NMB-ADP slows negative adaptation in utricular Y61G hair cells

When hair bundles are given negative displacements - i.e., pushed away from the tallest stereocilia - external forces are removed from adaptation motors, allowing them to climb up stereocilia at a constant rate. Negative displacements to Y61G homozygous hair cells revealed that slow negative adaptation was nearly twice as fast as wild-type (Fig. 22, $0.37 \pm 0.04 \text{ }\mu\text{m/s}$ for Wt; $0.62 \pm 0.17 \text{ }\mu\text{m/s}$ for Y61G), which agrees with the faster motility rate of Y61G (Fig. 20). Fast negative adaptation in Y61G hair cells was nearly one-third faster than C57BL/6 cells ($24 \pm 6 \text{ }\mu\text{m/s}$; $18 \pm 3 \text{ }\mu\text{m/s}$).

NMB-ADP inhibited fast and slow negative adaptation rates by $\sim 80\%$ (Fig. 22). Like its effects on positive adaptation, NMB-ADP inhibited both fast and slow negative adaptation in Y61G hair cells, indicating that Myo1c is intimately involved in both processes. These experiments were performed by Eric Stauffer and Jeff Holt.

Figure 22. **Fast and slow negative adaptation are slowed by NMB-ADP in Y61G utricular hair cells.** *A*, Negative adaptation from Y61G utricular hair cells dialyzed either with a control solution or with 250 μM NMB-ADP. Overshoots were converted to adaptation extent by comparison with the current-displacement curve. Data points were fit with sum exponential and linear functions. The gray line is C57BL6 control data. *B*, Fast (exponential) negative adaptation initial rates. **** $p < 0.05$** . *C*, Slow (linear) negative adaptation rates. Y61G, $0.62 \pm 0.17 \mu\text{m/s}$ (n=9); Y61G + NMB-ADP, $0.12 \pm 0.07 \mu\text{m/s}$ (n=7). Electrophysiology experiments were performed by Eric Stauffer.



DISCUSSION

As hoped, Y61G homozygous knock-in mice displayed no detectable abnormalities in the auditory system, as confirmed by normal auditory brainstem (ABR) responses. Nor did they demonstrate overt behavioral defects in the vestibular system. Moreover, Y61G homozygous mice properly splice Myo1c mRNA and produce wild-type levels of Myo1c protein in tissues that express Myo1c, including the cochlea and utricle. Biochemically, mouse Y61G behaved nearly the same as wild-type Myo1c in motility and ATPase assays, yet was potently inhibited by NMB-ADP. Taken together, these results suggest that Y61G knock-in mice in combination with NMB-ADP are suitable for studying Myo1c-dependent processes in the inner ear.

Early crosses of Y61G mice to C57BL/6 mice (generations F2 through F4) produced a subset (~10-20%) of heterozygotes and homozygotes with abnormally sparse hair around the face and back – giving mice an “Eddie Munster widow-peak phenotype”. Alopecia and hair thinning, however, were not detected in any of the subsequent generations. Differences in genetic background between early and later mouse generations might explain the coat features observed in the F2-F4s, or perhaps, an innocuous, skin-specific pathogen may have transiently infested the room in which the mice were housed during early backcrossing to C57BL/6 mice. This type of hair loss in mice is occasionally observed in the OHSU mouse facility (Dee Horne, Kamm Prognay, personal communication).

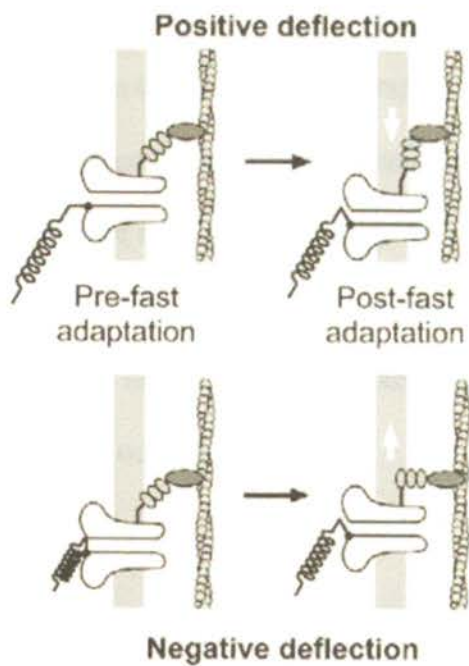
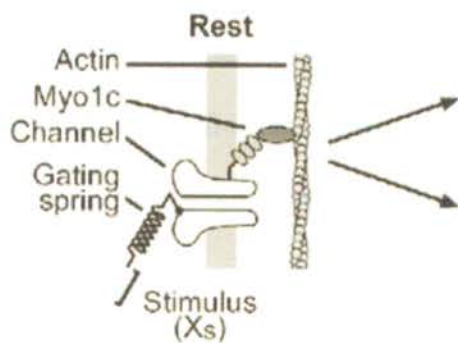
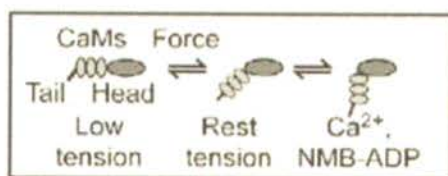
Analysis of transduction records from homozygous Y61G vestibular hair cells suggests that Myo1c mediates slow and fast adaptation in the utricle. As noted

previously (Gillespie et al., 1999; Holt et al, 2002), the “climbing” adaptation rate (i.e., slow linear negative adaptation rate) for Y61G knock-in hair cells was faster than wild-type (31 vs. 19 nm/s) and was similar to the rates measured using the in vitro motility assay (25 and 12 nm/s), suggesting that no other myosin isoform participates in slow adaptation.

Surprisingly, fast adaptation in vestibular hair cells requires Myo1c, which probably functions as a release element that “rocks” while remaining attached to actin during fast adaptation. Under control conditions, fast adaptation occurred more quickly in homozygous Y61G hair cells to either positive or negative stimuli, indicating that the molecular properties of Myo1c directly influence the rates of fast adaptation. Moreover, NMB-ADP slowed fast adaptation by more than 80% in Y61G knock-in cells, suggesting that when NMB-ADP is bound to the nucleotide-binding pocket of Y61G it affects its mechanical transitions, which underpin fast adaptation. Perhaps NMB-ADP forces Y61G-Myo1c into a conformation such that Ca^{++} can no longer trigger fast adaptation (Fig. 23). The NMB-ADP bound could either prevent the mechanical change in Y61G that causes fast adaptation or could promote the change prior to stimulation, inducing Y61G-Myo1c into a pre-stimulus configuration similar to the mechanical state when Ca^{++} is bound. The rocking behavior that Myo1c undergoes during fast adaptation should not depend on changes in acto-myosin interactions when Myo1c transits its ATPase cycle, but rather should rely on the speed of entry and exit of Ca^{++} and its binding kinetics for Myo1c.

Figure 23. Model for fast adaptation in response to positive and negative stimuli.

Force (downward in diagram) rotates the lever arm (extended IQ domains that bind calmodulin molecules [CaMs]). By reducing crossbridge stiffness, Ca^{2+} or NMB-ADP produces further rotation of lever arm under tension. During a positive deflection, tension in the gating spring increases; entering Ca^{2+} triggers lever arm movement. Tension decreases, allowing channels to close. Slow positive adaptation occurs as Myo1c molecules detach and reattach cyclically to further reduce tension (not shown). During a negative deflection, reduced gating spring tension (and reduction in intracellular Ca^{2+}) allows lever arm to rotate to the zero-force state, producing fast negative adaptation. Tension increases modestly in gating spring but is not enough to reopen channels. Slow negative adaptation occurs as Myo1c molecules detach and reattach cyclically to further increase tension (not shown).



Why did the previous study (Holt et al., 2002) using conventional Y61G transgenic mice not reveal a role for Myo1c in fast adaptation? These conventional transgenic mice contained adaptation motors with a mixture of Myo1c molecules, predominantly Wt and fewer mutant ones, which were sufficient in number to stall the motor complex and block slow adaptation in response to NMB-ADP. Residual fast adaptation persisted in a small fraction of Y61G transgenic hair cells (4 of 18, Y61G line 33; 2 of 14, Y61G line 9018) in the presence of NMB-ADP. A likely explanation is that Wt Myo1c molecules present in the composite motors could undergo the rapid conformational changes underlying fast adaptation since they were not bound by NMB-ADP. By contrast, the Y61G molecules present in the motors, being bound by the inhibitor, were unavailable for fast adaptation. The experiments with homozygous Y61G knock-in mice differ from the Holt et al. experiments in that motors from knock-in hair cells contain no wild-type Myo1c molecules to carry out fast adaptation.

FUTURE DIRECTIONS

Preliminary experiments have begun to investigate the role of Myo1c in cochlear outer hair cells from Y61G homozygous mice. Whether outer hair cells from mouse cochlea rely on fast and slow adaptation for proper function is not known, nor whether Myo1c activity is required for both processes. Kennedy et al., 2005 showed that fast adaptation in rat outer hair cells coincided with a large forward movement of the hair bundle, which is consistent with a release mechanism for fast adaptation in these cells. They noted that a molecule in series with the gating spring could rapidly reduce tension by rocking during fast adaptation. Perhaps Myo1c is that molecule.

Is Myo1c responsible for setting the transduction channel resting tension in hair cells? This exciting possibility could be addressed by pre-incubating Y61G knock-in hair cells with NMB-ADP, then applying small stimuli to measure displacement – P_{open} curves near a bundle's resting position. If Myo1c sets the resting sensitivity, then NMB-ADP inhibition in Y61G knock-in cells would cause mutant motors to slowly move down the actin cytoskeleton until they no longer maintain a resting tension. NMB-ADP dialysis in Y61G homozygous outer hair cells would result in a decline in resting sensitivity, a rightward shift of the displacement- P_{open} curve.

Once a membrane-permeable version of NMB-ADP becomes available, it will be much easier to inhibit Myo1c while recording from Y61G hair cells and examine the role of Myo1c in hair-cell transduction and adaptation. Whether a membrane permeable analog will behave similarly to NMB-ADP is not known. It will be particularly

interesting to test whether a membrane permeable analog acts like NMB-ADP, inducing Myo1c into a conformation that prevents or inhibits fast adaptation.

Aside from studying the role of Myo1c in hair-cell adaptation, the Y61G-Myo1c knock-in mice were engineered for the purpose of studying the role of Myo1c in *any* physiological process dependent on Myo1c in the cells that express it. Indeed, Myo1c is expressed at substantial levels in a variety of different organs (Fig. 13). What is it doing in these tissues? The development of a membrane permeable version of NMB-ADP will make it possible to readily examine the purported roles of Myo1c in a variety of physiological processes including transcription (Pestic-Dragovich et al., 2000), glucose transport in adipocytes (Bose et al., 2002), lamellopodial retraction of the neuronal growth cone (Diefenbach et al., 2002), and the formation of the immunological synapse in activated T lymphocytes (Krummel and Davis, 2002). Homozygous Y61G-Myo1c mice in combination with a membrane permeable inhibitor will be ideal reagents for directly exploring the role of Myo1c in these processes.

A membrane permeable analog also opens up the tantalizing possibility of directly testing the role of Myo1c in hearing and vestibular function *in a live mouse*. Using homozygous Y61G mice, one could develop a local delivery system to safely and reliably introduce the membrane permeable inhibitor into the mouse inner ear. Possibilities include surgically implanting a permanent pump in the cochlea or an external canula with access to the endolymphatic compartments. Because endolymph freely communicates between the cochlea and the vestibular organs of the membranous labyrinth via the *ductus reunions*, diffusion of a membrane permeable inhibitor in the inner ear could allow rapid inhibition Myo1c in the auditory and vestibular systems within a live mouse. Auditory function could be evaluated by ABR analysis; vestibular function by visual

monitoring mice for obvious balance defects. If Myo1c plays a significant role in transduction of cochlear outer hair cells as it does in utricular hair cells and is necessary for normal hearing and balance, then infusion of a membrane permeable inhibitor into the endolymphatic space of a homozygous Y61G mouse will likely result in FUBAR (Fully-Uncoupled Balance and Auditory Responses). Although this project is not without its challenges, if it worked it would strongly support the notion that Myo1c is required for normal auditory and vestibular function.

RESULTS II

CHARACTERIZATION OF THE Myo7a^{sh1-8J} MUTATION

Rationale for using 8J mice and characterizing the *Myo7a^{sh1-8J}* mutation

To determine whether either *Myo7a* transgene (Y114G-*Myo7a* or FlAsH-tagged *Myo7a*) was functional, we separately bred the different transgenic mouse lines onto a *Myo7a* null background. We predicted that a complete rescue would restore the balance and hearing defects observed in the *shaker-1* phenotype at the level of the whole animal, or that an incomplete rescue would result in partial restoration of one of these deficits. To more thoroughly assess the degree of rescue, we employed immunocytochemistry to examine hair-bundle morphology and *Myo7a* expression at the level of the hair cell; and also used immunoblotting to examine *Myo7a* expression in inner ears taken from 8J heterozygotes, 8J homozygotes, and *Myo7a* transgenics on a homozygous 8J background, as described below.

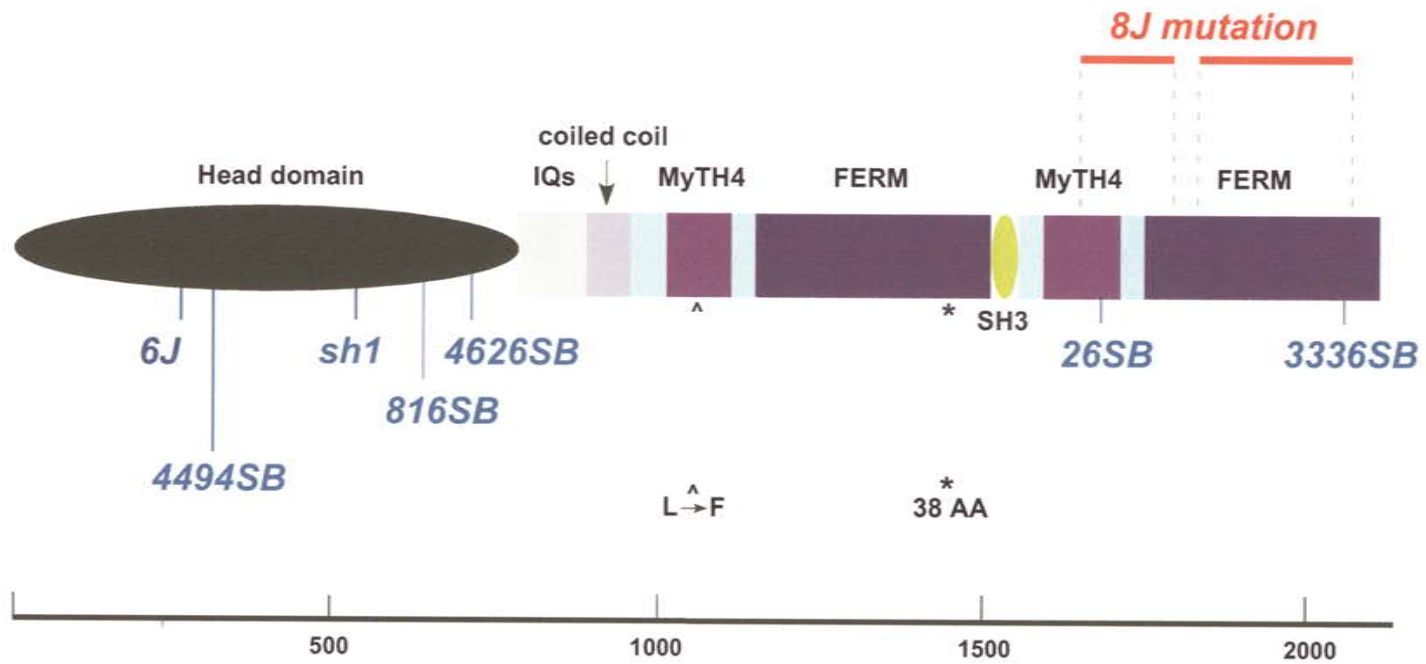
Of the seven well-characterized *shaker-1* alleles (table 2, Fig. 24), three (*816SB*, *4626SB*, *4494SB*) were ideal for the rescue experiment, because mice homozygous for these alleles express only trace amounts of *Myo7a*, effectively serving as a *Myo7a* null. Unfortunately, none of the well-characterized *shaker-1* strains were easily available, either because the mice were housed overseas or within facilities contaminated with mouse hepatitis virus (MHV) or other pathogens. To import and re-derive one of these strains to OHSU would have taken months and cost several thousand dollars.

Table 2. ***Shaker-1* alleles.** Features of the seven well-characterized *shaker-1* alleles are summarized and adapted from Mburu et al., 1997. Spontaneous mutations resulted in two of the alleles (*sh1* and *6J*), while the five other mutations were induced by *N*-ethyl-*N*-nitrosurea (ENU)-mutagenesis. Missense mutations accounted for the least severe alleles (*sh1*, *6J*, *26SB*). Nonsense mutations produced three *shaker-1* alleles (*3336SB*, *4494SB*, *4626SB*). Two alleles (*816SB*, *4494SB*) arose from sequence inversions (IVS) in the motor domain of *Myo7a*, resulting in mutations that yield very little *Myo7a* protein.

Table 2. *Shaker-1* alleles.

<i>Allele</i>	<i>Mutation</i>	<i>Protein level</i>	<i>Hair-bundle morphology</i>	<i>Cochlear responses</i>
<i>sh1</i>	CGG → CCG Arg-502 → Pro	0.93	Normal	Some
<i>6J</i>	CGT → CCT Arg-241 → Pro	0.21	Abnormal	Very few
<i>26SB</i>	TTT → ATT Phe-1800 → Ile	0.18	Abnormal	None
<i>816SB</i>	IVS 16 nt-2a → g 10 aa deletion	0.063	Abnormal	None
<i>3336SB</i>	TGT → TGA Cys-2182 → stop	0.13	Abnormal	None
<i>4494SB</i>	IVS 6 nt+2t → a stop 5 aa	0.0089	Abnormal	Very few
<i>4626SB</i>	CAG → TAG Gln-720 → stop	0.0072	Abnormal	None

Figure 24. **Functional domains of Myo7a with *shaker-1* mutations.** Myo7a includes a motor head domain, five IQ domains, a putative coiled-coil domain followed by two repeats of MyTH4 and FERM domains, which are separated by a putative Src homology 3 (SH3) domain. Indicated in blue are the locations of the seven known mutations in *Myo7a*, which are summarized in Table 2. Five alleles contain mutations in the motor head domain while two alleles have mutations in the tail of Myo7a. Indicated in red is the location of the 8J mutation, which resulted in the deletion of part of repeat 2 in the MyTH4 and FERM domains. A leucine (L) to phenylalanine (F) change at amino acid 1165 is present in the original human *MYO7A* cDNA clone (Chung et al. 1997) as well as the mouse *Myo7a* cDNA used to generate the Myo7a transgenic mice. An asterisk (*) indicates the small region encoding 38 amino acids of the first FERM domain not present in the cDNA that was used to engineer the transgenes in figure 36.



To pursue the rescue experiment, we decided to purchase an uncharacterized *shaker-1* strain ($Myo7a^{shl-8J}$ stock # 3184) from The Jackson Laboratory (Bar Harbor, ME) with the hope that this strain would be a *Myo7a* null. If so, then we would breed it with our *Myo7a* transgenics and look for rescue. Indeed, as described in this chapter, we found that the 8J mouse strain is effectively a *Myo7a* null.

Molecular characterization of the 8J mutation was essential; we had to design a PCR-based genotyping strategy to routinely differentiate mice of three genotypes (8J/+, 8J/8J, 8J/8J/Tg⁺) at the newborn stage. To characterize the 8J mutation, we took two parallel approaches. One approach required amplifying, TOPO-cloning, and sequencing all exons of $Myo7a^{shl-8J}$ genomic DNA. The second approach involved Southern blot analysis of genomic DNA from homozygous $Myo7a^{shl-8J}$ mice and from the two parental mouse strains (C57BL6/J and SJL) on which the $Myo7a^{shl-8J}$ mutation arose spontaneously.

$Myo7a^{shl-8J}$ Exon Sequencing

To locate the 8J mutation, we initially began amplifying and sequencing individual exons from $Myo7a^{shl-8J}$ genomic DNA in the hope that we would find a single nucleotide change (deletion, addition, or substitution) that resulted in a nonsense or missense mutation. Since the $Myo7a^{shl-8J}$ allele arose *spontaneously* at The Jackson Laboratory (Bar Harbor, ME) and the majority of spontaneous mutations result in a single nucleotide change, we had reason to follow this approach. We successfully amplified exons (1- 37) from $Myo7a^{shl-8J}$ genomic DNA, either as groups of exons or as individual ones with primers (table 3), and used the Ensembl *Myo7a* sequence for comparison. However,

Table 3. Primers used for *Myo7a* Exon Sequencing

<u>Primer sequence (5' to 3')</u>	<u>Primer</u>
CCGGAATTCTTCAGGATCTCCTGCCTACAGG	EX 1 FWD
CCGGAATTCATTGTCTTCATCATCCACCACC	EX 1 REV
CCGGAATTCGAACACTGGATATCCCCTCAGA	EX 2 FWD
CCGGAATTCACTCACATAGATGAGGTGGTCC	EX 2 REV
CCGGAATTCAGACGTACACAGGTTCCATCCT	EX 3/6 FWD
CCGGAATTCATGGCCAAGTAGTTGTAGTCA	EX 3/6 REV
CCGGAATTCCTCCTGCCCAGGGTAACTGCATCACCT	EX 7/10 FWD
CCGGAATTCCTGTTCACAGTGAAGTTCTCA	EX 7/10 REV
CCGGAATTCCTTCGAGCAGCTCTGCATTAAC	EX 11/13 FWD
CCGGAATTCTCTTACCATGGCAACGTCAGCT	EX 11/13 REV
CCGGAATTCTGTCTGTCTGTCCTCTGCCACAGGGTG	EX 14 FWD
CCGGAATTCCTCACCATGGGCTTCTTGAACTCATTG	EX 14 REV
CCGGAATTCCTCTTCGACCGGCACTTGTGTGTACGC	EX 15/16 FWD
CCGGAATTCCTCACCTTCAGAAAGATCTTGG	EX 15/16 REV
CCGGAATTCGACCACCATGACATGTTGCTGGAGGTG	EX 17 FWD
CCGGAATTCTGACACAGACCTGTCTTTGAAGCCCCG	EX 17 REV
CCGGAATTCTCTCCCTTCCAGGTCCAAC TTC	EX 18/20 FWD
CCGGAATTCCTTACCTGATGCTTGCGCTCAGCCTCC	EX 18/20 REV
CCGGAATTCTTACTCTGCGTCCCCCAACCTCAGGA	EX 21/24 FWD
CCGGAATTCCTCTTCTGTGAGTTTGGACTT	EX 21/24 REV

<u>Primer sequence (5' to 3')</u>	<u>Primer</u>
CCGGAATTCGTGACCAAGAGGCTGAACGATGGGGAA	EX 25 FWD
CCGGAATTCAGAAGCCCAGACACAGCATCCCCTGC	EX 25 REV
CCGGAATTCGGACGAGATTTACTGCCAGATC	EX 26/29 FWD
CCGGAATTCACCTTCTCACACCTGTACTCCC	EX 26/29 REV
CCGGAATTCTGTGTGTCACCCTCAGGAGGACGACCT	EX 30 FWD
CCGGAATTCTCCTACCTTCTTGTGGGCAGCAATGGC	EX 30 REV
CCGGAATTCGGAATTTATGCCAGAGGAGAACTGAC	EX 31/33 FWD
CCGGAATTCCCCTCACCAGGGTTAGGATTGTCCT	EX 31/33 REV
CCGGAATTCTAAGCTGGTGAGGAGTCAGGCT	EX 34/36 FWD
CCGGAATTCATATCTACAAAGGCCATGCAGG	EX 34/36 REV
CCGGAATTCCCTCTCACCTGTGCTCAAGTAC	EX 37 FWD
CCGGAATTCCCACAGTGTCGCTCACCTGATGTGAT	EX 37 REV
CCGGAATTCTTTCCCACAGGTACAGCGAAGA	EX 38/40 FWD
CCGGAATTCCCTTATCTGCGATTTTGACAAA	EX 38/40 REV
CCGGAATTCGTCATCAGCGTCCCAGAGAATGATTTC	EX 41/45 FWD
CCGGAATTCGCTCACCTTGGTTCTGGGATCGATGAG	EX 41/45 REV
CCGGAATTCGACATCCTGACTACTACCCCTTCACC	EX 46/47 FWD
CCGGAATTCAAAGAGGTTGCTTGATGGAGCTGGTCT	EX 46/47 REV
AGGTGTGAGAAGGAGGACGAA	EX 29/30 (For 38AA)
TGCAGTGCCACCACATACTTA	EX 33 (For 38AA)
CCTCTCACCTGTGCTCAAGTAC	EX 37A FWD
GAGCTCACTGACCAGATCTT	EX 37B FWD

sequencing of the first 37 exons revealed no mutations.

Using primers (table 4) spanning individual exons over a region encompassing exons 38-46, we amplified PCR products of the expected sizes from parental C57BL6/J and SJL genomic DNA (Fig. 25). We could not, however, amplify any PCR products with these same primers using *Myo7a*^{sh1-8J} genomic DNA as the template. This result suggested that a deletion spanning this region (exons 38-46) of *Myo7a* might be the causative mutation of the *Myo7a*^{sh1-8J} allele.

To test this possibility, we attempted to PCR amplify across the putative deletion and sequence the PCR products. Specific primers (table 5), spaced apart by 500 bp, for the large intron upstream of exon 38 were used in conjunction with a primer specific for the 3' untranslated region (UTR). One specific primer pair (47603 5', EX47B 3') amplified a PCR product of ~1590 bp (Fig. 26), which was TOPO-cloned and then sequenced.

Sequence analysis of this amplified ~1590 bp PCR product revealed a breakpoint (symbolized by ▼ in Fig. 27A) occurring ~1880 bp upstream of exon 38. The sequence skipped to the intron between exons 40 and 41 (~55 bp downstream of exon 40, ▼ in Fig. 27A) and ran uninterrupted to the next breakpoint, ▼ in Fig. 27A) located ~20 bp downstream of exon 41 in the intron between exons 41 and 42. The sequence then skipped to the intron between exons 46 and 47 (▼ in Fig. 27A).

A total of 6.412 kb appeared to be deleted from genomic DNA of 8J homozygotes (Fig. 27A). The upstream deletion included exons 38 through 40 for a total of 3.611 kb sequence. The second deletion encompassed exons 42 through 46, totaling of 2.811 kb of sequence. To confirm these sequencing results, Southern analysis was performed on

Table 4. Primers used for *Myo7a* Exon (38-47) Sequencing

<u>Primer sequence (5' to 3')</u>	<u>Primer</u>
GCCTGCCTTGAGGTAGTGAGTGCCT	EX 38 5'
GGTACTTCCGGGAGCCATTTCTG	EX 38 3'
CCTGAGTTCCACAGCTTGACGGTG	EX 39 5'
TGGAGTTTGAGGGCGAGAGGGAA	EX 39 3'
GGACTAGTCCTGTTTGGAGGGCCA	EX 40 5'
CGGAGACATTGTCTTTGGGTCCTCA	EX 40 3'
TGGAGGATCTGTGTCAGAGCTGGAC	EX 41 5'
GCAACTTGGGGATGCTAGGGAAGTA	EX 41 3'
ATTGGGCCTGTGCAGGTCTTGGT	EX 42 5'
GTACCATTCTCAGGCCCACTCCT	EX 42 3'
GCACAGGGACTTGCTGGCTTGAGAC	EX 43 5'
GAGGCTTCCCTTATCACACAGGAGG	EX 43 3'
AGGGGTTGAGACAGCAAGTGCTGG	EX 44 5'
CCACAGCCTCAAGGGTCCCTATAAG	EX 44 3'
GGAGGTTTGGCACTGGGACAAGA	EX 45 5'
CGGTCTGTGGCATCCAGTGACAT	EX 45 3'
CCAGGACATCCTGACTACTCACCCC	EX 46 5'
TCACCAGCGATGTCTCACAGAGCA	EX 46 3'
ATGGATGTGGGCCTTCAGCCCAT	EX 47 5'
CAAAGAGGTTGCATTGATGGAGCTG	EX 47 3'
TCAGTCCAGCTTCCCTGCCTA	EX47B 3'

Figure 25. **PCR amplification of *Myo7a* exons 38-46 from genomic DNA.** Primer pairs, designed to hybridize in flanking introns, were employed to amplify individual exons (38-46) of *Myo7a*. *A, B*, Amplification of PCR products for exons 38-46 was successful using genomic DNA from C57BL6 (*A*) or SJL (*B*), the parental strains of the original 8J mice. *C*, The same primer pairs failed to amplify PCR products for exons 38-46 from *Myo7a^{sh1-8J}* genomic DNA. PCR products were amplified from 1 μ l genomic mouse DNA and separated by agarose (1.4%) gel electrophoresis. A 1 kb plus ladder was loaded in the left-most lanes. Expected PCR products were as follows: EX38 (~1.2 kb), EX39 (~850 bp), EX40 (~850 bp), EX41 (~850 bp), EX42 (~850 bp), EX43 (~650 bp), EX44 (~830 bp), EX45 (~650 bp), EX46 (128 bp).

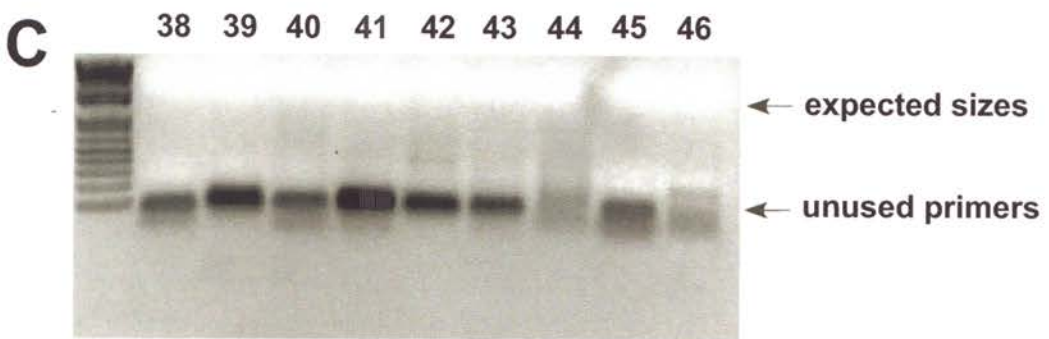
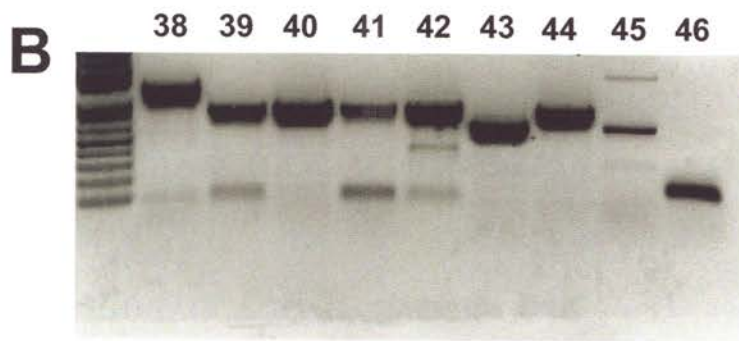
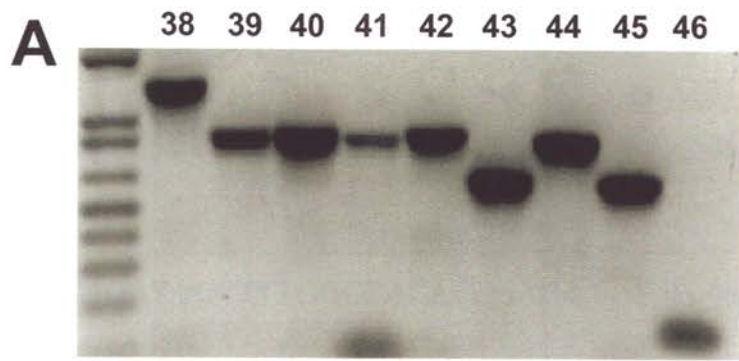
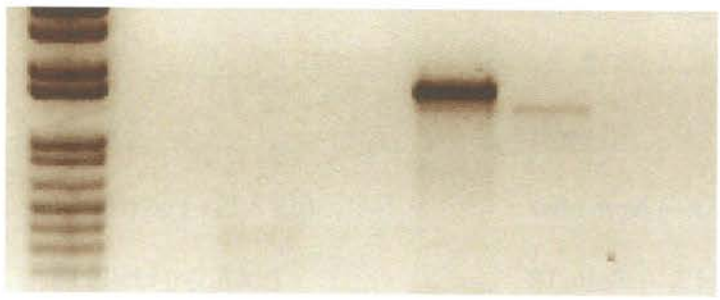


Table 5. Upstream Primers for Amplifying Across the 8J Deletion

<u>Primer sequence (5' to 3')</u>	<u>Primer</u>
CGGACACTGTGGGACCTCTTGAAG	44601 5' primer
CCATTCCTAGGAGACTGGGGCCCAT	45615 5' primer
CCAGATAGCTTTGGGTACACCGACA	46606 5' primer
ATTTGGGACAGATGTGATTGGTGGG	47603 5' primer
GAAACAAACTGCCAGGAGTTGGTGA	48641 5' primer
TCTGGAAGCAGCAGAGACCTTGGTC	49020 5' primer
ACTGTGGACTTTCATTCTGGCACCG	49507 5' primer

Figure 26. **PCR amplification across the 8J deletion.** 5' primers, designed to hybridize in the intron upstream of exon 38, were spaced apart by ~500 bp and employed with a 3' primer to amplify across the deleted region (exons 38-46) of *Myo7a^{sh1-8J}* genomic DNA. Each 5' primer was used in conjunction with a 3' primer (EX 47B 3') in an attempt to amplify a PCR product across the 8J deletion using homozygous 8J genomic DNA as template. PCR amplification with primers 47603 and EX 47B 3' (specific for exon 47) amplified ~ 1.59 kb product*, which was TOPO-cloned. Sequencing revealed exact breakpoints, which are displayed in figure 27. PCR products were amplified from 1 µl of genomic DNA obtained from 8J homozygous mice. Each lane was loaded with 25 µl PCR reaction and separated by agarose (1.4%) gel electrophoresis. A 1 kb plus ladder was loaded in the far left lane.

*



— ~1590 bp

Figure 27. **Diagram of the 8J allele and Southern analysis of 8J mutation.** *A*, Sequencing of the 8J allele revealed ~6.412 kb of deleted sequence, which is highlighted in red. The symbol ▼ demarcates the breakpoints and boundaries of missing regions of *Myo7a*. Also shown are the predicted sizes of genomic DNA from wild-type or 8J homozygous mice digested with *EcoR* I or with *Hind* III and analyzed by Southern blotting with a 3' external probe (~469 bp):

EcoR I

wild-type (~13.8 kb)

8J allele (~7.3 kb)

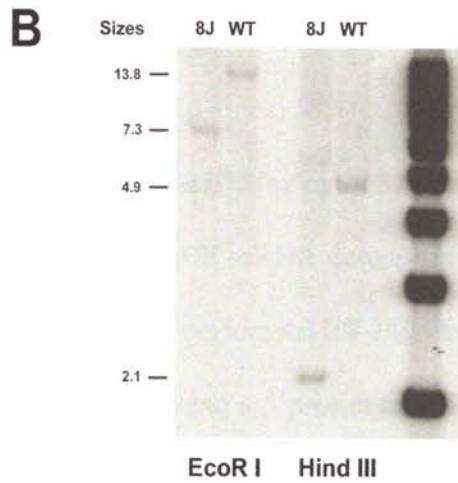
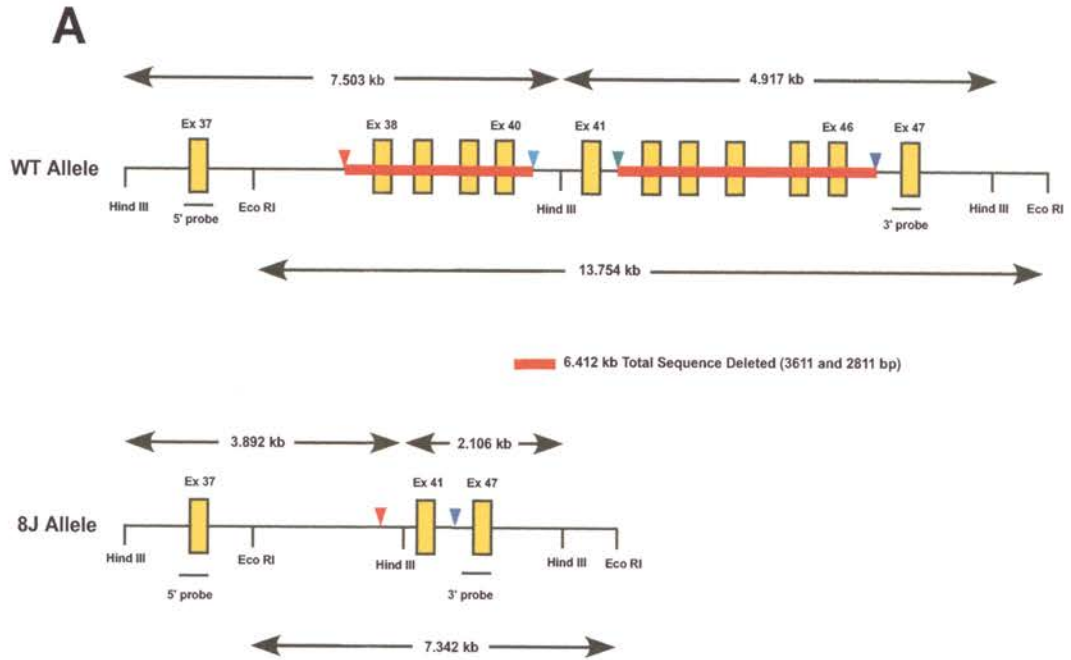
Hind III

wild-type (~4.9 kb),

8J allele (~2.1 kb).

B. Southern blot analysis indicating predicted results.

8J Mutation/Characterization



genomic DNA from *Myo7a*^{sh1-8J} homozygotes and from mice of the two parental mouse strains, C57BL6/J and SJL.

Southern analysis of wild-type and *Myo7a*^{sh1-8J} homozygous mice

To confirm the ~6.42 kb deletion within the *Myo7a*^{sh1-8J} allele, mouse genomic DNA from one of three strains (C57BL6/J, SJL, homozygous *Myo7a*^{sh1-8J}) was treated with either restriction enzyme *EcoR* I or *Hind* III, and separated by agarose gel electrophoresis. Using a 3' probe specific for exon 47, we then performed Southern blot analysis on the digested genomic DNA from wild-type (C57BL6/J or SJL) or 8J homozygous mice (Fig. 27B).

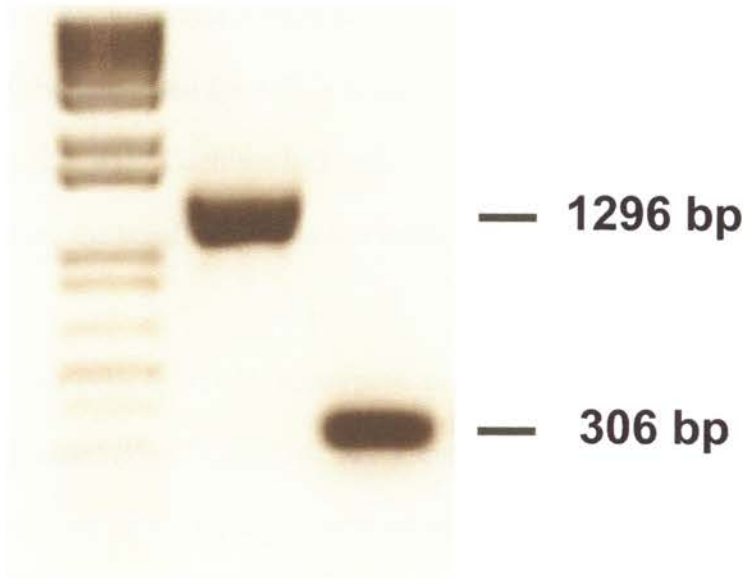
EcoR I digestion of wild-type and 8J/8J samples gave band sizes of ~13.75 kb and ~7.3 kb, respectively; *Hind* III digestion produced ~4.9 kb wild-type band and ~2.1 kb 8J/8J band. These sizes were expected for wild-type and for the 8J homozygote, if the 8J mutation resulted in a ~6.412 kb deletion in the *Myo7a* gene. Thus, Southern analysis confirmed that 6.412 kb sequence was deleted in the 8J allele, supporting the results of sequencing the 1590 bp PCR product.

RT-PCR analysis using primers specific for exon 37 and the 3' UTR

To examine the splicing of *Myo7a* mRNA across the 8J mutation and test for the deletion with a different strategy, we performed RT-PCR analysis on total RNA isolated from wild-type and 8J/8J kidneys. Using a 5' primer (EX 37B FWD) specific for exon 37 and a 3' primer (EX47B 3') specific for 3'UTR, we amplified a PCR product encompassing exons 37 through 47 (Fig. 28). The product amplified from the 8J

Figure 28. **RT-PCR analysis of kidney RNA *Myo7a*^{sh1-8J} and C57BL/6 mice.** Total RNA was processed from mouse kidneys from wild-type (C57BL/6) and homozygous *Myo7a*^{sh1-8J} mice, and reverse-transcribed to cDNA. Primers (EX 37B FWD/ EX47B 3') specific for exons 37 and 47 of *Myo7a* were used to amplify PCR products from cDNA, which were then separated by agarose (1.4%) gel electrophoresis. Amplification resulted in the predicted product sizes: wild-type – 1296 bp; homozygous *Myo7a*^{sh1-8J} 306 bp.

WT 8J



homozygote sequence was 306 bp in size, which agrees with the predicted size.

Immunocytochemistry

To inspect *Myo7a* expression in hair cells from 8J homozygous and 8J heterozygous mice, whole cochlear epithelia were harvested from mice (aged P0-P2, P4, P6) and stained with phalloidin-FITC (0.25 μ M) and a *Myo7a* specific antibody. Mouse genotypes were readily distinguished by PCR genotyping (Fig. 29) at P0-P1 prior to immunocytochemical analysis.

Using confocal microscopy, we noted normal bundle morphology in all hair cells within whole cochlear epithelia harvested from 8J heterozygote mice, for all ages examined (Figs. 30A, 31A, 32A, 41). Cochlear hair cells from these mice stained intensely for *Myo7a*, including the bundles and the cell bodies of inner and outer hair cells.

By contrast, cochlear hair cells from 8J homozygote mice were consistently disorganized at the ages examined (Figs. 30A, 31A, 32A), even at P0 (Fig. 41). Hair cells from these mice stained very dimly for the *Myo7a* antibody, suggesting either that *Myo7a* is not expressed in 8J/8J hair cells or that the 8J mutation results in an unstable form of *Myo7a*. It seems very unlikely that the 8J mutation results in a stable, truncated form of *Myo7a*; otherwise staining in 8J/8J hair cells would have been more intense with the *Myo7a* specific antibody and would have labeled a truncated product, since this antibody is specific against a section of *Myo7a* (880-1070 amino acids) more N-terminal of the putative region missing in the 8J protein (Fig. 24).

Figure 29. **Genotyping 8J mice.** Genomic DNA was processed from mouse tails of three different genotypes (wild-type, 8J heterozygote, 8J homozygote) and used for PCR amplification. A ~1590 bp region of *Myo7a* flanking the 8J mutation was amplified using 8J primers (47603 5' / EX 47 3'). The predicted PCR product (~1590 bp) was amplified only in samples containing the 8J allele - 8J homozygote and 8J heterozygote. Conditions were chosen to avoid amplification of a large PCR product (7.97 kb) from Wt samples. A separate Wt primer pair (EX 44 5' / EX 44 3') amplified a PCR product (~850 bp) only in samples containing exon 44 of *Myo7a* - wild-type and 8J heterozygote. As predicted, the Wt primer pair did not amplify a product from genomic DNA from 8J homozygous mice because exon 44 was removed by the 8J deletion. PCR products were separated by agarose (1.4%) gel electrophoresis. A 1 kb plus DNA marker ladder was loaded in far left lane.

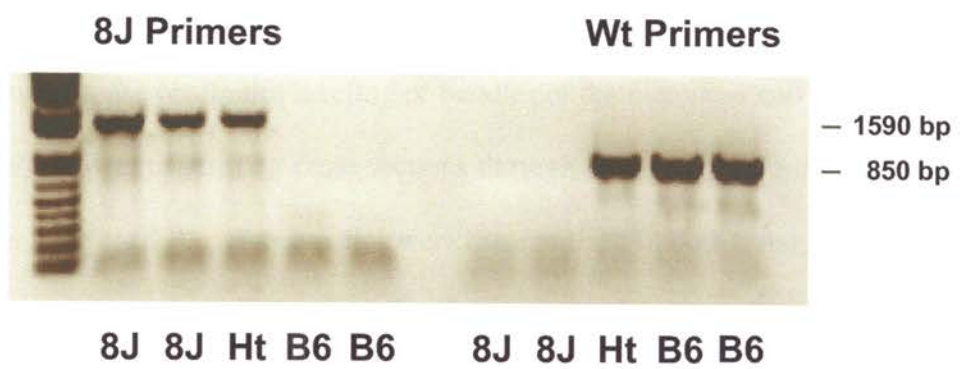


Figure 30. **Phalloidin labeling of organ of Corti from 8J mice (aged P1).** Top panels (A), cross sections through the organ of Corti from 8J heterozygote mice aged P1. Small arrows point to hair bundles of the outermost row of outer hair cells. Cochlear hair cells from two 8J heterozygotes displayed tightly formed v-shaped hair bundles of outer hair cells and more intense phalloidin labeling of bundles of the inner hair cell row (arrowheads). Lower panels (B), cross sections through the organ of Corti from 8J homozygote mice aged P1. Hair bundles were disorganized in both outer hair cells (small arrows) and inner hair cells (arrowhead) from two 8J homozygotes. Images were taken with a 60× objective lens. C, Diagram of the mammalian organ of Corti and a shadowed rectangle outlining the approximate region projected by confocal images. IHC, inner hair cell; OHC, outer hair cell.

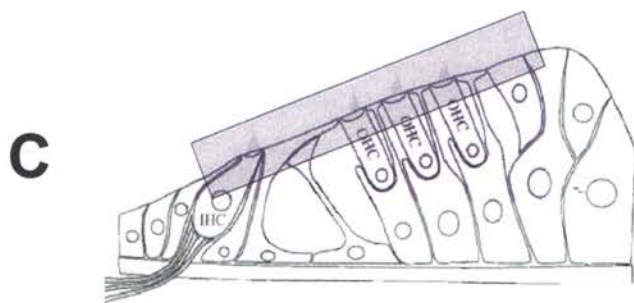
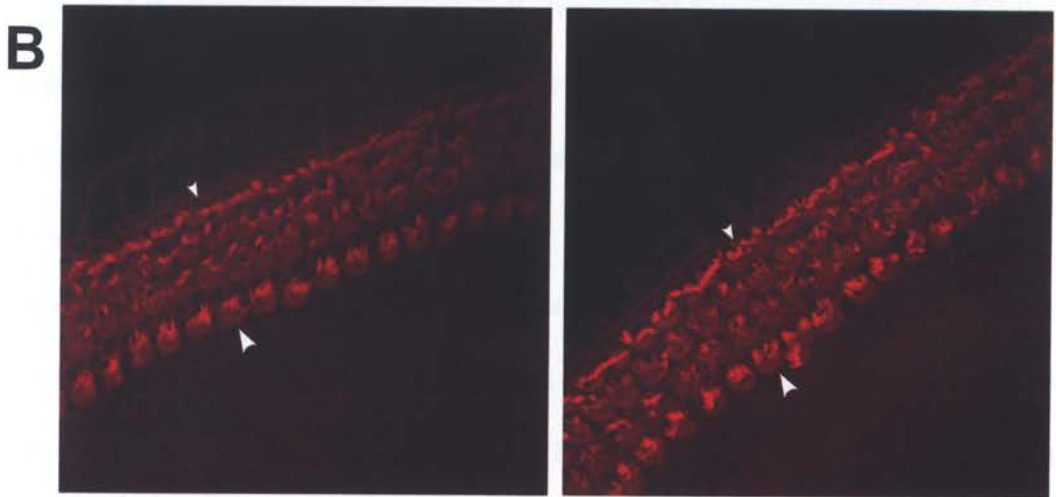
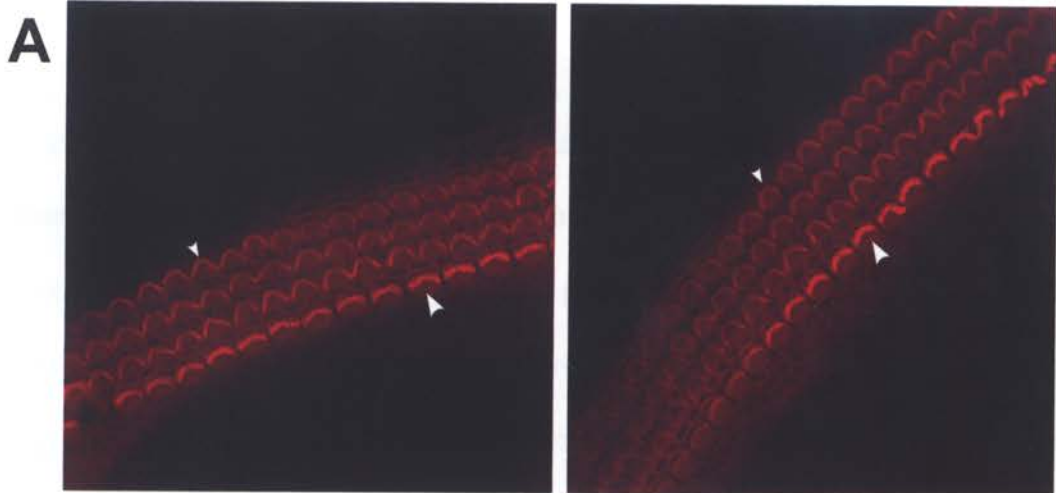


Figure 31. Localization of Myo7a in organ of Corti from mice (aged P4) by immunofluorescence and immunocytochemistry. Cross-sections through the mouse organ of Corti from three genotypes. Left panels, actin (FITC-phalloidin, shown in red); middle panels, Myo7a immunolabeling (green); right panels, combined actin (red) and Myo7a (green). In the left panels, small arrows point to hair bundles of the second row of outer hair cells. *A*, Cochlear hair cells from an 8J heterozygote displayed tightly formed v-shaped hair bundles of outer hair cells and Myo7a reactivity within the bundles of outer hair cells and the somas (arrowhead) of inner hair cells. *B*, Hair bundles of cochlear hair cells from an 8J homozygote were disheveled and dimly labeled for phalloidin (actin) and Myo7a. *C*, Cochlear hair cells from an 8J homozygote with a single Y114G transgene copy also demonstrated disorganized hair bundles, but slightly greater Myo7a immunoreactivity than the 8J homozygote sample, most notably in the inner row of hair cells (arrowhead). Images were taken with a 40× objective. *D*, Diagram of the mammalian organ of Corti and a shadowed rectangle outlining the approximate region projected by confocal images. IHC, inner hair cell; OHC, outer hair cell.

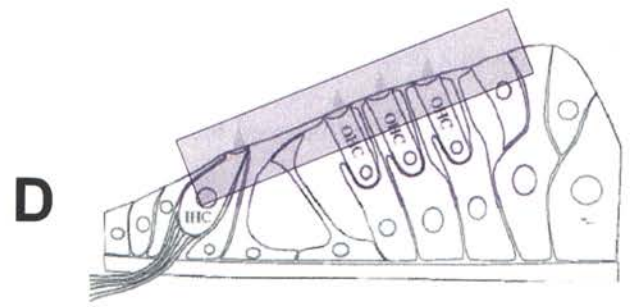
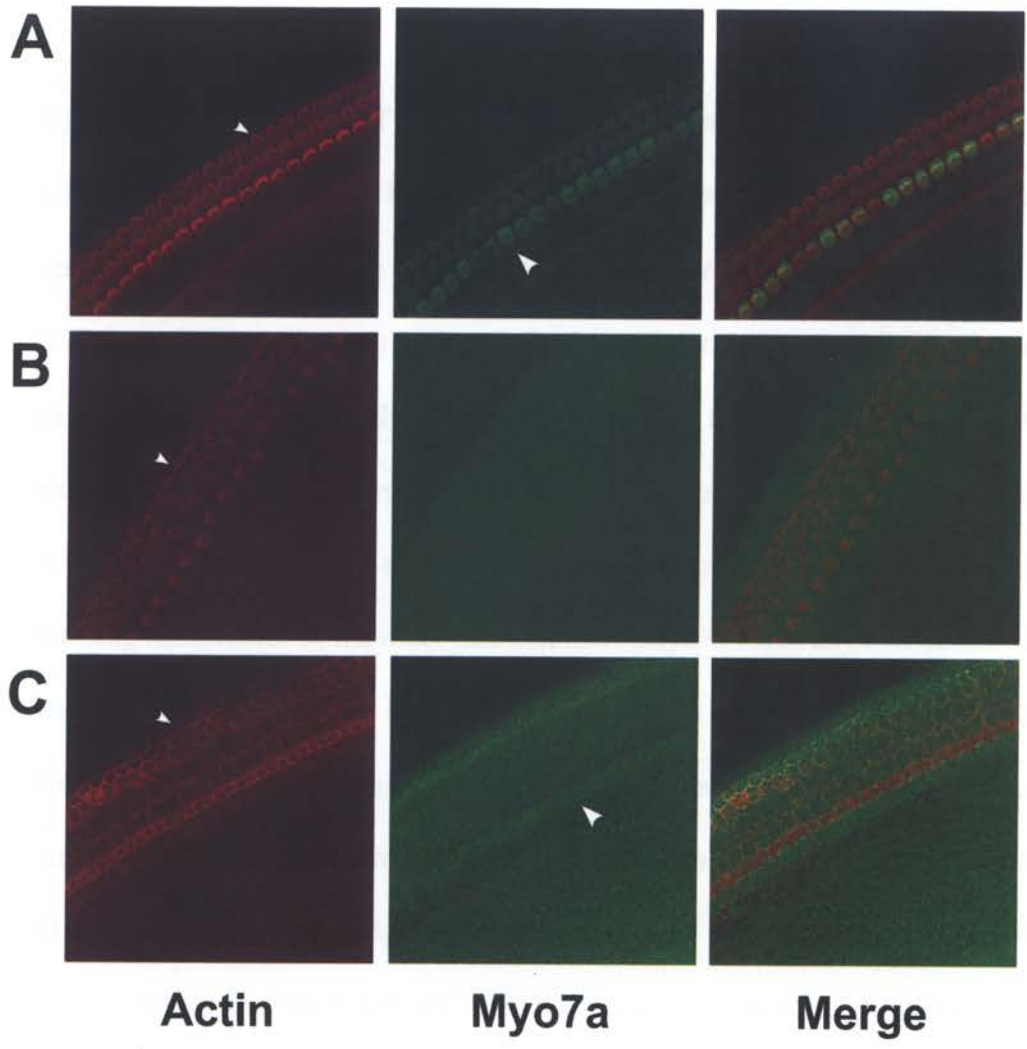
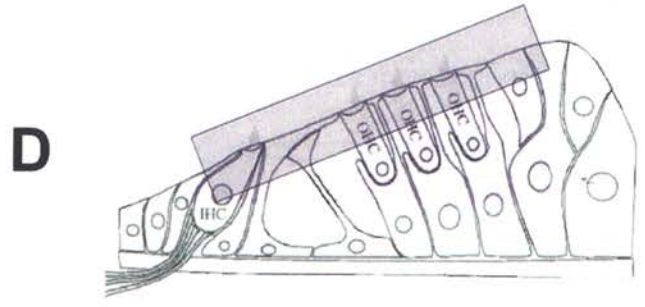
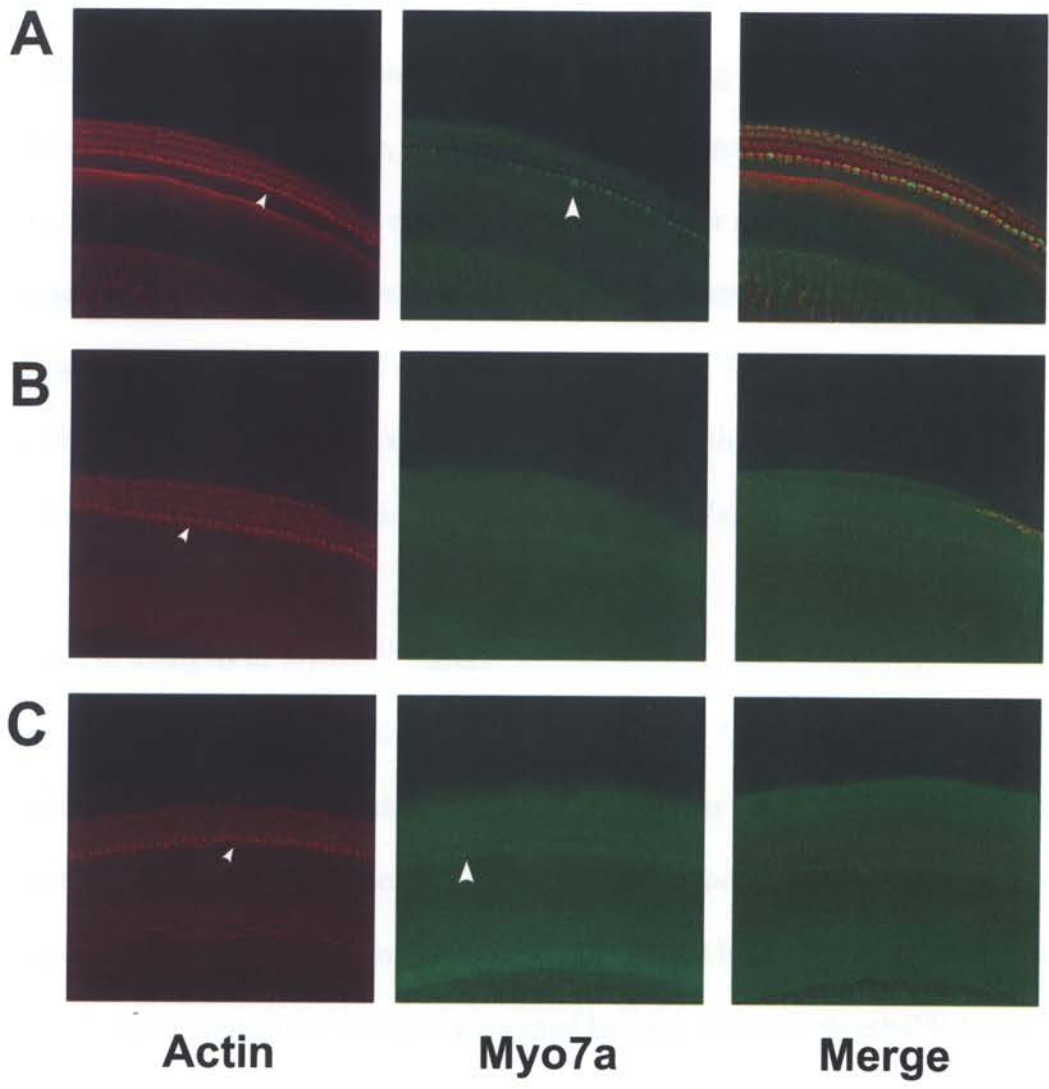


Figure 32. **Localization of Myo7a in organ of Corti from mice (aged P6) by immunofluorescence and immunocytochemistry with a 20× objective lens.** Cross-sections through the mouse organ of Corti from three genotypes. Left panels, actin (FITC-phalloidin, shown in red); middle panels, Myo7a immunolabeling (green); right panels, combined actin (red) and Myo7a (green). In the left panels, small arrows point to hair bundles of the row of inner hair cells. *A*, Cochlear hair cells from an 8J heterozygote displayed tightly formed v-shaped hair bundles of outer hair cells and intense phalloidin labeling the bundles of the inner hair cell row. Myo7a reactivity was demonstrated within the bundles of outer hair cells and the somas (arrowhead) of inner hair cells. *B*, Hair bundles of cochlear hair cells from an 8J homozygote were disheveled and dimly labeled for phalloidin (actin) and Myo7a. *C*, Hair bundles of cochlear hair cells from an 8J homozygote with a single Y114G transgene copy were also disorganized, but showed greater Myo7a immunoreactivity than the 8J homozygote sample, most notably in the inner row of hair cells (arrowhead). Images were taken with a 20× objective lens. *D*, Diagram of the mammalian organ of Corti and a shadowed rectangle outlining the approximate region projected by confocal images. IHC, inner hair cell; OHC, outer hair cell.



Immunoblot analysis of tissues for Myo7a expression in the 8J mouse

As an additional test to compare Myo7a expression in mice homozygous or heterozygous for the 8J allele, we used the Myo7a-specific antibody that was used in the immunocytochemistry experiments for immunoblotting of mouse organ extracts. Lysates from kidney, cochlea, utricle, retina were prepared from 8J heterozygous and 8J homozygous littermates and equal amounts (1-5 µg per sample) of protein extracts were loaded onto gels. Blot analysis revealed that 8J homozygous mice did not express Myo7a in any of the tissues sampled (Fig. 33, 34). Moreover, 8J heterozygotes expressed in the kidney, cochlea, utricle, and retina a ~220 kD protein that was reactive to the Myo7a antibody, the same size predicted for full-length Myo7a.

ABR of analysis of *Myo7a^{sh1-8J}* Mice

Auditory-evoked brainstem responses (ABR) were performed to determine the degree of hearing loss of 8J homozygous mice in comparison with age-matched 8J heterozygous controls. As expected, we found that 8J homozygous mice (aged P36) did not hear normally as compared with 8J heterozygous controls. 8J heterozygote control mice displayed normal hearing, with low thresholds for the frequency and intensities tested (Fig. 35). By contrast, abnormal ABR thresholds were raised by more than 40 db SPL across all frequency and stimulus intensities tested in the 8J homozygotes, even to high stimulus trains, indicating that these mice were profoundly deaf.

Figure 33. **Protein immunoblot analysis of Myo7a expression in tissues from Y114G transgenic and 8J mice.** Immunoblotting of mouse tissues with anti-Myo7a antibody. Equal amounts of total protein from tissues (kidney, cochlea, utricle, retina) were loaded ($\sim 5 \mu\text{g}$ per lane) on SDS polyacrylamide gels. Indicated are tissue sampled, genotype, and Myo7a position (~ 220 kDa). Twenty ear equivalents (cochlea, utricle) were loaded per lane for inner ear tissues. 8J heterozygote mice express Myo7a protein in kidney, retina, cochlea, and utricle. Bands of lower intensity and size were detected in transgenic samples (Y114G⁺/8J/8J) only from kidney and cochlea, but not utricle or retina. Myo7a was not detected in any of the 8J homozygous tissue samples.

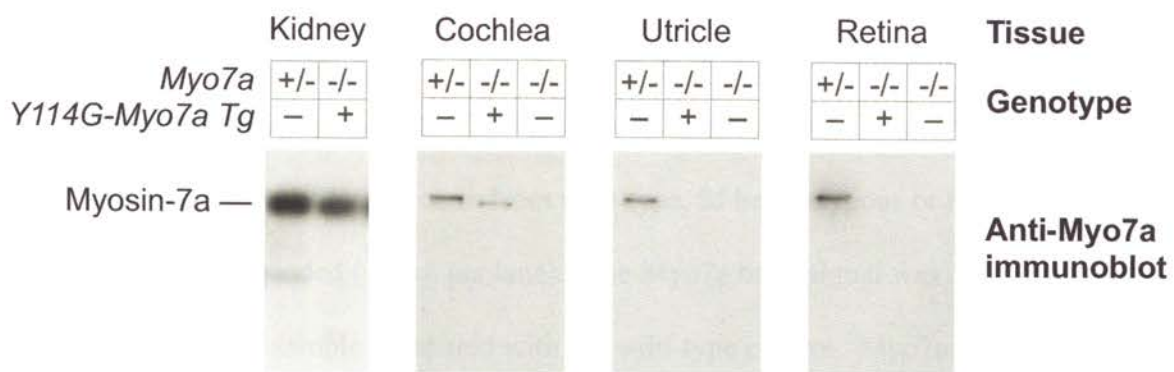


Figure 34. **Protein immunoblot analysis of Myo7a expression in kidneys from wild-type and 8J mice.** Immunoblotting of mouse kidneys with anti-Myo7a antibody. Equal amounts of total protein from wild-type, 8J heterozygous or 8J homozygous kidney lysates were loaded ($\sim 5 \mu\text{g}$ per lane). The Myo7a band signal was $\sim 50\%$ reduced in the heterozygous sample compared with the wild-type control. Myo7a position ($\sim 220 \text{ kDa}$) is indicated.

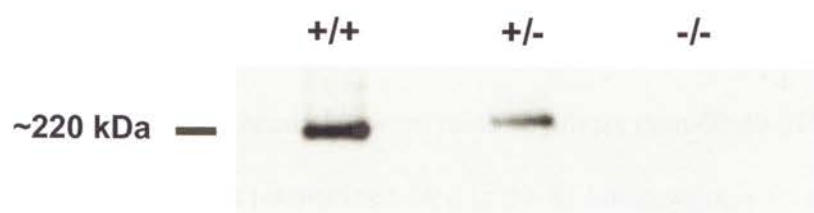
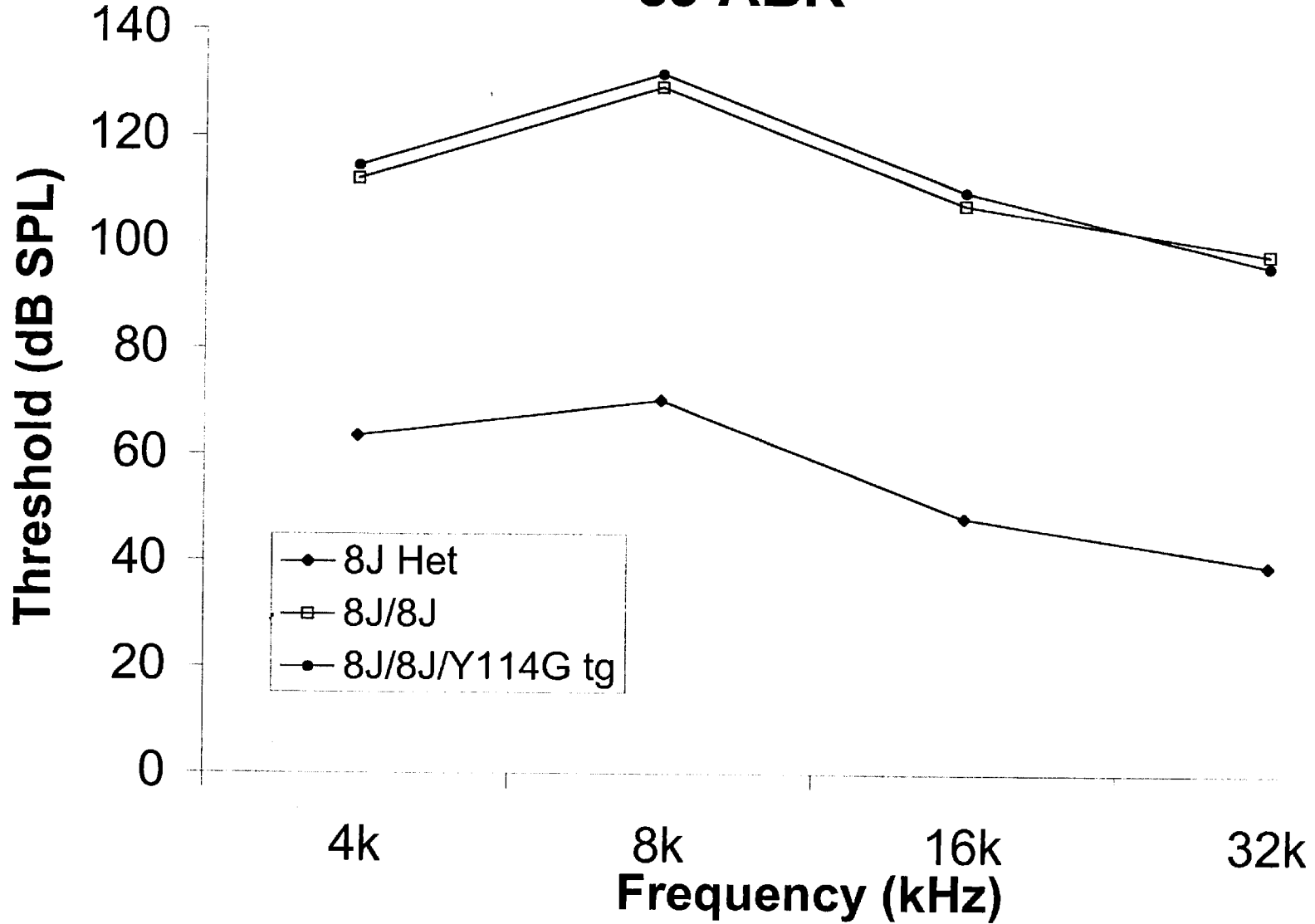


Figure 35. **Auditory-evoked brainstem response (ABR) analysis of 8J mice.** ABR audiometry to pure tones was used to evaluate cochlear function of 8J heterozygous (control) and of 8J homozygous mice +/- Y114G transgene aged P36. Auditory-evoked brainstem responses (ABRs) were elicited to tone-burst stimuli at 4, 8, 16, and 32 kHz and thresholds were obtained from left ears. Animals were tested with high intensity stimulus trains. ABR thresholds were raised by more than 40 db SPL across all frequency and stimulus intensities tested in the 8J homozygotes +/- a single copy of the Y114G transgene (line 56), indicating that they were deaf. Thresholds were comparable at all values tested in these mice. By contrast, 8J heterozygote control mice had normal ABRs and could hear. Stimulus frequency (kHz) is plotted on the *x*-axis and the minimum threshold (dB SPL) that elicited a response on the *y*-axis.

8J ABR



DISCUSSION II

Complementation testing at the Jackson Laboratory revealed that the 8J mutation is an allele of *Myo7a*. We characterized the defect molecularly and found that a large deletion (6.412 kb) within *Myo7a* resulted in the 8J mutation, which occurred spontaneously on the transgenic mouse strain B6/SJL-TgN (c177lacZ) at the Jackson Laboratory (Bar Harbor, ME). Sequence analysis of a PCR product spanning the 8J mutation as well as RT-PCR and Southern analysis of 8J homozygous genomic DNA disclosed that part of the coding region for the MyTH4 and FERM domains of repeat 2 was missing in the 8J mutant. Apparently, this defect in the *Myo7a* tail produces very little *Myo7a* protein, as demonstrated by immunoblotting with a *Myo7a*-specific antibody of several 8J homozygous tissues (kidney, utricle, cochlea, and retina). *Myo7a* immunocytochemistry of cochlea epithelia also revealed negligible *Myo7a* expression in 8J mutant hair cells, which correlates with its severe auditory and vestibular phenotype. We confirmed by ABR analysis that homozygous 8J mice were deaf in comparison to 8J heterozygotes, and displayed the *shaker-1* vestibular phenotype, which included hyperactivity, head bobbing, and circling.

Studies in *Myo7a* mutants in mouse (*shaker-1*) and zebrafish (*mariner*) highlight the functional importance of the C-terminal regions of *Myo7a*. Two *shaker-1* mutations (*26SB*, *3336SB*) in the tail of *Myo7a* lead to reduced *Myo7a* expression (18% and 13% respectively) and a severe bundle phenotype. The *26SB* mutation lies within the second MyTH4 domain, altering a conserved phenylalanine residue to isoleucine. The *3336SB* mutant leads to the deletion of the last 35 amino acids. The 8J protein allele, missing

exons 38-40 and 42-46, may give rise to an unstable truncated protein and also supports the idea that the C-terminus of Myo7a is required for Myo7a protein stability.

Like the *shaker-1* mutant 3336SB, which is characterized by a severe bundle defect, the zebrafish equivalent, C2144X (*mariner*^{tn4503}), results in the profound splaying of inner ear hair bundles of mutant *mariner* larvae (Ernest et al., 2000). These results suggest that the last 35 amino acids may be required for bundle formation or maintaining structural integrity.

A second *mariner* mutant, G2073D (*mariner*^{tr202b}), which carries a missense mutation in the C-terminus of the second FERM domain, however, resulted in mostly intact hair bundles. The second FERM domain, therefore, may not be involved in bundle integrity, or perhaps this mutation does not significantly impair the ability of Myo7a to bind ligands that are required for bundle maintenance. Although bundle disorganization was not a prominent feature of this *mariner* mutant, extracellular hair cell potentials were dramatically reduced, suggesting that the second FERM domain may play a role in bundle mechanics and is required for proper mechanotransduction. Perhaps large sections of the FERM and MyTH4 domains of repeat 2 are required for proper hair bundle formation and integrity, since loss of regions of these domains in the 8J mutation resulted in a severe bundle defect, even at P0.

We were able to develop a convenient PCR genotyping strategy for rapidly identifying postnatal mice bearing the 8J allele (Fig. 29). This was crucial for expression analysis of the various *Myo7a* transgenic lines (described in Chapter 3), as the *shaker-1* phenotype does not become readily apparent until P12. From our own observations, we learned that at P5 we could tell apart an 8J heterozygote from an 8J homozygote by

flipping the pups over on their backs, and measuring how long it took for the mice to “right” themselves. 8J heterozygotes righted themselves in 1-2 seconds, whereas 8J homozygotes took 5-10 seconds or longer. Nevertheless, the PCR genotyping scheme was essential in distinguishing newborn 8J homozygotes +/- transgene from 8J heterozygotes.

Characterization of the *Myo7a*^{sh1-8J} mutation revealed that mice homozygous for the 8J allele expressed trace amounts of Myo7a, and could serve as a *Myo7a* null. The 8J homozygous mouse was thus an ideal background on which to breed our *Myo7a* transgenics to test for Myo7a expression and functional rescue of the hair cell defect and the *shaker-1* phenotype. Furthermore, developing a convenient PCR genotyping strategy made it possible for us to distinguish newborn mice at P0 and test for rescue of the 8J phenotype in postnatal 8J/8J/Y114G transgenic mice.

RESULTS III

GENERATION AND CHARACTERIZATION OF Y114G-AND FLAsH-TAGGED Myo7A TRANSGENIC MICE

Mutant-Inhibitor Strategy

The chemical-genetic approach that was successfully applied to Myo1c involved changing the tyrosine (Y61) residue of Myo1c to glycine, in order to expand its nucleotide pocket to accept N⁶-modified analogs of ADP, e.g. NMB-ADP. Since the analogous tyrosine residue (Y114) is conserved in Myo7a, we applied the mutant/inhibitor strategy to this motor protein. To allow for selective inhibition of Myo7a, we created the Y-to-G mutation at tyrosine 114 in the hope that it would have little effect on ATP hydrolysis and motor activity, but would sensitize Myo7a to NMB-ADP or to other N⁶-modified ADP analogs in the inner ear.

FLAsH-FALI Strategy

With the intent of studying Myo7a function in the inner ear, we also pursued an alternative strategy to the Y-to-G approach by using FLAsH technology (Invitrogen, Carlsbad, CA.), which involved genetically engineering the “FLAsH-tag” into Myo7a of mice. Rarely occurring in nature, the FLAsH tag is a tetracysteine motif (TGC TGC CCC GGC TGC TGC) with the capacity to bind tightly, via its cysteines, with one of two non-fluorescent, biarsenical fluorophores - Lumio Red and Lumio Green (Invitrogen, Carlsbad, CA.). Upon binding, Lumio becomes highly fluorescent, permitting

visualization of the FLAsH-tagged protein in a living cell and real-time monitoring of the protein in a physiological process within the cell (Tour et al., 2003). An additional feature of covalently bound Lumio is that high intensity light induces the fluorophore to locally produce reactive oxygen species at the site of the tag, in turn destroying the protein. Thus, a protein's role can be directly linked to a particular physiological process and function assigned by this powerful method of FALI (fluorescent-assisted light inactivation).

Generating Y114G- and FLAsH-tagged Myo7a transgenic mice

To apply the inhibitor-sensitization and FLAsH strategies for Myo7a to hair cells, we generated transgenic mice that expressed Y114G-Myo7a and FLAsH-tagged-Myo7a under a hair-cell specific promoter (Boëda et al., 2001). To ensure that the levels of transgenic Myo7a were similar to endogenous, wild-type Myo7a, we included tandem copies of insulator sequence from the chicken *beta-globin* locus, which has been shown to minimize position effects of transgene integration (Boëda et al., 2001). These sequences also have the ability to prevent DNA methylation and histone deacetylation of the transgene (Chung et al., 1997).

John Mercer's group at the McLaughlin Institute in Montana microinjected the transgenic constructs (Y114G-Myo7a, FLAsH-tagged-Myo7a; Fig. 36) into FVB/NCr mouse oocytes and produced several founders (shown below). In all cases, the transgenic founders were backcrossed to the parental FVB strain before they were transported to OHSU. Upon arrival, lines were crossed with the FVB strain for three generations, then onto C57BL6/J. Duplicate transgenic lines were kept in Montana for breeding on the 8J

Figure 36. Schematic diagram of the Y114G-Myo7a and FAsH-tagged *Myo7a* transgenes. Except for a small region encoding 38 amino acids in the first FERM domain (Fig. 24), the transgenes included a full-length *Myo7a* cDNA sequence driven by a minimal hair-cell specific promoter (Boëda et al., 2001). Tandem core insulators from chicken β -*globin* were engineered at either end of the transgenes. The Y114G transgene contained coding for the Y114G mutation at amino acid residue 114 in exon 4, which created a *BamH*I restriction site. The FAsH-tagged *Myo7a* transgene contained an in-frame insertion of the FAsH sequence (TGC TGC CCC GGC TGC TGC) between the coding region for the second and third amino acids of *Myo7a*. Treatment with restriction enzymes (*Not*I and *Age*I) were used to linearize the transgenes.



homozygous background to attempt rescue of the *shaker-1* phenotype by any of the lines, which was assessed by auditory brainstem analysis (ABR) and visual inspection of behavior.

Founders:

FVB/NCr Tg Myo7a FAsH 2

FVB/NCr Tg Myo7a FAsH 5

FVB/NCr Tg Myo7a FAsH 15

FVB/NCr Tg Myo7a FAsH 23

FVB/NCr Tg Myo7a FAsH 25

FVB/NCr Tg Myo7a FAsH 26

FVB/NCr Tg Myo7a wt 26

FVB/NCr Tg Myo7a Y114G 55

(multiple insertions, personal communication D. W. Provance)

FVB/NCr Tg Myo7a Y114G 56

(multiple insertions, personal communication D. W. Provance)

FVB/NCr Tg Myo7a Y114G 71

RT-PCR/Southern analysis of FAsH-tagged Myo7a transgenic mice

To determine which FAsH-tagged Myo7a transgenic lines were likely to express the most protein, an RT-PCR/Southern was performed on five of the transgenic lines. As described in the Materials and Methods, total RNA from transgenic inner ear tissue was reverse-transcribed to generate cDNA, which then was used as template for PCR

amplification with primers spanning the FAsH-tagged site. Successful amplification resulted in 710 and 726 bp products. To determine the relative copy number of each transgenic line, equal amounts of amplified cDNA PCR products were loaded on an agarose (1.4%) gel and analyzed by Southern blotting with a short oligo probe (ggta TGC TGC CCC GGC TGC TGC) that included the FAsH tag. The Southern (Fig. 37) results indicated that lines 15 and 25 gave the greatest band signals for both cochlea and utricle, line 23 gave faint signals, while lines 2 and 5 showed no bands. These results were corroborated by a separate strategy: RT-PCR amplification of transgenic message followed by *EcoR* V treatment of the PCR products. These experiments showed that lines 23 and 25 were indeed the only ones that expressed the FAsH-tagged transgene (Fig. 38). Thus, lines 23 and 25 were used for FAsH labeling experiments to determine whether hair cells from these mice expressed the FAsH-tagged Myo7a transgene.

FAsH labeling of inner ear tissues from Lines 23 and 25 (FAsH-tagged transgenics)

To determine whether either of these lines expressed FAsH-tagged Myo7a protein in hair cells, cochlear or utricular whole epithelia from postnatal transgenic mice (P4-P8) were labeled with Lumio green (Fig. 39). Cocktails of 15-25 μ M EDT (1,2-ethanedithiol) and Lumio green (1.5-5.0 μ M) were used empirically to label transgenic inner ear tissue (details outlined in Materials and Methods), and then were examined by confocal microscopy. High background levels always resulted, in both transgenic and control inner ear tissue, even with four 15-minute washes containing EDT at 750 μ M. Hair bundles and hair cells often labeled more intensely with lumio green than surrounding cell types. Comparable signals were consistently observed between FAsH

Figure 37. RT-PCR/Southern analysis of FAsH-tagged *Myo7a* transgenic lines.

Total RNA was prepared from mouse inner ear tissue and reverse-transcribed to cDNA. A 724 bp region of *Myo7a* flanking the FAsH insertion was amplified from transgenic cDNA using primers (7aprB/ primer C). Equal amounts of PCR product from each sample were loaded onto 1.4 % agarose gels and separated by electrophoresis before transfer onto a Genescreen membrane. The 5'-OH (hydroxyl group) of an oligo probe (ggta tgc tgc ccc ggc tgc tgc ata) was labeled with [γ -³²]ATP by T4 PNK treatment and then used to compare expression level between the FAsH-tagged transgenic lines. Expected band sizes were 706 or 724 bp for wild-type and transgenic PCR amplified products, respectively. Lines 15, 23, 25 expressed the transgene in the utricle; lines 23, 25 also expressed the transgene in the cochlea.

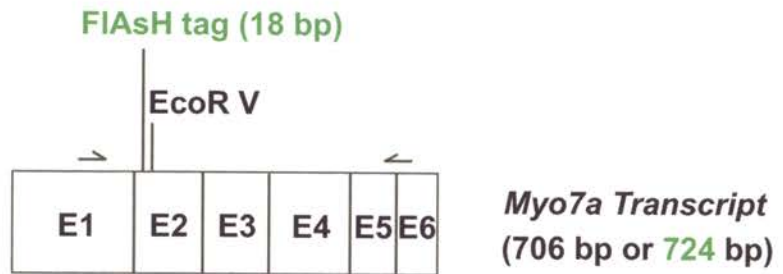
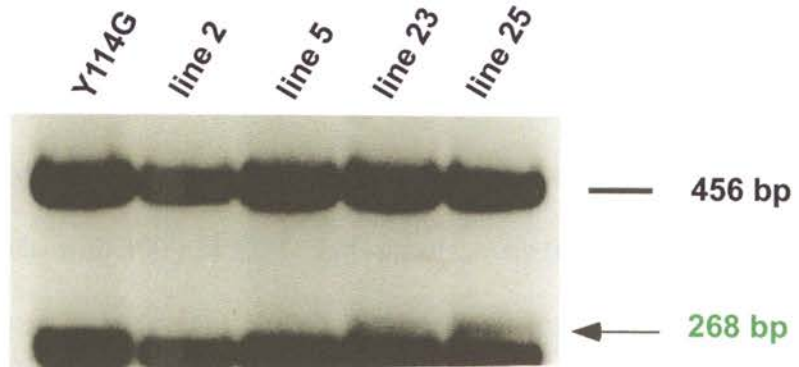
Utricle

Cochlea



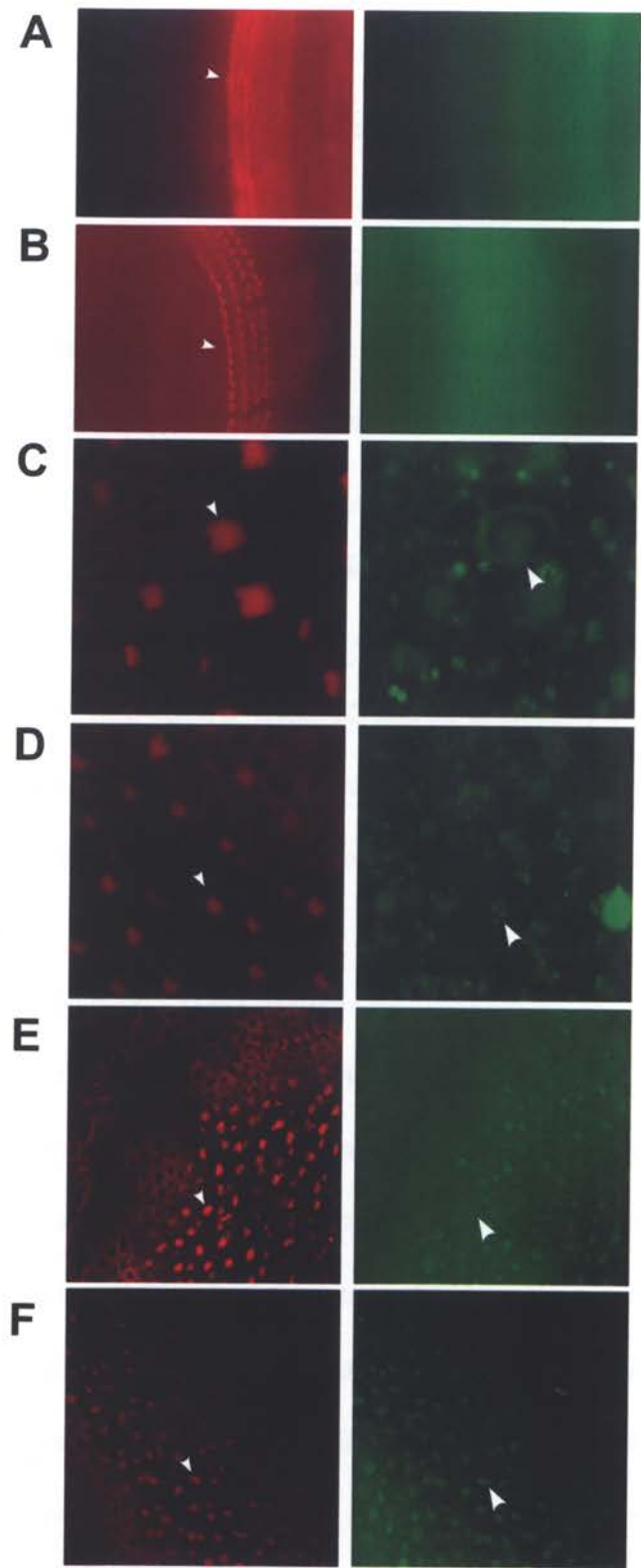
Figure 38. **RT-PCR/ *EcoR V* digestion analysis of FAsH-tagged *Myo7a* transgenic lines.** Total RNA was prepared from inner ear tissue of transgenic mice and reverse-transcribed to cDNA. Primer pairs (7aprB/ primer C) selective for a region flanking the engineered FAsH insertion were used to amplify PCR products from cDNA. PCR products were subsequently treated with *EcoR V* restriction enzyme to estimate the relative fraction of wild-type and transgenic message, since the FAsH tag (tgc tgc ccc ggc tgc tgc ata) insertion increases the transcript size by 18 bp. Primers amplified PCR products of 706 or 724 bp for wild-type and transgenic sequence, respectively. Expected band sizes with *EcoR V* treatment are indicated. An agarose (1.4%) gel revealed that only transgenic lines 23, 25 expressed the FAsH-tagged transcript in the cochlea.

cochlea



Transcript	Predicted Sizes	
	<i>Wt</i>	250 bp
<i>FIAsH tg</i>	268 bp	456 bp

Figure 39. **Localization of inner ear Myo7a in FAsH-tagged Myo7a transgenic mice line 25 by lumio green labeling.** Cross-sections through the organ of Corti and utricles from mice (aged P8). Inner ear tissue was harvested in MEM with 25 mM HEPES, incubated with 2.5 μ M lumio-green and 20 μ M EDT for 30 minutes, then bathed four times (15 minutes each) with 300 μ M EDT. Left panels, actin (660-phalloidin, shown in red); right panels, lumio green (green). In left panels, small arrows indicate phalloidin-labeled hair bundles of the hair cell rows. In the lower right four panels, arrowheads indicate the equivalent positions. *A*, The organ of Corti from a wild-type mouse aged P8 labeled with phalloidin. Right panel reveals intense lumio green labeling and high background fluorescence. *B*, The organ of Corti from a FAsH-tagged transgenic mouse aged P8 labeled with phalloidin. Tissue was also intensely labeled with lumio green. *C*, *E*, Phalloidin labeling of utricular hair bundles from *wild-type* mice aged P8. Hair bundles (small arrows) also labeled with lumio green (arrowhead). *D*, *F*, Utricular hair bundles from *transgenic* mice line 25 labeled with phalloidin. In the lowest panels (*F*), the small arrow indicates a phalloidin-labeled hair bundle that also labeled with lumio green (arrowhead).



transgenic and control cochlear and utricular epithelia, which strongly suggested that Myo7a protein was not being expressed at an appreciable level from the FlAsH-tagged Myo7a transgene to allow for Myo7a detection by Lumio green.

RT-PCR analysis of Y114G-Myo7a transgenic mice

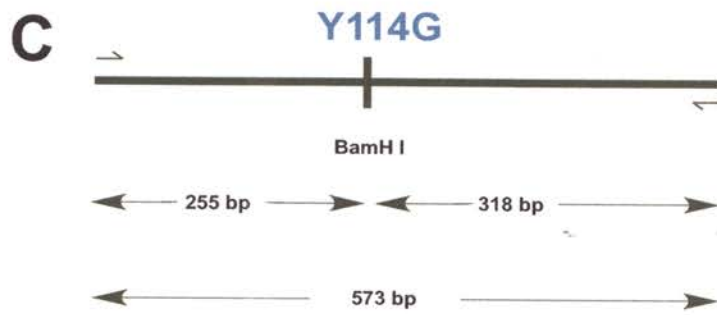
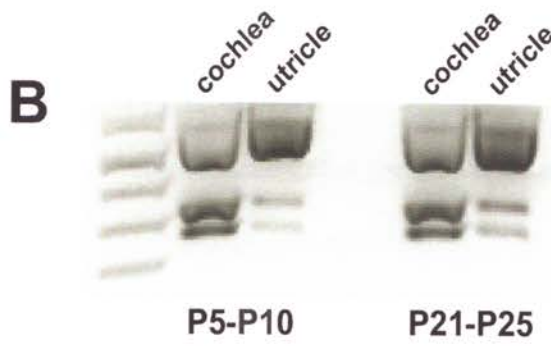
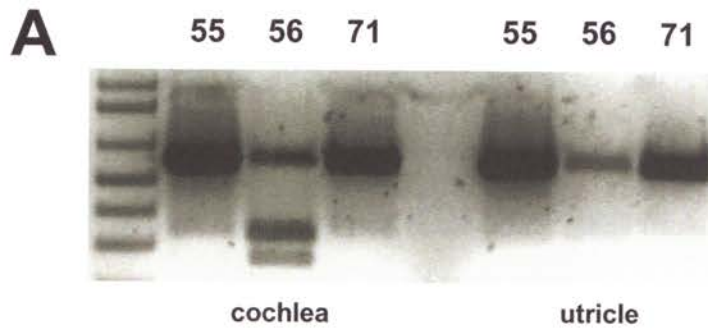
To determine which of the three Y114G transgenic lines expressed Y114G-Myo7a transcripts, RT-PCR analysis was performed on cochlear and utricular cDNA from mice of two different ages (P5-10 and P21-25), using primers that amplify both wild-type and transgenic cDNA. Because the Y114G site introduces a *Bam*HI restriction site, we treated amplified PCR products with this enzyme to estimate the relative amounts of wild-type and transgenic cDNA. Lines 55 and 56 demonstrated expression of the transgene (Fig. 40). In line 56, mRNA transcribed from the Y114G transgene accounted for ~55% of the total Myo7a transcript population in the cochlea.

Immunoblot analysis of Y114G tissues

To confirm expression of the Y114G-Myo7a transgene in cochlea and utricle from line 56, we harvested inner ear tissue from transgenic mice. Using an antibody that recognizes amino acids 880-1080 of Myo7a, we performed immunoblotting of whole organ extracts from cochlea, utricle, retina, and kidney taken from mice of three genotypes: Y114G transgenics (line 56) on an 8J homozygote (*Myo7a* null) background, 8J heterozygotes, and 8J homozygotes. Equal amounts of protein were loaded in 8% SDS gels (see Materials and Methods).

In the kidney, nearly comparable band intensities appeared for transgenic and 8J

Figure 40. **RT-PCR analysis of cochlea and utricle from Y114G transgenic mice.** *A*, Total RNA was processed from mouse cochleas and utricles of Y114G transgenic lines 55, 56, 71 and reverse-transcribed to cDNA. A 573 bp region of *Myo7a* flanking the Y114G site by 318 and 255 bp was amplified using primers. PCR products were subsequently treated with *Bam*HI restriction enzyme to estimate the relative fraction of wild-type and transgenic message, since the Y114G mutation creates a *Bam*HI restriction site. Treatment with *Bam*HI was predicted to split the amplified transgenic PCR product into 318 and 255 bp fragments. An agarose (1.4%) gel revealed that ~55% of the cochlear *Myo7a* message expressed by line 56 was transgenic, as determined by densitometry using an Alpha Innotech imaging system. *B*, The steady state level of Y114G transgene expression from line 56 in the cochlea and utricle did not change between ages P5-10 and P21-25. PCR products were separated by agarose (1.4%) gel electrophoresis. A 1 kb plus DNA marker ladder was loaded in far left lanes.



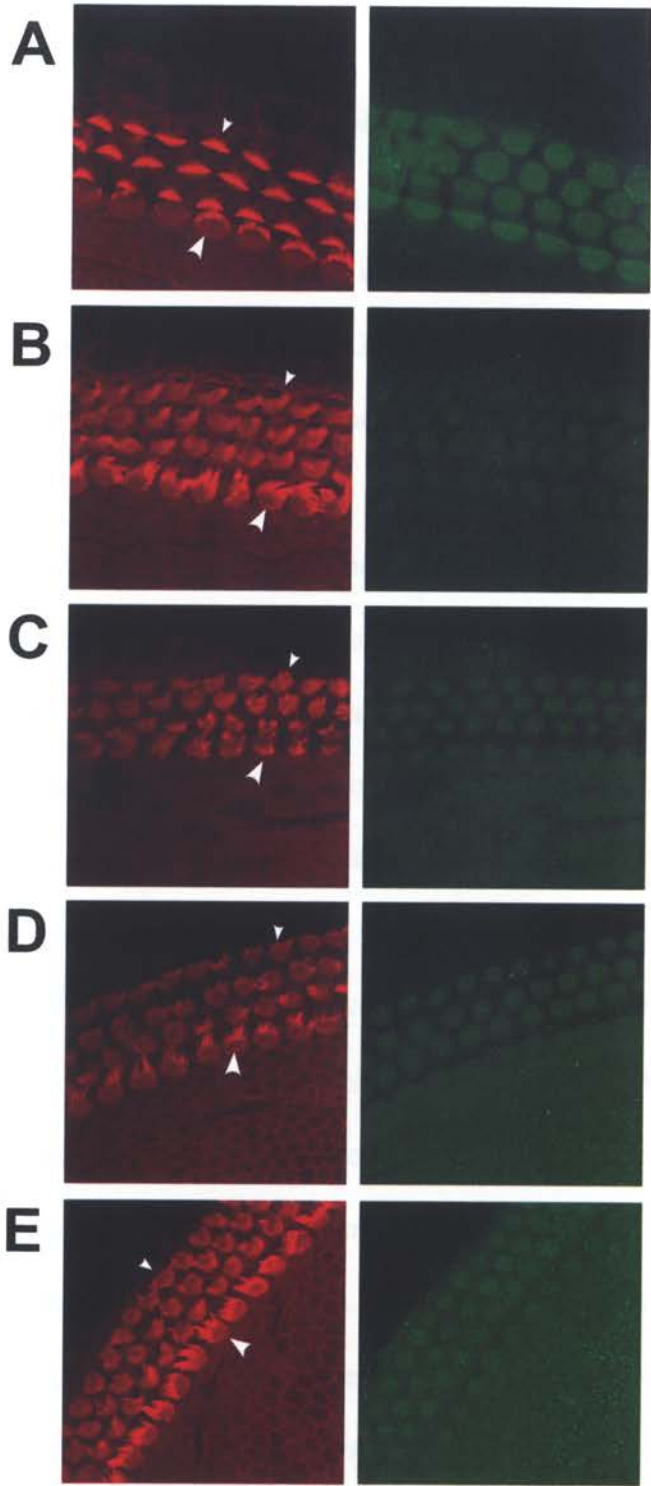
heterozygous samples, indicating roughly equivalent Myo7a expression (Fig. 33). However, the transgenic band ran slightly lower than the ~220 kD band of the 8J heterozygote, probably because the cDNA used to create the Y114G transgene was cloned from a plasmid missing 38 amino acids in-frame of the full-length cDNA sequence (see Fig. 24). In cochlea, the Y114G transgene was expressed at reduced levels compared with wild-type Myo7a and was not detectable in the utricle or retina.

Immunocytochemistry of Y114G cochleas

To look specifically for transgene expression in cochlear hair cells of line 56, we performed immunocytochemistry with the same antibody used for immunoblotting that recognizes amino acids 880-1080 of Myo7a. Cochleas were harvested from postnatal mice (P0-P2, P4, P6) of one of three genotypes, 8J homozygotes +/- Y114G line 56 or 8J heterozygotes, which were readily distinguished by PCR genotyping at P0-P1 prior to immunocytochemical analysis.

The Myo7a antibody strongly labeled inner and outer hair cells from 8J heterozygote mice that expressed a normal Myo7a copy, both along the length of the stereocilia and in the soma (Figs. 31, 32, 41), which is consistent with previous studies (Hasson et al., 1997; Rzadzinska et al. 2004) that examined hair cells from wild-type mice. By contrast, the hair cells from 8J homozygote mice stained very dimly with the Myo7a antibody (Figs. 31, 32, 41). More intense Myo7a labeling was observed in Y114G transgenics on an 8J homozygote background (Figs. 31, 32, 41), demonstrating Myo7a expression of the transgene. Faint expression was observed in the cell bodies and possibly in the stereocilia (Fig. 41) of transgenic inner and outer hair cells at P0.

Figure 41. Localization of Myo7a in organ of Corti from single or double transgenic Y114G mice (aged P0) by immunofluorescence and immunocytochemistry. Cross-sections through the mouse organ of Corti from newborn (P0) mice: 8J heterozygote, 8J homozygote, 8J homozygotes with one or two copies of the Y114G transgene. Left panels, actin (FITC-phalloidin, shown in red); right panels, Myo7a immunolabeling (green). Top panels (A), cross sections through the organ of Corti from an 8J heterozygote mouse aged P0. Small arrow points to a tightly formed hair bundle from an outer hair cell of the outermost row of cells. Hair bundles of the inner row of hair cells were also organized (arrowhead). Right panel reveals strong immunoreactivity for Myo7a in hair cells. (B), Cross sections through the organ of Corti from an 8J homozygote mouse aged P0. Hair bundles were disorganized in both outer hair cells (small arrows) and inner hair cells (arrowhead). Hair cells were dimly labeled with Myo7a. C, D, E, Organ of Corti from three separate newborns derived from 8J homozygous single Y114G transgenic parents. Hair bundles from the three samples were disorganized. Hair cells displayed greater Myo7a immunoreactivity in all hair cells compared with the 8J homozygote sample. (E) Sample with the greatest Myo7a immunoreactivity of the 17 progeny born from the cross between the 8J homozygous single Y114G transgenic parents. Therefore, this representative may have contained two copies of the Y114G transgene. Images were taken with identical gain and confocal settings.



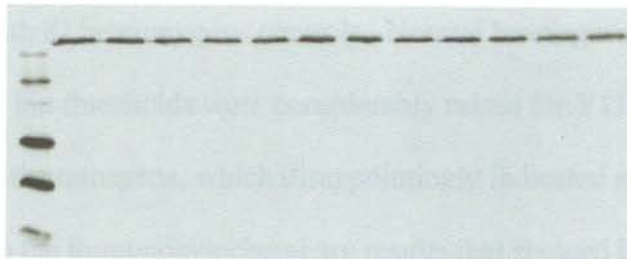
Expression of the transgene in outer hair cells declined at P4 and P6 while inner hair cell expression was still detected.

Stereocilia from 8J homozygotes +/- a single Y114G transgene copy were consistently disorganized despite Myo7a expression, in comparison with the tight bundles observed in 8J heterozygous controls, at all ages evaluated (Figs. 31, 32, 41). Thus, expression of a single copy of the Y114G transgene from line 56 failed to rescue the stereociliary anomaly seen in the 8J homozygote. Alternatively, the Y114G-Myo7a protein might not be functional.

To assess whether two copies of the Y114G-Myo7a transgene could rescue the 8J defect, we set up crosses between 8J/8J/single transgenic Y114G parents to generate double transgenic 8J/8J progeny for immunoblotting of kidney lysates (Fig. 42) and for immunocytochemical analysis of organ of Corti Myo7a at age P0 (Fig. 41). A quarter of the progeny from this cross were predicted to be double Tg/8J/8J if the transgene did not integrate in an essential gene. Of the 17 progeny born to the parents [8J/8J/single Y114G tg ♂ × 8J/8J/single Y114G tg ♀], cochlear hair bundles were disorganized in all samples examined despite immunocytochemical detection of Myo7a (Fig. 41). Two of the 17 progeny may indeed have been double transgenic because Myo7a expression in hair cells from these samples (a representative is shown in Fig. 41E) was more intense than other samples tested (Fig. 41 C, D). Thus, it appears that two copies of the Myo7a transgene might be insufficient to rescue the 8J homozygous phenotype. However, immunoblotting for Myo7a in kidney lysates showed equivalent band signals for Myo7a across all samples, so it is possible that none of the 17 progeny were double transgenic.

Separate progeny from these crosses [8J/8J/single Y114G tg ♂ × 8J/8J/single

Figure 42. **Immunoblot analysis of Myo7a expression in kidneys from single or double Y114G transgenic mice (line 56).** Immunoblotting of mouse kidneys with anti-Myo7a antibody. Lysates were prepared from progeny born from a cross between 8J/8J/single transgenic Y114G parents. A quarter of the progeny were predicted to be double transgenic 8J/8J if the transgene did not integrate within an essential gene. Equal amounts of total protein were loaded ($\sim 5\mu\text{g}$ per lane). Myo7a position (~ 220 kDa) is indicated. The Myo7a band signals were nearly identical for all samples, indicating similar Myo7a transgene expression.



— Myosin-7a

Anti-Myo7a
immunoblot

Kidney

Y114G tg $\frac{0}{1}$] have been saved for ABR analysis; yet so far, all have displayed the typical *shaker-1* phenotype (hyperactivity, circling, head bobbing). We will identify authentic double transgenics by breeding them to wild-type mice and then verify by PCR genotyping that *all* progeny from these crosses are transgenic.

Phenotype Analysis

Auditory-evoked brainstem responses were performed to determine whether Y114G transgenic mice on an 8J homozygous background hear normally, i.e., at a level comparable with 8J heterozygous controls. Normal hearing was observed in 8J heterozygotes, but thresholds were considerably raised for Y114G transgenic harboring a single copy of the transgene, which disappointingly indicated no auditory rescue and was consistent with the immunocytochemistry results that showed little Myo7a hair-cell expression. In fact, ABR thresholds were raised by more than 40 db SPL across all frequency and stimulus intensities tested in the 8J homozygotes +/- a single copy of the Y114G transgene (line 56), revealing that they were deaf (Fig. 35). These results suggest that one copy of the Y114G-Myo7a transgene was insufficient to rescue the auditory defect in 8J homozygous mice. Ryan Karchar of John Mercer's group independently confirmed these ABR results. They also found that none of the Myo7a transgenics (FlAsH or Y114G lines) rescued the 8J homozygous auditory defect.

To assess vestibular function, we visually monitored the behavior of mice. The shaker phenotype (circling, tremors, and head bobbing) was seen in all 8J homozygotes and in those with one copy of the Y114G transgene line 56. Again, Ryan Karchar found the same result: none of the Myo7a transgenic lines on the 8J homozygous background

rescued the *shaker-1* vestibular defect. All transgenic mice displayed the typical shaker phenotype (hyperactivity, circling, head bobbing).

DISCUSSION III

Interpretation of Myo7a Transgenic Mice

Why did none of the Myo7a transgenics rescue the 8J homozygote *shaker-1* phenotype?

Failure of rescue may have resulted either because the promoter did not express in the right cell type in the inner ear for rescue or was too weakly expressed or both.

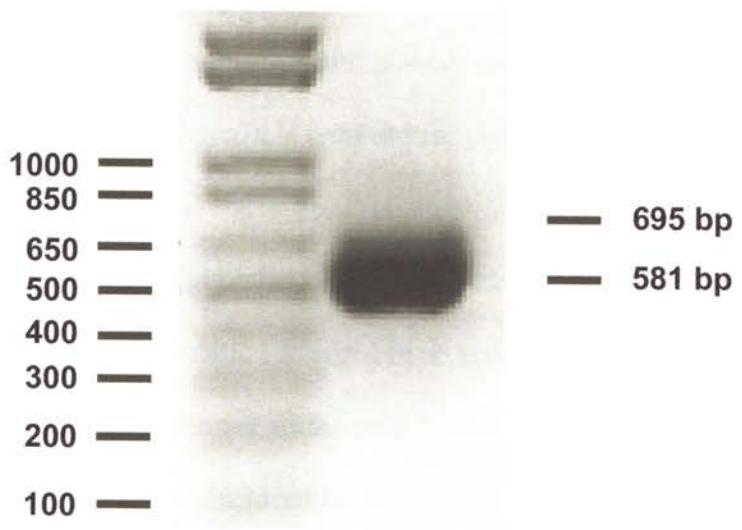
Perhaps the C57BL/6 minimal promoter (-118 to +1776) used in the transgenes was too minimal, and more upstream C57BL/6 genomic sequence was needed for more robust hair-cell specific expression or for targeting to the right cell type. We found eleven single nucleotide differences in the minimal Myo7a promoter that we amplified from C57BL/6 genomic DNA (correct sequence was confirmed against the C57BL/6 *Myo7a* sequence using Ensembl) compared with the minimal Myo7a promoter used in Boëda et al., which came from the C3H mouse strain (Larin et al., 1991). Although Myo7a does not contain a typical kozak sequence [(gcc)gccrcc atg g], the sequence for C57BL/6 (gacgtagaagc atg g) differs from the Boëda et al. C3H sequence (gacgtagaagc cgcg g atg g). Perhaps, these slight sequence differences accounted for the tissue expression profile of our transgenes and weaker transgene expression.

Perhaps the minimal promoter from either strain should not be expected to rescue either the hearing or the vestibular defect observed in the *Myo7a* null phenotype. Boëda et al. drove GFP expression from their minimal Myo7a promoter and created four transgenic lines. In only one of these four lines did they see GFP expression in nearly all utricular hair cells and a subset of cells of the cochlear apex - inner hair cells and border fibrocytes. We observed transient outer hair cell expression of our Y114G transgene at

P0 (Fig. 41) and none in the utricle (Fig. 33). Therefore, we might not see rescue of the *hearing* defect without sufficient *Myo7a* expression in outer hair cells or rescue of the *balance* defect without sufficient *Myo7a* expression in utricular hair cells. Only when GFP expression was driven with a YAC containing 200 kb of upstream C3H *Myo7a* sequence from the starting ATG did Boëda et al. observe slight expression in outer hair cells in the cochlear apex. All transgenic lines derived from the YAC expressed GFP in inner hair cells along the entire length of the cochlea and in all utricular hair cells.

Perhaps the hair cell requires for proper function a *Myo7a* isoform that contains the 38 amino acid coding region that was missing in our transgenic *Myo7a* cDNA. This possibility would be surprising given our RT-PCR results that showed the predominant *Myo7a* transcript in wild-type cochlea does not contain this coding region (Fig. 43). Another group (Mburu et al., 1997) performed RT-PCR analysis of multiple tissues (cochlea, retina, kidney, and testis) derived from a different mouse strain (CBA/Ca) and *only* detected a *Myo7a* transcript missing the 38 amino acid coding region in all tissues sampled, consistent with our RT-PCR analysis of wild-type (C57BL/6) cochlea (Fig. 43). Moreover, hair cells are the only cell type in the cochlea that express *Myo7a* (Hasson et al., 1995). Our RT-PCR analysis examined transcripts from whole cochlea; perhaps single-cell RT-PCR analysis of cochlear inner or outer hair cells would reveal that these cells express an isoform with the 38 amino acid coding region in greater abundance than whole cochlea. Maybe the isoform with the 38 amino acid insertion is delivered to the hair bundle and is required for proper bundle formation and maintenance. Interestingly, an alternative spliced transcript containing the 38 amino acid coding region has been found in human tissues: testis, lymphocytes (Chen et al., 1996), and retina (Weil et al.,

Figure 43. **RT-PCR analysis of wild-type cochlea to test for the presence of a 38 amino acid coding region of *Myo7a* in exons 32 and 33.** Total RNA was processed from wild-type (C57BL6/J) mouse cochlea and reverse-transcribed to cDNA. To determine whether wild-type cochlea encodes an isoform of *Myo7a* that includes 38 amino acids of the first FERM domain (indicated by an asterisk* in figure 24), primers (EX 29-30/ EX 33) specific to a flanking region of *Myo7a* were used to amplify PCR products from cDNA. If the 38 amino acid region were present, a 695 bp PCR product was predicted; if absent, a 581 bp product was predicted. An agarose (1.4%) gel revealed that the predominant *Myo7a* isoform in wild-type cochlea does not include the 38 amino acids. This information was important, since the *Myo7a* cDNA used to construct the *Myo7a* transgenes did not include the 38 amino acid coding region. A 1 kb plus ladder was loaded in the left lane; marker sizes (100-1000 bp) are indicated.



1996).

In favor of the cochlea requiring a *Myo7a* isoform with the 38 amino acid insertion for proper function are our immunoblotting results from mouse cochlea (Fig. 33), which are in stark contrast to our RT-PCR results and those of Mburu et al. (1997) detecting only a *Myo7a* transcript without the 38 amino acid coding region in wild-type cochlea. A higher molecular weight wild-type species of *Myo7a* was detected in the 8J heterozygote sample in cochlea and kidney versus in the transgenic/8J/8J sample. Perhaps then the cochlea predominantly expresses a *Myo7a* protein with the 38 amino acids even if its transcript is produced in the minority. If this were the case in the hair cell, then maybe the 38 amino acid region in *Myo7a* is required for proper hair-cell function in the cochlea and hair-bundle integrity.

An unstable *Myo7a* might have been expressed from our Y114G-*Myo7a* transgene either because the Y114G mutation resulted in an unstable *Myo7a* protein or because the cDNA included a phenylalanine at amino acid 1156 instead of a leucine, which is present in the C57BL/6 sequence (as disclosed by the Ensembl *Myo7a* sequence). However, a phenylalanine does occur at this position in the human MYO7A (Chen et al., 1996; Weil et al., 1996).

RT-PCR analysis revealed robust transgene (Y114G line 56) expression in cochlea; by densitometry, transgene message levels were slightly higher than wild-type message (55% versus 45%) at two different ages, P5-P10 and at P21-25 (Fig. 40).

Immunoblotting with a *Myo7a* specific antibody, however, suggested that expression was poor in the cochlea (30% vs heterozygous levels; Fig.33), perhaps too low to rescue the hearing defect in 8J mice. The absence of *Myo7a* expression in the utricle of this line

explains the lack of rescue of the vestibular defect. Immunocytochemistry for organ of Corti Myo7a also supported a substantially lower expression level of Myo7a in transgenic cochlear hair cells on an 8J homozygous background than compared with the 8J heterozygote controls. Because hair bundles were disorganized at all ages examined, expression of a single copy of the Y114G transgene line 56 was insufficient to rescue the 8J homozygous cochlear hair cell defect. Expression from the other two Y114G transgenic lines (55 and 71) likely would not have rescued the 8J defect because expression from these lines was nearly nonexistent (Fig. 40).

Two copies of the transgene from line 56 may also be insufficient to rescue the bundle defect and auditory 8J phenotype. As highlighted in the results section, cochlear hair bundle morphologies were disorganized from 17 pups (aged P0) of a cross between 8J/8J/single Y114G tg (♂) × 8J/8J/single Y114G tg (♀) parents. By contrast, expression of a single wild-type copy of Myo7a was enough to result in tight bundle morphology and normal auditory function, as observed in 8J heterozygous controls. Maybe the Y114G Myo7a protein is functional but the gene dosage of either the single or double transgenic was not high enough to result in normal hair bundle formation or auditory function. Indeed, immunoblotting of cochlear tissues (Fig. 33) revealed that Myo7a signal from a single transgenic was ~20-30% compared to the level of the heterozygote.

Chance predicts that a quarter of the pups would have been double transgenic/8J homozygote from the cross [8J/8J/single Y114G tg (♂) × 8J/8J/single Y114G tg (♀)]. Therefore, it seems likely that two copies of the transgene did not rescue the Myo7a null phenotype. However, as noted earlier, the Myo7a expression level in kidneys

from these 17 progeny was nearly identical (12 of 17 are shown in Fig. 42). Therefore, it is possible that none of the pups were double transgenic. The results could also be explained if the Y114G transgene from line 56 integrated into the locus of an essential gene, requiring at least one copy for viability.

FUTURE DIRECTIONS III

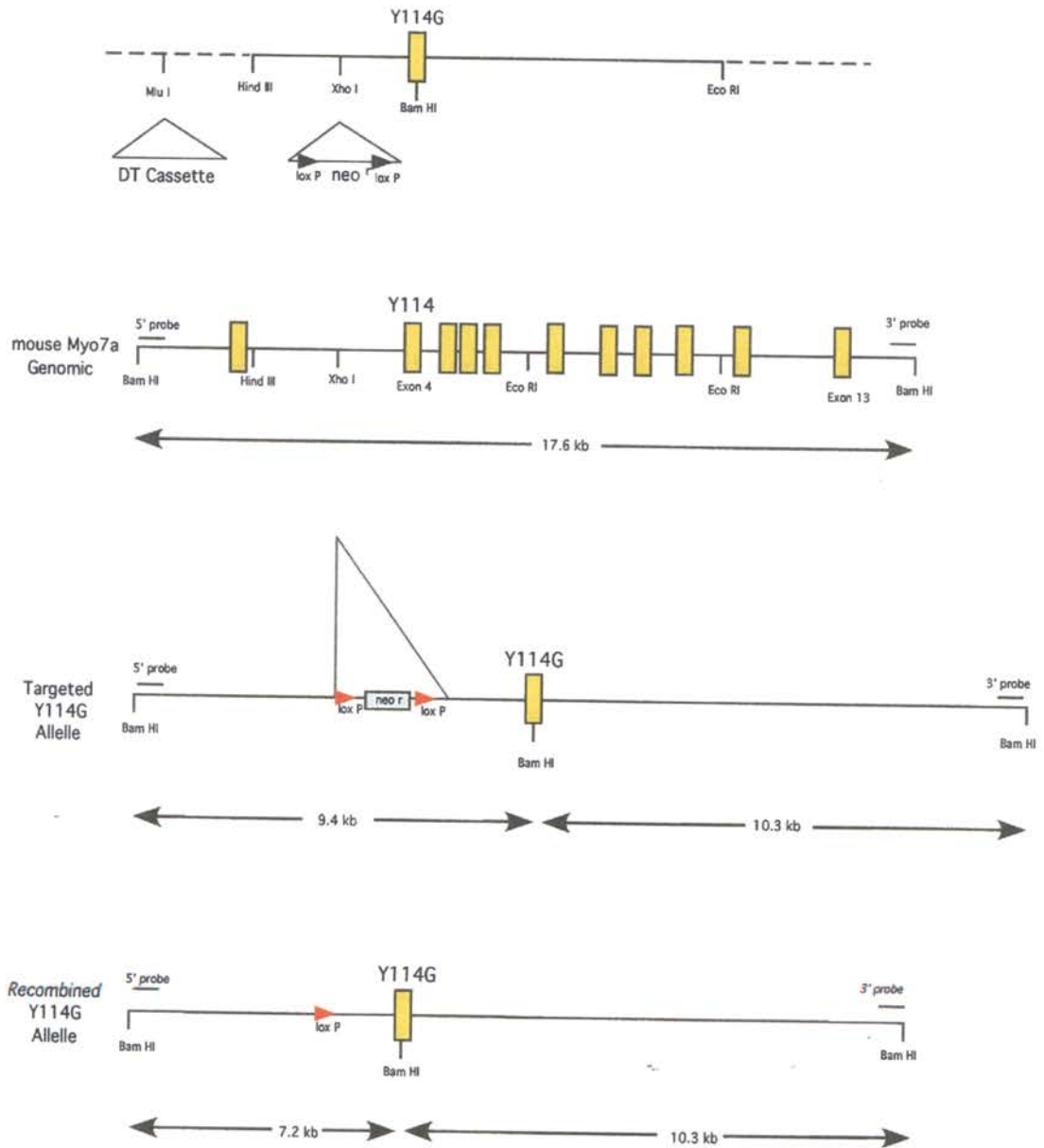
Remaking the Y114G transgenic mice with an insertion containing the 38 amino acid coding region into the *Myo7a* cDNA might result in achieving higher transgene expression in the cells targeted by the minimal hair-specific promoter or in producing a *Myo7a* isoform necessary for proper hair cell function. If the hair bundle requires this isoform for formation and maintenance, then reinsertion of this region might possibly rescue the 8J bundle defect. However, there is little information about the *Myo7a* isoforms required for hair-cell function, so this approach should not be a priority.

The most decisive experiment, however, is to make the Y114G-*Myo7a* knock-in mouse (Fig. 44). Correct targeting of the Y114G mutation into the endogenous *Myo7a* locus would ensure the inclusion of the mutation in *every* *Myo7a* isoform, however many there may be. Then again, it is not known whether the hair cell expresses alternatively spliced forms of *Myo7a* that exclude exon 4, the region coding for tyrosine 114. An unusual, alternatively spliced retinal cDNA of *Myo7a* missing exons 8, 9, and 13 of the head domain was detected in the minority of the cDNA clones isolated from a human retinal cDNA library (Weil et al., 1996).

Whether the Y114G-*Myo7a* protein is functional or not could be assessed quickly and easily at the level of the whole animal or the hair cell in the Y114G knock-in mouse. Chimeras generated from a correctly targeted Y114G-*Myo7a* ES cell clone should transmit the Y114G mutation to the germline because even if the Y114G mutation resulted in a non-functional *Myo7a*, a heterozygote mouse would express a wild-type copy of *Myo7a*, thus ensuring normal hair cell structure and function. As demonstrated

Figure 44. **Targeting Strategy for the Y114G Knock-in Construct.** Sequence coding for the Y114G mutation at amino acid residue 114 in exon 4 will result in a new *Bam*HI restriction site. The loxP-flanked *neomycin*-resistance cassette can be introduced into the large intron between exons 3 and 4 at an *Xho* I restriction site.

Y114G-Myo7a Knock-in Strategy



by 8J heterozygotes, mice function normally with a single wild-type Myo7a copy. Alternatively, if the Y114G allele resulted in a gain-of-function change in the Myo7a protein that led to the destruction of wild-type Myo7a in a dominant-negative fashion, no Y114G heterozygotes would be found in the F1 progeny (i.e., offspring from wild-type mated to the chimeras).

Once Y114G chimeras transmit to the germline and Y114G heterozygous mice are identified, they will be available for intercrossing at 8 weeks of age. One quarter of the progeny from this cross $Y114G/+ (\text{♂}) \times Y114G/+ (\text{♀})$ should be Y114G homozygous. If the Y114G allele is non-functional, a quarter of the progeny will display the *shaker* phenotype at P12. Given the fact that making a targeted mutation in mice is now trivial, pursuing the Y114G is the most reasonable course of action. An answer as to whether the Y114G allele is functional could be gained within four months of generating Y114G-targeted chimeras.

Biochemical characterization of Y114G-Myo7a will remain a challenge until conditions are worked out to conveniently produce soluble Myo7a. While mouse Myo7a can be expressed using several systems, solubilization of mouse Myo7a has been extraordinarily problematic (pages 91-94, Materials and Methods III) and has also proven evasive for others (De LaCruz, personal communication). Alternatively, one could engineer the Y114G mutation in rat Myo7a and pursue biochemical characterization of it. Additionally, if Y114G homozygous mice display no *shaker* phenotype, it would suggest that the Y114G protein is functional. Perhaps then, an analog of ADP (e.g. NMB-ADP) could be used empirically to determine whether it inhibited the function of Y114G-Myo7a in homozygote knock-in hair cells.

Another option to study Myo7a function in the hair cell is to introduce the improved FLAsH sequence (Martin et al., 2005) into the endogenous *Myo7a* locus, creating a knock-in mouse. The improved FLAsH sequence - FLNCCPGCCMEP – imparts greater sensitivity to Lumio Red labeling compared with the original tetracysteine sequence (CCPGCC). Choosing the best location within *Myo7a* to insert the tag could be approached two ways. First, alignments of Myo7a from several species could point to poorly conserved surface loops of Myo7a as potential sites for FLAsH tag insertion. These locations must be within 3-4 nm of the actin-binding regions of Myo7a (Tour et al. 2003), since the goal would be to sever the acto-Myo7a linkage by single reactive oxygen species produced upon high intensity light induction. Second, a structural program could be used to view the motor domain of a crystallized myosin to corroborate each of the proposed insertion points in the surface loops. The FLAsH tag could then be introduced individually at sites identified and Myo7a versions could be expressed in vitro. If solubilization conditions could be worked out to generate modest amounts of *soluble* Myo7a, FLAsH-tagged versions of Myo7a could be used in actin-cosedimentation assays. Using light-assisted actin release from FLAsH-tagged Myo7a, one could identify the ideal mutant and then assay it by a second system – Myo7a-dependent entry of *Listeria* or of latex beads coated with *Listeria* internalin A into human E-cadherin⁺ fibroblasts.

Since the entry of *Listeria monocytogenes* into human cells appears to require Myo7a (Sousa et al., 2003), the ideal FLAsH-tagged mutant identified in the actin release assay could be tested for its ability to prevent *Listeria* entry upon light inactivation. Stably transfected L2071 fibroblasts expressing human E-cadherin (L2071 hEcad)

internalize latex beads coated with purified internalin A (InIA), a surface protein of *L. monocytogenes* required for cell entry through its receptor, E-cadherin.

The approach of introducing the FLAsH sequence into the *Myo7a* locus has risks though; the original shaker mutant (*sh¹*) is due to a nucleotide substitution (CGG to CCG; Arg 502 to Pro) in a poorly conserved surface loop (Mburu et al., 1997) in the head domain. Although these mutants express close-to-normal levels of *Myo7a* and display normal hair bundle development, even into adulthood, the mutation results in diminished hair-cell transduction responses and the *shaker* phenotype (table 2, page 144). Perhaps insertion of the FLAsH tag into a different surface loop would result in milder functional impairment of *Myo7a* or none at all.

SUMMARY AND CONCLUSIONS

In vitro biochemical characterization of mouse Y61G demonstrated that it behaved nearly the same as wild-type Myo1c in motility and ATPase assays, yet was potently inhibited by NMB-ADP. Homologous recombination of the Y61G knock-in construct with the endogenous *Myo1c* locus yielded two correctly targeted ES cell clones (G8, B3), one (G8) of which transmitted to the germline. Mice homozygous for the Y61G mutation appeared normal in every aspect and had no apparent phenotypic deficits. In particular, Y61G homozygotes had normal hearing, as determined by ABR analysis, and showed no obvious vestibular dysfunction. Homozygotes properly spliced Y61G-Myo1c message and produced Myo1c comparable to wild-type levels in all tissues sampled. Thus, the Y61G knock-in mice, in combination with NMB-ADP, were suitable for studying Myo1c-dependent processes in the inner ear. In the future, Y61G knock-in mice will be useful for defining functions of Myo1c in cell types other than vestibular hair cells, particularly when an effective membrane permeable version of NMB-ADP is developed and becomes available.

Eric Stauffer's and Jeff Holt's electrophysiology experiments in homozygous Y61G knock-in cells confirmed that Myo1c mediates slow adaptation in vestibular hair cells. Their experiments also suggest that fast adaptation in vestibular hair cells occurs when Myo1c rapidly releases or adopts a relaxed configuration. Mice homozygous for this sensitized (Y61G) allele are now being used to investigate whether Myo1c activity is necessary for fast and slow adaptation in mouse outer hair cells. If fast adaptation in cochlear hair cells requires the mechanical release of Myo1c, then Myo1c may contribute

substantially to cochlear amplification, the process by which outer hair cells boost faint mechanical stimuli (e.g., soft sounds).

The contribution of *Myo7a* to hair-cell adaptation and transduction remains unresolved. With the hope of sensitizing this motor protein to NMB-ADP and directly testing the role of *Myo7a* in hair cell adaptation, we extended the inhibitor-sensitization strategy to *Myo7a* and generated mice that expressed the analogous Y-to-G mutation in *Myo7a* (Y114G) under a hair-cell specific promoter (Boëda et al., 2001). To determine whether the Y114G-*Myo7a* transgene was functional, we first characterized the genetic defect of a *Myo7a*-null allele, *Myo7a*^{sh1-8J}. RT-PCR analysis, Southern blotting, and direct sequencing of a PCR product spanning the 8J mutation revealed that a large deletion (~6.4 kb) in the MyTH4 and FERM domains of repeat 2 in the tail of *Myo7a* was responsible for the 8J allele.

Using *Myo7a* immunocytochemical analysis of 8J homozygous organ of Corti, we demonstrated that the 8J defect expressed negligible *Myo7a* in cochlear hair cells and resulted in a severely disorganized bundle phenotype; thus, the 8J homozygote was effectively a *Myo7a* null background and was ideal to assess rescue by our Y114G-*Myo7a* transgenics. Interestingly, one or two copies of the Y114G transgene on the 8J/8J background failed to rescue the bundle defect despite the expression of a transgenic isoform of *Myo7a* in the cochlea. Y114G/8J/8J transgenics had disheveled hair bundles and were profoundly deaf; ABR analysis disclosed comparable thresholds that were raised by more than 40 db SPL across all frequency and stimulus intensities between 8J homozygotes +/- a single copy of the Y114G transgene. Perhaps the exclusion of a 38 amino acid in-frame coding region accounted for the failure of the Y114G-*Myo7a*

transgene to rescue the 8J/8J phenotype. Whether the Y114G-Myo7a allele produces a functional protein or not will be assessed in knock-in mice homozygous for the Y114G-Myo7a mutation.

REFERENCES

- Albanesi J.P., H. Fujisaki, J.A. Hammer, E.D. Korn, R. Jones, and M.P. Sheetz. 1985. Monomeric *Acanthamoeba* myosins I support movement in vitro. *J. Biol. Chem.* 260:8649-8652.
- Anderson, D.W., F. J. Probst, I.A. Belyanueva, R.A. Fridell, L. Beyer, D.M. Martin, D. Wu, B. Kachar, T.B. Friedman, Y. Raphael, and S.A. Camper. 2000. The motor and tail regions of myosin XV are critical for normal structure and function of auditory and vestibular hair cells. *Hum. Mol. Genet.* 9:1729-1738.
- Assad, J.A., G.M.G. Shepherd, and D.P. Corey. 1991. Tip-link integrity and mechanotransduction in vertebrate hair cells. *Neuron.* 7:985-994.
- Assad, J.A., and D.P. Corey. 1992. An active motor for adaptation by vertebrate hair cells. *J Neurosci.* 12:3291-3309.
- Avraham, K.B., T. Hasson, K.P. Steel, D.M. Kingsley, L.B. Russell, M.S. Mooseker, N.G. Copeland, and N.A. Jenkins. 1995. The mouse Snell's waltzer deafness gene encodes an unconventional myosin required for structural integrity of inner ear hair cells. *Nat. Genet.* 11:369-375.

Berg, J.S., B.C. Powell, and R.E. Cheney. 2001. A millennial myosin census. *Mol. Biol. Cell.* 12:780-794.

Boëda B., and C. Petit. 2001. A specific promoter of the sensory cells of the inner ear defined by transgenesis. *Hum. Mol. Genet.* 10:1581-1589.

Boëda, B., A. El-Amraoui, A. Bahloul, R. Goodyear, L. Daviet, S. Blanchard, I. Perfettini, K.R. Fath, S. Shorte, J.Reiners, A. Houdusse, P. Legrain, U. Wolfrum, G. Richardson, and C. Petit. 2002. Myosin VIIa, harmonin, and cadherin 23, three Usher I gene products that cooperate to shape the sensory hair cell bundle. *EMBO.* 24:6689-99.

Bozovic, D., and A.J. Hudspeth. 2003. Hair-bundle movements elicited by transepithelial electrical stimulation of hair cells in the sacculus of the bullfrog. *Proc. Natl. Acad. Sci. USA* 100:958-963.

Bishop, A., J.Ubersax, D. Petch, D. Matheos, N. Gray, J. Blethrow, E. Shimizu, J. Tsien, P. Schultz, M. Rose, J. Wood, D. Morgan, and K. Shokat. 2000. A chemical switch for inhibitor-sensitive alleles of any protein kinase. *Nature.* 407:395-401.

Bishop A., O. Burko, S. Heyeck-Dumas, I. Jung, B. Kraybill, Y. Liu, K. Shah, S. Ulrich, L. Witucki, F. Yang, C. Zhang, and K. Shokat. 2000. Unnatural ligands for engineered proteins: new tools for chemical genetics. *Ann. Rev. Biophys. Biomol. Struct.* 29:577-606.

- Bose, A., A. Guilherme, S.I. Robida, S.M. Nicoloso, Q.L. Zhou, Z.Y. Jiang, D.P. Pomerleau, and M.P. Czech. 2002. Glucose transporter recycling in response to insulin is facilitated by myosin Myo1c. *Nature*. 420:821-4
- Chen, Z-Y., T. Hasson, P.M. Kelley, B.J. Schwender, M.F. Schwartz, M. Ramakrishnan, W.J. Kimberling, M.S. Mooseker, and D.P. Corey. 1996. Molecular cloning and domain structure of human myosin-VIIa, the gene product defective in Usher syndrome 1B. *Genomics*. 36:440-448.
- Chen, Z-Y., T. Hasson, D-S. Shang, B. Schwender, B. Derfler, M.S. Mooseker, and D.P. Corey. 2001. Myosin-VIIb, a novel unconventional myosin, is a constituent of microvilli in transporting epithelia. *Genomics*. 72:285-296.
- Cheung E.L., and D. P. Corey. 2005. Ca^{++} changes the force sensitivity of the hair-cell transduction channel. *Biophys. J.*
- Chung, J.H., A.C. Bell, and G. Felsenfeld. 1997. Characterization of the chicken beta-globin insulator. *Proc. Natl. Acad. Sci. USA* 94: 575-580.
- Corey, D.P., and A.J. Hudspeth. 1979a. Ionic basis of the receptor potential in vertebrate hair cell. *Nature*. 281:675-677.
- Corey, D.P. and A.J. Hudspeth. 1979b. Response latency of vertebrate hair cells. *Biophys. J.* 26:499-506.

Corey, D.P. and A.J. Hudspeth. 1983. Kinetics of the receptor current in bullfrog saccular hair cells. *J. Neurosci.* 3:962-976.

Corey, D.P. 2003. New TRP channels in hearing and mechanosensation. *Neuron.* 39:585-588.

Denk, W., J. R. Holt, G. M. Shepherd, and D. P. Corey. 1995. Calcium imaging of single stereocilia in hair cells: localization of transduction channels at both ends of tip links. *Neuron.* 15:1311-1321.

DeRosier, D.J., L.G. Tilney, and E. Egelman. 1980. Actin in the inner ear: the remarkable structure of the stereocilium. *Nature.* 287: 291-296.

Diefenbach, T.J., M. Vaughan, M. Latham, D. Yimlamai, C.A. Liu, I. M. Herman and D. G. Jay. 2002. Myosin 1c and myosin IIB serve opposing roles in lamellipodial dynamics of the neuronal growth cone. *J Cell Biol.* 158:1207-17.

Dumont, R.A., Y-D Zhao, J. Holt, M. Bähler, and P.G. Gillespie. 2002. Myosin-I isozymes in neonatal rodent auditory and vestibular epithelia. *JARO.* 03:375-389.

Eatock, R.A., D.P. Corey, and A.J. Hudspeth. 1987. Adaptation of mechano-electrical transduction in hair cells of the bullfrog's sacculus. *J. Neurosci.* 7:2821-2936.

Ernest, S., G.J. Rauch, P. Haffter, R. Geisler, C. Petit, and T. Nicholson. 2000. Mariner is defective in myosin VIIA: a zebrafish model for human hereditary deafness. *Hum. Mol. Genet.* 9:2189-2196.

Etournay, R. A., A. El-Amraoui, A. Bahloul, S. Blanchard, I. Roux, G. Pezeron, N. Michalski, L. Daviet, J.P. Hardelin, P. Legrain, and C. Petit. 2005. PHR1, an integral membrane protein of the inner ear sensory cells, directly interacts with myosin 1c and myosin VIIa. *J. Cell Sci.* 118:2891-2899.

Furness, D.N., and C.M. Hackney. 1985. Cross-links between stereocilia in the guinea pig cochlea. *Hear. Res.* 18:177-188.

Gale, J.E., W. Marcotti, H.J. Kennedy, C.J. Kros, and G.P. Richardson. FM1-43 dye behaves as a permeant blocker of the hair-cell mechanotransducer channel. 2001. *J. Neuroscience.* 21:7013-7025.

Garcia, J.A., A.G. Yee, P.G. Gillespie, and D.P. Corey. 1998. Localization of myosin-I beta near both ends of tip links in frog saccular hair cells. *J. Neurosci.* 18:8637-8647.

Gibson, F., J. Walsh, P. Mburu, A. Varela, K.A. Brown, M. Antonio, K.W. Biesel, K.P. Steel, and S.D.M. Brown. 1995. A type VII myosin encoded by the mouse deafness gene *shaker-1*. *Nature.* 374:62-65.

Gillespie, P.G. and A.J. Hudspeth. 1991. High-purity isolation of bullfrog hair bundles and subcellular topological localization of constituent proteins. *J. Cell Biol.* 112:625-640.

Gillespie, P.G., M.C. Wagner, and A.J. Hudspeth. 1993. Identification of a 120kD hair-bundle myosin located near stereociliary tips. *Neuron.* 11:581-594.

Gillespie, P.G., and A.J. Hudspeth. 1993. Adenine nucleoside diphosphates block adaptation of mechano-electrical transduction in hair cells. *Proc. Natl. Acad. Sci. USA.* 90:2710-2714.

Gillespie, P.G., S.K.H. Gillespie, J.A. Mercer, K. Shah, and K.M. Shokat. 1999. Engineering of the myosin I β nucleotide-binding pocket to create selective sensitivity to N⁶-modified ADP analogs. *J. Biol. Chem.* 274:31373-81.

Gillespie PG, Gillespie SK. 1997. Improved electrophoresis and transfer of picogram amounts of protein with hemoglobin. *Anal Biochem.* 246:239-45.

Gillespie, P.G. and J. L. Cyr. 2004. Myosin-1c, the hair cell's adaptation motor. *Annu. Rev. Physiol.* 66:521-545.

Gillespie, P.G., R.A. Dumont, and B. Kachar. 2005. Have we found the tip link, transduction channel, and gating spring of the hair cell? *Curr. Opin. Neurobiol.* 15:389-396.

Goldberg, M.E. and A.J. Hudspeth. The vestibular system. In: *Principles of Neural Science*, edited by E. Kandel, J. Schwartz, T. Jessell. New York: McGraw-Hill. 2000. Chapter 40.

Goodyear, R. J., W. Marcotti, C. J. Kros, and G. P. Richardson, (2005). Development and properties of stereociliary link types in hair cells of the mouse cochlea. *J. Comp. Neurol.* 485:75-85.

Hasson, T., P.G. Gillespie, J.A. Garcia, R.B. MacDonald, Y. Zhao, A.G. Yee, M.S. Mooseker, and D.P. Corey. 1997. Unconventional myosins in inner-ear sensory epithelia. *J. Cell Biol.* 137:1287-1307.

Hasson, T., M.B. Heintzelman, J. Santos-Sacchi, D.P. Corey, and M.S. Mooseker. 1995. Expression in cochlea and retina of myosin VIIa, the gene product defective in Usher syndrome type 1B. *Proc Natl Acad Sci U S A.* 92:9815-9.

Hasson, T., J. Walsh, J. Cable, M.S. Mooseker, S.D. Brown, and K.P. Steel. 1997. Effects of shaker-1 mutations on myosin-VIIa protein and mRNA expression. *Cell Motil Cytoskeleton.* 2:127-38.

Holt, J., S.K.H Gillespie, D.P. Corey, J. Mercer, K. Shokat, and P.G. Gillespie. 2002. A role for Myosin-1c in hair cell adaptation. *Cell.* 108:371-381.

Homma, K., M. Yoshimura, J. Salto, R. Ikebe, and M. Ikebe. 2001. The core of the motor domain determines the direction of myosin movement. *Nature*. 412:831-834.

Howard, J., and J.F. Ashmore. 1986. Stiffness of sensory hair bundles in the sacculus of the frog. *Hear. Res.* 23:93-104.

Howard, J. and A.J. Hudspeth. 1987. Mechanical relaxation of the hair bundle mediates adaptation in mechano-electrical transduction by the bullfrog's saccular hair cell. *Proc. Natl. Acad. Sci. USA*. 84:3064-3068.

Howard, J. and A.J. Hudspeth. 1988. Compliance of the hair bundle associated with gating of mechano-electrical transduction channels in the bullfrog's saccular hair cell. *Neuron*. 1:189-199.

Hudspeth, A.J. and R. Jacobs. 1979. Stereocilia mediate transduction in vertebrate hair cells (auditory system/cilium/vestibular system). *Proc. Natl. Acad. Sci. USA*. 76:1506-1509.

Hudspeth, A.J. Hair-bundle mechanics and a model for mechano-electrical transduction by hair cells. 1982. *Soc. Gen. Physiol. Ser.* 47: 357-370.

Hudspeth, A.J. and P.G. Gillespie. 1994. Pulling springs to tune transduction: adaptation in hair cells. *Neuron*. 12:1-9.

Hwang, Y-W., and D.L.Miller. 1987. A mutation that alters the nucleotide specificity of elongation factor tu, a GTP regulatory protein. *J. Biol. Chem.* 262:13081-85.

Inoue A., and M. Ikebe. 2003 Characterization of the motor activity of mammalian myosin VIIA. *J. Biol. Chem.* 278:5478-5487.

Jacobs, R.A., and A.J. Hudspeth. 1990. Ultrastructural correlates of mechano-electrical transduction in hair cells of the bullfrog's internal ear. *Cold Spring Harbor Symp. Quant. Biol.* 55:547-561.

Kachar, B., M. Parakkal, M. Kurc, Y. Zhao, and P.G. Gillespie. 2000. High-resolution structure of hair-cell tip links. *Proc. Natl. Acad. Sci. USA.* 97:13336-13341.

Kennedy, H.J., A.C. Crawford, and R. Fettiplace. Force generation by mammalian hair bundles supports a role in cochlear amplification. 2005. *Nature.* 433:880-883.

Kennedy, H.J., M.G. Evans, A.C. Crawford, and R. Fettiplace. Fast adaptation of mechano-electrical transducer channels in mammalian cochlear hair cells. 2003. *Nature Neurosci.* 6:832-836.

Kros, C.J., W. Marcotti, S.M. van Netten, T.J. Self, R.T. Libby, S.D.M. Brown, G. P. Richardson, and K.P. Steel. 2002. Reduced climbing and increased slipping adaptation in cochlear hair cells of mice with mutations in the *Myo7a* gene. *Nature Neurosci.* 5:41-47.

Krummel, M.F., and M.M. Davis. 2002. Dynamics of the immunological synapse: finding, establishing and solidifying a connection. *Curr Opin Immunol.* 14:66-74.

Küssel-Andermann, P., A. El-Amraoui, S. Safieddine, J. Nouaille, I. Perfettini, M. Lecuit, P. Cossart, U. Wlofrum, and C. Petit. 2000. Vezatin, a novel transmembrane protein, bridges myosin VIIA to the cadherin-catenins complex. *EMBO.* 19:6020-6029.

Küssel-Andermann, P., A. El-Amraoui, S. Safieddine, J-P. Hardelin, S. Nouaille, J. Camonis, and C. Petit. 2000. Unconventional myosin VIIA is a novel A-kinase anchoring protein. *J. Biol. Chem.* 275, 38:29654-29659.

Larin, Z., A.P. Monaco, and H. Lehrach. 1991. Yeast artificial chromosome libraries containing large inserts from mouse and human DNA. *Proc. Natl. Acad. Sci.* 88 :4123-4127

LeMasurier, M. and P.G. Gillespie. 2005. Hair-cell mechanotransduction and cochlear amplification. *Neuron.* 48:403-415.

Lewis, E.R., E.L. Leverenz, and B.S. Bialek. 1985. The Vertebrate Inner Ear. Boca Raton, FL. CRC Press.

Libby, R.T., and K. P. Steel. 2000. The roles of unconventional myosins in hearing and deafness. *Essays Biochem.* 35:159-174.

Liu Y., K. Shah, F. Yang, L. Witucki, and K. Shokat. 1998. Structural basis for selective inhibition of *src* family kinases PP1. *Chem. Biol.* 5:91-10.

Liu, X.Z., J. Walsh, Y. Tamagawa, K. Kitamura, M. Nishizawa, K.P. Steel, and S.D. Brown. 1997. Autosomal dominant non-syndromic deafness caused by a mutation in the myosin VIIA gene. *Nat. Genet.* 17:268-9.

Lord, E.M. and H.W. Gates. 1929. Shaker, a new mutation of the house mouse (*Mus musculus*) *Am. Nat.* 63: 435-442.

Martin, B.R., B.N. Giepmans, S.R. Adams, and R.Y. Tsien. 2005. Mammalian cell-based optimization of the biarsenical-binding tetracysteine motif for improved fluorescence and affinity. *Nat Biotechnol.* 10:1308-14.

Martin, P., D. Bozovic, Y. Choe, and A.J. Hudspeth. 2003. Spontaneous oscillation by hair bundles of the bullfrog's sacculus. *J. Neurosci.* 23:4533-4548.

Mburu, P., X.Z. Liu, J. Walsh, D. Saw Jr, M.J. Cope, F. Gibson, J. Kendrick-Jones, K.P. Steel, and S.D. Brown. 1997. Mutation analysis of the mouse myosin VIIA deafness gene. *Genes Funct.* 3:191-203.

Mermall, V., P.L. Post, and M.S. Mooseker. 1998. Unconventional myosins in cell movement, membrane traffic, and signal transduction. *Science*. 279:527-33.

Mitchell, C., J.B. Kempton, T. Creedon, and D. Trune. 1996. Rapid acquisition of auditory brainstem responses with multiple frequency and intensity tone-bursts. *Hear. Res.* 99:38-44.

Ostap, E.M. and T. Pollard. 1996. Biochemical kinetic characterization of *Acanthamoeba* myosin-I ATPase. *J. Biol. Chem.* 132:1053-1060.

Pestic-Dragovich, L., L. Stojiljkovic, A.A. Philimonenko, G. Nowak, Y. Ke, R.E. Settlage, J. Shabanowitz, D.F. Hunt, P. Hozak, and P. de Lanerolle. 2000. A myosin I isoform in the nucleus. *Science*. 290:337-41.

Pickles, J.O., S.D. Comis, and M.P. Osborne. 1984. Cross-links between stereocilia in the guinea pig organ of Corti, and their possible relation to sensory transduction. *Hear Res.* 15:103-112.

Pollard, T.D. 1982. Assays for myosin. *Methods Enzymol.* 85:123-130.

Provance, D.W., C.R. Gouley, C.M. Silan, L.C. Cameron, K.M. Shokat, J.R. Goldenring, K. Shah, P.G. Gillespie, and J.A. Mercer. 2004 Chemical-genetic inhibition of a

sensitized mutant myosin Vb demonstrates a role in peripheral-pericentriolar membrane traffic. *Proc. Natl. Acad. Sci. USA* 101: 1868-73.

Ricci, A.J., and R. Fettiplace. 1997. The effects of calcium buffering and cAMP on mechano-electrical transduction in turtle auditory hair cells. *J. Physiology*. 501:111-124.

Ricci, A.J. A.C. Crawford, and R. Fettiplace. 2002. Mechanisms of active hair bundle motion in auditory hair cells. *J. Neurosci*. 22:44-52.

Richardson, G.P., A. Forge, C.J. Kros, J. Fleming, S.D. Brown, and K.P. Steel 1997. Myosin VIIA is required for aminoglycoside accumulation in cochlear hair cells. *J. Neurosci*. 17:9506-19.

Rzadinska, A.K., M.E. Schneider, C. Davies, G.P. Riordan, and B. Kachar. 2004. An actin molecular treadmill and myosins maintain stereocilia functional architecture and self-renewal. *J. Cell Biol*. 164:887-897.

Self, T., M. Mahony, J. Fleming, J. Walsh, S.D. Brown and K.P. Steel. 1998. Shaker-1 mutations reveal roles for myosin VIIA in both development and function of cochlear hair cells. *Development*. 125:557-566.

Shah K., Y. Liu, C. Deirmengian, and K. Shokat. 1997. Engineering unnatural nucleotide specificity for Rous sarcoma virus tyrosine kinase to uniquely label its direct substrates. *Proc. Natl. Acad. Sci. USA.* 94:3565-3570.

Shotwell, S.L., R. Jacobs, and A.J. Hudspeth. 1981. Directional sensitivity of individual vertebrate hair cells to controlled deflection of their bundles. *Ann. N.Y. Sci.* 374:1-10.

Siemens, J., C. Lillo, R.A. Dumont, A. Reynolds, D.S. Williams, P.G. Gillespie, and U. Müller. 2004. Cadherin 23 is a component of the tip link in hair-cell stereocilia. *Nature.* 428:950-955.

Slepecky, N. Structure of the mammalian cochlea. In: *The Cochlea*, edited by P. Dallos, A.N. Popper, and R.R. Fay. New York: Springer-Verlag. 1996. Chapter 2.

Söllner, C., G.J. Rauch, J. Siemens, R. Geisler, S.C. Schuster, U. Müller, and T. Nicolson. 2004. Cadherin 23 is a component of the tip link in hair-cell stereocilia. *Nature.* 428:955-959.

Sousa, S., D. Cabanes, A. El-Amraoui, C. Petit, M. Lecuit, and P. Cossart. 2004. Unconventional myosin VIIa and vezatin, two proteins crucial for *Listeria* entry into epithelial cells. *J Cell Sci.* 117:2121-30.

Stauffer*, E.A., J.D. Scarborough*, M. Hirono, E.D. Miller, K. Shah, J.A. Mercer, J.R. Holt, and P.G. Gillespie. 2005. Fast adaptation in vestibular hair cells requires myosin-1c activity. *Neuron*. 47:541-553. * Equal contributions.

Steyger, P.S., P.G. Gillespie, and R.A. Baird. 1998. Myosin I β is located at tip link anchors in vestibular hair bundles. *J. Neurosci*. 18:4603-4615.

Tilney, L.G., E.H. Egelman, D.J. DeRosier, and J.C. Saunders. 1983. Actin filaments, stereocilia, and hair cells of the bird cochlea. II. Packing of actin filaments in the stereocilia and in the cuticular plate and what happens to the organization when the stereocilia are bent. *J. Cell Biol*. 96:822-834.

Tour, O., R.M. Meijer, D.A. Zacharias, S.R. Adams, and R.Y. Tsien. 2003 Genetically targeted chromophore-assisted light inactivation. *Nat Biotechnol*. 12:1505-8.

von Békésy, G. (1960). *Experiments in Hearing*. (New York: McGraw-Hill Inc.).

Wangemann, P. and J. Schacht. Homeostatic mechanisms in the cochlea. In: *The Cochlea*, edited by P. Dallos, A.N. Popper, and R.R. Fay. New York: Springer-Verlag. 1996. Chapter 3.

Weil, D., S. Blanchard, J. Kaplan, P. Guilford, F. Gibson, J. Walsh, P. Mburu, A. Varela, J. Levilliers, and M.D. Weston. 1995. Defective myosin VIIA gene responsible for Usher syndrome type 1B. *Nature* 374:60-61.

Weil, D., P. Kussel, S. Blanchard, G. Levy, F. Levi-Acobas, M. Drira, H. Ayagi, and C. Petit. 1997. The autosomal recessive isolated deafness, DFNB2, and the Usher1B syndrome are allelic defects of the myosin-VIIA gene. *Nat. Genet.* 16:191-3.

Wu, Y., A. Ricci, and R. Fettiplace. 1999. Two components of transducer adaptation in auditory hair cells. *J. Neurophysiol.* 82:2171-2181.

Wu, X.S., K. Rao, H. Zhang, F. Wang, J. Sellers, L. Matesic, N. Copeland, N. Jenkins, and J. Hammer III. 2002. Identification of an organelle receptor for myosin-Va. *Nature Cell Biology.* 4:271-278.

Xu, S., Y. Wang, H. Zhao, L. Zhang, W. Xiong, K.W. Yau, H. Hiel, E. Glowatzki, D.K. Ryugo, and D. Valle. 2004. PHR1, a PH domain-containing protein expressed in primary sensory neurons. *Mol. Cell. Biol.* 24:9137-9151.

Yamoah, E.N., and P.G. Gillespie. 1996. Phosphate analogs block adaptation in hair cells by inhibiting adaptation-motor force production. *Neuron.* 17:523-533.

Zhao, Y., E.N. Yamoah, and P.G. Gillespie. 1996. Regeneration of broken tip links and restoration of mechanical transduction in hair cells. *Proc. Natl. Acad. Sci. USA*. 93:15469-15474.

Zheng, L., G. Sekerkova, K. Vranich, L.G. Tilney, E. Mugnaini, and J.R. Bartles. 2000. The deaf jerker mouse has a mutation in the gene encoding espin actin-bundling proteins of hair cell stereocilia and lacks espins. *Cell*. 102:377-385.